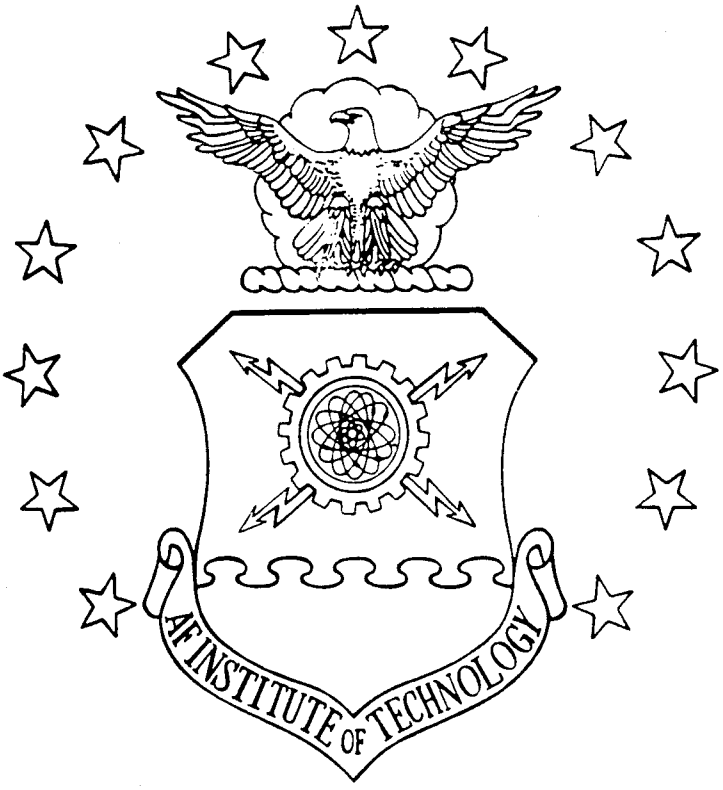

FATIGUE BEHAVIOR OF A CROSS-PLY CERAMIC MATRIX COMPOSITE AT ELEVATED TEMPERATURES UNDER TENSION-TENSION LOADING

THESIS

Craig D. Steiner
Captain, USAF
AFIT/GAE/ENY/94D

DEPARTMENT OF THE AIR FORCE
AIR UNIVERSITY
AIR FORCE INSTITUTE OF TECHNOLOGY

Wright-Patterson Air Force Base, Ohio

AFIT/GAE/ENY/94D-9

FATIGUE BEHAVIOR OF A CROSS-PLY CERAMIC MATRIX COMPOSITE AT ELEVATED TEMPERATURES UNDER TENSION-TENSION LOADING

THESIS

Craig D. Steiner
Captain, USAF
AFIT/GAE/ENY/94D

AFIT/GAE/ENY/94D-9

FATIGUE BEHAVIOR OF A CROSS-PLY CERAMIC MATRIX COMPOSITE AT ELEVATED TEMPERATURES UNDER TENSION-TENSION LOADING

THESIS

Presented to the faculty of the Graduate School of

Engineering of the Air Force Institute of Technology

Air University

In Partial Fulfillment of the

Requirements for the Degree of

Master of Science in Mechanical Engineering

Craig D. Steiner

Captain, USAF

December 1994

Approved for public release; distribution unlimited

Preface

The primary purpose of this study was to investigate the damage mechanisms and fatigue behavior of a ceramic matrix composite, SiC/MAS, at elevated temperature. This material is being studied for possible high temperature applications, including gas turbine engines and hypersonic airframes.

I would like to thank my advisor, Dr. Shankar Mall for his guidance and patience throughout the whole program and especially this project. My thanks must also go to Dr. Palazotto and Dr. Hall for serving on my graduate committee.

I would also like to acknowledge the AFIT laboratory personnel for their fine efforts in maintaining the laboratory facilities. I especially want to thank Mr. Mark Derriso for his tireless efforts in maintaining the test stations. Without his efforts there would be no data.

I would also like to thank my sponsors Mr. Ted Fecke of WL/POTC and Dr. Walter Jones of AFOSR/NA.

Table of Contents

	Page
Preface	ii
List of Figures and Tables	vi
Abstract	xii
I. Introduction	1
II. Background	6
III. Experimental Procedure	11
A. Test Set-Up	11
B. Calibration	13
C. Material Details and Specimen Preparation	14
D. Experimental Procedure	17
IV. Results and Discussion	23
A. Monotonic Tensile Tests	24
A.1. Monotonic Test 566°C	26
A.2. Monotonic Test 1093°C	27
A.3. Monotonic Test Comparison 566°C vs 1093°C	28
B. Fatigue Life	30
B.1. Fatigue Tests 10 Hz	30
B.2. Fatigue Tests 1 Hz	35
B.3. Fatigue Tests 566°C	37

B.4. Fatigue Tests 1093°C 38

C. Modulus Degradation. 41

C.1. Modulus Degradation 566°C 42

C.2. Modulus Degradation 1093°C. 46

C.3. Modulus Degradation 10 Hz 49

C.4. Modulus Degradation 1 Hz 51

D. Strain Data 53

D.1. Strain Data 566°C 10 Hz 53

D.2. Strain Data 566°C 1 Hz 56

D.3. Strain Data 10 Hz vs 1 Hz at 566°C 58

D.4. Strain Data 1093°C 10 Hz 61

D.5. Strain Data 1093°C 1 Hz 63

D.6. Strain Data 10 Hz vs 1 Hz at 1093°C . . 66

D.7. Strain Data 566°C vs 1093°C at 10 Hz . . 71

D.8. Strain Data 566°C vs 1093°C at 1 Hz . . 74

E. Hysteresis Loops 77

E.1. Energy Loops 566°C 77

E.2. Energy Loops 1093°C. 80

F. Damage Mechanisms 83

F.1. Monotonic Tensile Tests 84

F.2. Fracture Surface 10 Hz 566°C. 87

F.3. Fracture Surface 1 Hz 566°C 94

F.4. Fracture Surface 10 Hz 1093°C . . . 101

F.5. Fracture Surface 1 Hz 1093°C . . . 107

F.6 Over-all Comparison 114

V. Conclusions 118

VI. Recommendations 121

Bibliography 122

Appendix A 124

Appendix B 125

Appendix C 127

Vita 133

List of Figures and Tables

Figure #		Page
1.	Stress Strain Curve for 566°C.	26
2.	Stress Strain Curve for 1093°C	27
3.	Stress Strain Curve Comparison 566°C vs 1093°C . . .	28
4.	Fatigue Life Curves 10 Hz 566°C vs 1093°C	31
5.	Fatigue Life Curves 10 Hz 566°C vs 1093°C Magnified . .	32
6.	Normalized Fatigue Life Curves 10 Hz 566°C vs 1093°C . .	32
7.	Fatigue Life Curves SiC/MAS vs SiC/CAS Low Temperature .	33
8.	Fatigue Life Curves SiC/MAS vs SiC/CAS High Temperature .	34
9.	Normalized Fatigue Life Curves SiC/MAS vs SiC/CAS . .	34
10.	Fatigue Life Curves 1 Hz 566°C vs 1093°C	35
11.	Fatigue Life Curves 1 Hz 566°C vs 1093°C Magnified . .	36
12.	Normalized Fatigue Life Curves 1 Hz 566°C vs 1093°C . .	36
13.	Fatigue Life Curves 566°C 1 Hz vs 10 Hz	37
14.	Fatigue Life Curves 566°C 1 Hz vs 10 Hz	38
15.	Fatigue Life Curves 1093°C 1 Hz vs 10 Hz	39
16.	Fatigue Life Curves 1093°C 1 Hz vs 10 Hz	40
17.	Fatigue Life Curves 1093°C vs 566°C	40
18.	Modulus Degradation 566°C 10 Hz	42
19.	Modulus Degradation 566°C 1 Hz	44

20. Modulus Degradation 566°C 137.9 MPa 45

21. Modulus Degradation 566°C 120.66 MPa 45

22. Modulus Degradation 566°C 103.43 MPa 46

23. Modulus Degradation 1093°C 10 Hz 47

24. Modulus Degradation 1093°C 1 Hz 47

25. Modulus Degradation 1093°C 137.9 MPa 10 Hz vs 1 Hz . . 48

26. Modulus Degradation 1093°C 103.43 MPa 10 Hz vs 1 Hz . . 49

27. Modulus Degradation 10 Hz 137.9 Mpa 1093°C vs 566°C . . 50

28. Modulus Degradation 10 Hz 103.43 Mpa 1093°C vs 566°C . . 50

29. Modulus Degradation 1 Hz 137.9 Mpa 1093°C vs 566°C . . 51

30. Modulus Degradation 1 Hz 103.43 Mpa 1093°C vs 566°C . . 52

31. Maximum Strain 10 Hz 566°C 54

32. Minimum Strain 10 Hz 566°C 54

33. Strain Difference 10 Hz 566°C 55

34. Maximum Strain 1 Hz 566°C 56

35. Minimum Strain 1 Hz 566°C 57

36. Strain Difference 1 Hz 566°C 57

37. Maximum Strain 566°C 137.9 MPa 10 Hz vs 1 Hz . . . 58

38. Strain Difference 566°C 137.9 MPa 10 Hz vs 1 Hz . . . 59

39. Maximum Strain vs Time 566°C 137.9 MPa 10 Hz vs 1 Hz . . 60

40. Maximum Strain 566°C 103.43 MPa 10 Hz vs 1 Hz. . . 60

41. Strain Difference 566°C 103.43 MPa 10 Hz vs 1 Hz . . . 61

42. Maximum Strain 10 Hz 1093°C 62

43. Minimum Strain 10 Hz 1093°C 62

44. Strain Difference 10 Hz 1093°C 63

45. Maximum Strain 1 Hz 1093°C 64

46. Minimum Strain 1 Hz 1093°C 64

47. Strain Difference 1 Hz 1093°C 65

48. Maximum Strain 1093°C 137.9 MPa 1 Hz vs 10 Hz . . . 66

49. Strain Difference 1093°C 137.9 MPa 1 Hz vs 10 Hz . . . 67

50. Maximum Strain 1093°C 103.43 MPa 1 Hz vs 10 Hz. . . 67

51. Strain Difference 1093°C 103.43 MPa 1 Hz vs 10 Hz . . 68

52. Strain Difference vs Time 1093°C 137.9 MPa 1 Hz vs 10 Hz . 69

53. First Cycle Stress Strain 566°C 1 Hz vs 10 Hz . . . 70

54. First Cycle Stress Strain 103.43 Mpa 566°C vs 1093°C . . 71

55. Maximum Strain 10 Hz 137.9 MPa 566°C vs 1093°C . . 72

56. Strain Difference 10 Hz 137.9 MPa 566°C vs 1093°C . . 72

57. Maximum Strain 10 Hz 103.43 MPa 566°C vs 1093°C . . 73

58. Strain Difference 10 Hz 103.43 MPa 566°C vs 1093°C . . 73

59. Maximum Strain 1 Hz 137.9 MPa 566°C vs 1093°C . . 74

60. Strain Difference 1 Hz 137.9 MPa 566°C vs 1093°C . . 75

61. Maximum Strain 1 Hz 103.43 MPa 566°C vs 1093°C . . 75

62. Strain Difference 1 Hz 103.43 MPa 566°C vs 1093°C . . 76

63. Hysteretic Energy 10 Hz 566°C 77

64. Hysteretic Energy 1 Hz 566°C 78

65. Hysteretic Energy 566°C 120.66 MPa 1 Hz vs 10 Hz . . 79

66. Hysteretic Energy 566°C 103.43 MPa 1 Hz vs 10 Hz . . 80

67. Hysteretic Energy 1093°C 10 Hz 81

68. Hysteretic Energy 1093°C 1 Hz 81

69. Hysteretic Energy 1093°C 96.53 MPa 1 Hz vs 10 Hz . . 82

70. Hysteretic Energy 1093°C 103.43 MPa 1 Hz vs 10 Hz . . 83

71. Fracture Profile, Monotonic Tensile, 566°C, 7X . . . 85

72. Fracture Profile, Monotonic Tensile, 1093°C, 10X . . . 85

73. Fracture Surface, Monotonic Tensile, 1093°C, 20.4X . . 86

74. Fracture Surface, Monotonic Tensile, 566°C, 15.2X . . . 87

75. Matrix Crack, 10 Hz, 566°C, 137.9 MPa 100X . . . 88

76. Fracture Profile, 10 Hz, 566°C, 103.43 MPa, 10X . . . 89

77. Fracture Surface, 10 Hz, 566°C, 137.9 MPa, 15.7X . . . 90

78. Fracture Surface, 10 Hz, 566°C, 103.43 MPa, 26.2X . . 91

79. Fiber Surface, 10 Hz, 566°C, 137.9 MPa 685X . . . 92

80. Fiber Surface, 10 Hz, 566°C, 103.43 MPa, 470X . . . 92

81. Fracture Surface, 10 Hz, 120.66 MPa, 566°C, 560X . . . 93

82. Matrix Crack, 1 Hz, 120.66 MPa, 566°C, 100X . . . 94

83. Fracture Profile, 1 Hz, 137.9 MPa, 566°C, 10X . . . 95

84. Fracture Surface, 1 Hz, 566°C, 137.9 MPa, 20.8X . . . 96

85. Fracture Surface, 1 Hz, 566°C, 103.43 MPa, 28.8X . . . 97

86. Fiber Surface, 1 Hz, 566°C, 137.9 MPa, 685X . . . 98

87. Fiber Surface, 1 Hz, 566°C, 120.66 MPa, 525X . . . 99

88. Fracture Surface, 1 Hz, 566°C, 660X 100

89. Matrix Crack, 10 Hz, 1093°C, 96.53 MPa, 100X . . . 101

90. Fracture Profile, 10 Hz, 1093°C, 137.9 MPa, 10X . . . 102

91. Fracture Surface, 10 Hz, 1093°C, 137.9 MPa, 18.4X . . 103

92. Fracture Surface, 10 Hz, 1093°C, 103.43 MPa, 18X . . . 104

93. Fiber Surface, 10 Hz, 1093°C, 137.9 MPa, 815X . . . 105

94. Fiber Surface, 10 Hz, 1093°C, 96.53 MPa, 855X . . . 106

95. Fracture Surface, 10 Hz, 1093°C, 720X 107

96. Matrix Crack, 1 Hz, 1093°C, 96.53 MPa, 100X . . . 108

97. Fracture Profile, 1 Hz, 1093°C, 137.9 MPa, 10X . . . 108

98. Fracture Surface, 1 Hz, 1093°C, 137.9 MPa, 11.4X . . . 109

99. Fracture Surface, 1 Hz, 1093°C, 103.43 MPa, 25X . . . 110

100. Fiber Surface, 1 Hz, 1093°C, 137.9 MPa, 625X . . . 111

101. Fiber Surface, 1 Hz, 1093°C, 96.53 MPa, 575X . . . 112

102. Fracture Surface, 1 Hz, 137.9 MPa, 1093°C, 655X . . . 113

103. Fracture Surface, 1 Hz, 120.66 MPa, 1093°C, 17.6X . . 115

104. Fracture Surface, 10 Hz, 96.53 MPa, 1093°C, 19.9X . . 116

105. Fracture Surface, 1 Hz, 96.53 MPa, 1093°C, 20X . . . 116

Table # Page

1. Specimen Dimensions 16

2. Test Matrix 25

3. Material Properties 29

Abstract

The purpose of this study was to investigate the effect of loading rate and elevated temperature on the fatigue behavior of a model ceramic matrix composite with a cross-ply lay-up. The material used in this study was a potassium borosillicate glass (BSG) doped (5%) magnesium aluminosilicate (MAS) cordierite matrix reinforced with Nicalon (silicon carbide, SiC) fibers in a $[0/90]_{4s}$ lay-up. The composite was forty percent fiber by volume. The BSG dopant in the MAS matrix serves as a source of boron which diffuses into the interface between the fiber and the matrix during hot consolidation. The boron serves to keep the interface thin and more oxidatively stable than a purely carbon interface, which is present in the earlier version of this ceramic composite, SiC/CAS.

Initially, monotonic tensile tests were conducted at 566°C and 1093°C. These tests provided that this composite system had an initial modulus of 118 GPa at 566°C and 96 GPa at 1093°C. They also provided baseline data for the ultimate strength of the material which was 292 MPa at 566°C and 209 MPa at 1093°C. These two temperatures were chosen to correspond to those used in work previously done with this material so that results obtained here could be compared with the available data.

Tension-tension fatigue tests with an R value ($\sigma_{min} / \sigma_{max}$) of 0.1 were conducted at two frequencies; 10 Hz and 1 Hz. A total of ten tests were conducted at a frequency of 10 Hz. Five tests were conducted at 566°C with maximum stresses ranging from 137.9 MPa to 86.19 MPa. Another five tests were conducted at 1093°C with the same value of maximum stresses. There were nine tests performed at 1 Hz. Five tests

were conducted at 1093°C and four tests were conducted at 566°C. The maximum stresses for the tests conducted at 566°C ranged from 137.9 MPa to 99.98 MPa. For the tests conducted at 1093°C, the maximum stresses ranged from 137.9 MPa to 96.53 MPa.

Load and strain data were recorded during cycling of all specimens. Post-mortem fractographic analysis, with optical and scanning electron microscopes, was also performed on all the specimens. These load and strain data were then used to assess the fatigue damage mechanisms by analyzing modulus degradation curves, fatigue-life curves, hysteretic loop energy curves and minimum, maximum and strain difference curves.

The present results indicate that the frequency of the triangular loading waveform has no effect on the fatigue life of the specimen in terms of time. It was also seen that the SiC/MAS material has a shorter fatigue-life at elevated temperature, regardless of the frequency of the loading. The fatigue damage mechanisms involved the combination of fiber-matrix debonding and a time dependent environmentally assisted crack growth. The amount of time dependent environmentally assisted crack growth in the specimen is independent of the frequency of the cyclic loading, but dependent on test duration. The specimens cycled at an elevated temperature, 1093°C, had more time dependent environmentally assisted crack growth than the specimens cycled at 566°C.

FATIGUE BEHAVIOR OF A CROSS-PLY CERAMIC MATRIX COMPOSITE AT ELEVATED TEMPERATURES UNDER TENSION-TENSION LOADING

I. Introduction

Ceramics have been in use for many centuries. The ability of ceramics to withstand high temperatures has made them attractive for many different applications. A relatively low density, and the ease of structural tailoring allowed for the ability to create lightweight ceramic objects that were easy to handle. Unfortunately a low ductility and fracture toughness made the type of loading environment and handling critical to the life of these materials.

In the past few years the need for low weight, high strength materials in applications such as engine components has led to the investigation of ceramics as a possible solution. The addition of high strength fibers to the ceramic material led to the development of ceramic matrix composites which have the high strength and thermal durability of ceramic material but a much higher toughness due to the inclusion of the fibers. The orientation of the fibers in the ceramic matrix can be altered to create different or directional properties, and plies with different orientations can be stacked to create optimum performance of the material.

Because the loading environments in applications such as aircraft engines are highly dynamic, it is very important to determine not only the static but also the dynamic properties and capabilities of any material that will be used in that environment. In addition, these environments routinely see, and in fact strive for, extremely high temperatures. For these reasons one of the most important things to determine about a new material that is being considered for these applications is its fatigue behavior at elevated temperatures. Also, it is equally as important to determine the damage mechanisms at high temperature under cyclic loading.

Because of the promising characteristics of the ceramic matrix composites, many different studies have been performed to evaluate and characterize the properties of a wide range of ceramic matrix composite systems [2,3,5,6,8,9,10,12,13,14,15]. These studies all indicate that there is a large reduction in the static and fatigue properties of the ceramic matrix composite at elevated temperatures. This study concentrates on the fatigue life and damage mechanisms of one particular system, a potassium borosillicate glass (BSG) doped (5%) magnesium aluminosilicate (MAS) cordierite matrix reinforced with Nicalon (silicon carbide, SiC) fibers in a $[0/90]_{4s}$ lay-up, SiC/MAS.

The SiC/MAS system is from a family of composites consisting of silicon carbide fibers in a glass ceramic matrix. These glass ceramics are characterized by a weak interfacial bond between the fiber and the matrix which increases the toughness of the composite. The interface between the fiber and matrix is typically susceptible to oxidation, which is more aggressive at elevated temperatures. This oxidation of the interface reduces the toughness of the composite and causes the fatigue properties to be

significantly reduced. The reason this system was chosen for investigation is that it was specifically developed in an attempt to improve its properties at high temperatures. The method used to try to improve the properties of the material was to dope the matrix with a borosilicate glass which diffuses into the interface during hot consolidation. This serves to create a thinner interface which is less susceptible to oxidation and ought to improve the fatigue behavior of the material at high temperature.

With this in mind, the objective of these tests was to determine the fatigue behavior and damage mechanisms of a cross-ply laminate of this ceramic matrix composite, SiC/MAS, at elevated temperature. The fatigue behavior was evaluated by comparing the fatigue life and damage mechanisms resulting from four different loading cases. These cases involved two different frequencies, 1 Hz and 10 Hz, and two different temperatures, 566°C and 1093°C. This allowed for the determination of the effect of frequency, as well as temperature, on the fatigue behavior and damage mechanisms. A final objective of this study was to compare the fatigue behavior and damage mechanisms of this ceramic matrix composite (CMC) system to that of an earlier version of this ceramic matrix composite, SiC/CAS.

The approach taken in this study was to conduct monotonic tensile tests at two different temperatures, 566°C and 1093°C, and fatigue tests at two different frequencies, 1 Hz and 10 Hz, at the same two temperatures. The monotonic tests were conducted to determine baseline information for the material, such as ultimate strength, strain at failure, and initial modulus at the two different temperatures. The next step was to conduct fatigue tests for each of the four loading cases at different stress levels. The data from the

fatigue tests, at each of the frequencies and temperatures, allowed for the determination and comparison of fatigue life curves. The combination of the data from the monotonic and fatigue tests allowed for the determination and comparison of normalized fatigue life curves for each of the four loading cases. Stress-strain data were taken during each of the fatigue tests in order to evaluate the modulus degradation and strain progression during cycling of these tests. The modulus degradation and strain progression plots were used to evaluate the damage mechanisms.

The final step of the approach was the post-mortem fractographic analysis of the failed specimens. Optical microscopes were used to document the failure profiles and the extent of fiber pullout on the fractured surface. A scanning electron microscope was used to document a closer view of the fractured surface and the fibers after failure. This documentation was used to compare the damage mechanisms of the four different loading cases.

The remainder of this document is set up in the following manner. Chapter 3 is a detailed discussion of the preparation of the specimen and the development of the test set-up. This chapter also discusses the methods used to perform the tests and collect the data. Chapter 4 is divided into six sections which discuss the reduction of the data and the conclusions that can be drawn regarding the fatigue life and the damage mechanisms. The first section discusses the monotonic tests conducted at the two temperatures. The next section is a discussion of the fatigue life curves. In this section, comparisons of the fatigue life and normalized fatigue life curves between the two temperatures and the two frequencies are provided. Finally, comparisons between the fatigue life curves of the

present system, SiC/MAS, and the SiC/CAS system are made. Following this is a section on the modulus degradation which also makes comparisons between the two temperatures and the two frequencies as well as comparisons between the different stress levels. A discussion of the strain progression throughout each of the tests is included. This discussion compares the maximum strain, minimum strain, and strain difference of the tests conducted at different stress levels, different frequencies and different temperatures. A short discussion of the loop hysteretic energy is also included. These are provided to assess the fatigue damage mechanisms from the stress strain information obtained during cycling. Next, a section on fractography compares the failure surface, the fracture profile, and the condition of the fibers after failure between the four different loading cases as well as between the different stress levels. Chapter 5 summarizes all the conclusions that can be drawn from this study and Chapter 6 contains recommendations for future work.

II. Background

Ceramic matrix composites have been developed in order to meet the demand for high strength materials with the ability to withstand high temperature environments. Among the many applications that fit this description are components in air breathing propulsion engines. Ceramic matrix composites (CMC's) combine the qualities of high strength, thermal durability, and relative ease of structural tailoring, along with a greater fracture toughness and ductility than non fiber-reinforced ceramics, to be ideal for these applications.

Because of the promise of the ceramic matrix composite, much work has been done over the years in developing and studying this family of composites. The CMC system being studied here is from a class of composites known as glass ceramic matrix composites. These systems are characterized by a weak interfacial bond between the fiber and the matrix which increases the toughness of the material but the interface is susceptible to oxidation. A lot of work has been done at high temperature, and with cyclic loading, in order to characterize these materials in the environment in which they will most likely be utilized [2, 5, 6, 9, 10, 12]. One of the problems that has been encountered is the embrittlement of the fiber matrix interface at high temperatures [12]. This embrittlement of the fiber matrix interface occurs much more readily at high temperatures and reduces the ultimate strength and the fatigue life of the material [8, 10, 12]. The material investigated in this study, SiC/MAS, is a magnesium aluminosilicate (MAS) glass ceramic

matrix reinforced with silicon carbide (SiC) fibers. The matrix material was doped with 5 percent potassium borosilicate glass (BSG) in an attempt to prevent or reduce the oxidation of the fiber matrix interface.

Larsen et al showed that the fiber matrix interface of the BSG doped SiC/MAS CMC was significantly thinner, 70 percent, than the interface with an undoped matrix. In addition the interface was only 70 atomic percent carbon as opposed to the undoped interface which is typically at or near 100 percent [7]. These two developments lead to an interface which is less susceptible to oxidation and therefore creates a CMC which is more thermally durable. Larsen used stepped stress rupture tests and monotonic tensile tests to show that the ultimate tensile strength of this material with a doped matrix exhibits a load history independence up to 5000 hours at 1093°C [7]. Another result of this study was that the doping of this material has a large impact on the ultimate tensile strength and strain at failure at high temperature, 1093°C, but only a minor influence on these properties at intermediate temperatures, 566°C [7].

Worthem performed a study comparing the thermomechanical characteristics of three model CMC systems from 600 °C to 1100 °C in laboratory air [14]. One of the materials included in the study was MAS-5. By comparing the fatigue life of a unidirectional lay-up to that of a cross-ply lay-up, Worthem determined that fiber failure determined the composite failure, regardless of the phase angle between the thermal and mechanical loading [13]. A comparison of the fatigue lives of SiC/CAS and SiC/MAS unidirectional lay-ups showed that the SiC/MAS system has a considerably improved

thermomechanical fatigue life [13]. This was attributed in large part to the dopant in the matrix which altered the fiber matrix interface.

Allen, Beevers, and Bowen performed a study on another model CMC system, SiC/CAS, in which they explored, among other things, the effect of cyclic loading on the time to failure of specimens at 1000 °C in laboratory air [3]. They determined that cyclic loading at an elevated temperature air environment would cause failure in identical specimens, under a static load equivalent to the maximum load in the fatigue test, in the same amount of time [3]. This led to the conclusion that there is a lower limit to the stress that is required to initiate environmental attack and a time dependent fracture toughness will be exhibited at elevated temperatures in air.

Holmes investigated the load rate dependence of a CMC system by comparing tests conducted at frequencies of 1 Hz and 10 Hz [6]. Although the material used, a woven carbon fiber SiC system, is quite different from the present cross-ply system of interest (SiC/MAS), the load rate dependence trends are still of interest. Holes determined that both the mean crack spacing and the modulus degradation at room temperature were greater for the tests conducted at 1 Hz than for the tests conducted at 10 Hz [6]. This indicated that the rate of damage during the initial stages of the tests conducted at 1 Hz was higher than that of the tests conducted at 10 Hz. He also determined that, after the crack spacing had reached a plateau, there was still some decrease in the modulus [6]. This was attributed to the increase in the amount of fiber matrix debonding along the interface and additional fiber fracture. Another observation made by Holmes was that, at stress levels below the proportional limit and at room temperature, there is a partial

recovery of the modulus [6]. This time dependent partial recovery of the modulus in fatigue tests was attributed to the interaction of the fiber matrix interface with the environment.

Lee performed a study investigating the damage development and the mechanical response of a heat treated Nicalon/CAS composite system [8]. He found that the heat treated specimens exhibited a brittle matrix crack propagation and a fracture surface characterized by uneven fiber pullout. This fiber pullout was attributed to matrix cracks allowing oxygen to diffuse to the fiber matrix interface, causing embrittlement and debonding.

A number of studies have been performed investigating the fatigue behavior of model ceramic matrix composites at high temperature. The study by Holmes [6] indicated that the effect of a high temperature air environment was to cause the oxidation of the carbon in the fiber matrix interface. His observation was that the oxidation of this interface would act to significantly reduce the fatigue life of the Nicalon fiber. Rousseau also performed a study investigating the effect of elevated temperature on the fatigue life of a Nicalon/CAS cross-ply laminate [10]. This study also indicated that the effect of the elevated temperature was to reduce the fatigue life of the material. This was attributed to the matrix cracks allowing the fiber-matrix interface to be exposed to oxygen in the air and become embrittled.

Tuznik performed a study investigating the tension-tension fatigue behavior and the failure mechanisms of a cross-ply ceramic matrix composite, SiC/CAS, at 10 Hz [12]. He noted that at elevated temperatures the debonding of the fiber from the matrix altered

the fatigue behavior of the material. He observed that there was a large amount of debonding of the fibers at high temperature that was not seen at low temperature. The conclusion was that the debonding of the fibers was due to the embrittlement of the interface between the fiber and the matrix.

In a similar study by Agins, the static behavior of a cross-ply ceramic matrix composite, SiC/CAS, system was studied [2]. The effect of elevated temperature upon the fracture behavior was studied. He determined that the dominant failure mechanism at high temperature was fiber debonding due to oxidation of the fiber matrix interface. He observed larger and longer amounts of fiber pullout at this high temperature.

III. Experimental Procedure

This chapter deals with the details of the experiments. A description of the test equipment, composite material, specimen preparation, and the test procedure will be presented. All of the tests were performed in the Aeronautics and Astronautics Laboratory of the Air Force Institute of Technology located at Wright-Patterson Air Force Base.

A. Test Set-Up

There were two test set-ups employed to gather data in this investigation. A description of the set-up used by the author to gather the majority of the data will be given here. A description of the other set-up can be found in the work done by Grant [5]. The set-up consisted of four main components, materials test equipment, a control system, a data acquisition system and a heating and cooling system.

The material test equipment consisted of three components. These components were a hydraulic actuator, hydraulic grips, and an extensometer. The servo-ram actuator was used in concert with an MTS Load Transducer with a 25 kN/5500 lb capability. The grips used were MTS hydraulic wedge grips that had been modified during a previous study [13]. This modification was the addition of internal channels to allow for the cooling of the grips during the high temperature testing. The grip pressure was supplied by an MTS 685.03 3 ksi Hydraulic Grip Supply. A grip pressure of 250 lb was used for all of

the tests. The final part of the test stand was an MTS 632.65B-03 extensometer with quartz rods. The rods were sharpened and the extensometer calibrated to a gauge length of 2.54 cm prior to each of the tests. The extensometer was air cooled with air bled off the facility supply and regulated to 206 kPa.

The control system used was the MTS 458.20 Microconsole. The console had an MTS 458.13 AC controller for the displacement control and a pair of MTS 458.11 DC controllers for the load and strain control. All the tests were conducted under load control and the controllers for the displacement and the strain were used primarily to control test limits. For example, if the extensometer slipped during a test the strain controller limits would be violated and it would shut the test down. In addition, two Barber Coleman 560 temperature controllers were used to control the output of the heat lamps used in the test.

The data acquisition system consisted of a Zenith Data Systems 486 personal computer and Materials and Test Environment (MATE) software. The system collected load data from the transducer and displacement data from the extensometer. For each fatigue cycle in which data were taken, the system took 1000 instantaneous values of different data, load and displacement, and stored it in a separate file. The cycle in which the data was taken was run at 1 Hz.

The heating part of the heating and cooling system was performed by two locally fabricated heat lamps which were placed on each side of the specimen. Each lamp consisted of an aluminum housing and two quartz bulbs. The housing was cooled by both water and air. The air was bled off the facility supply and regulated to 206 kPa. The bulbs in the front lamp were controlled by one of the Miller Barber units and the bulbs in

the back lamp were controlled by the other. This allowed the lamps to work independently.

The cooling part of the system was performed by the Neslab Coolflow refrigerated recirculator. This unit was used to run water to the grips, the actuator, the lamps, and the heat shields. These heat shields were in the form of collars that were placed between the lamps and the hydraulic grips. The water that was fed through the cooling system was kept at 20°C for all of the tests.

The heat shields, the modified grips, and the lamps were all constructed for, and used in, past studies conducted at AFIT [9,12].

B. Calibration

As mentioned previously, the extensometer was calibrated prior to each test. The method of calibration was fairly simple. A digital micrometer was used to establish a baseline gauge length of 2.54 cm. Then an MTS vertical micrometer was used, in conjunction with the MATE calibration module, to step the extensometer rods through 10 increments of displacement, up to 1.5 times the maximum expected displacement. This was a two way calibration so the rods were stepped back down to zero in each calibration. The calibration was checked each time by loading a machined aluminum specimen and confirming that the modulus was accurate to within 5 percent of the expected value. This was done with the MODULUS.EXE program, developed by Sanders [11], which recorded load and displacement data as the load was manually

increased to a level below the elastic limit of the aluminum and then back down to zero. The program performed a linear curve fit to the data to determine the modulus.

The test stand itself was calibrated by laboratory personnel prior to the beginning of this effort but the alignment of the grips was checked. The method used was similar to that employed by Opalski [9]. A square piece of stainless steel was machined and instrumented with strain gauges. Incremental loads were applied to the specimen and the strains were monitored to determine if there was any bending in the specimen. The grips were adjusted until there was less than two percent bending strain in the specimen.

C. Material Details and Specimen Preparation

The material used in this investigation was a ceramic matrix composite manufactured by Corning Glass. The fiber was Nicalon, a predominately silicon amorphous/crystalline fiber produced by the Nippon Carbon Company. The average diameter of the fibers is on the order of 15 microns. The matrix was a barium-stuffed magnesium aluminosilicate (MAS) cordierite matrix. The average grain size in the matrix was less than 1 micron and it was doped with 5 percent borosillicate glass (BSG). The SiC/MAS composite was designed to be thermally durable and resistant to oxidation embrittlement [7].

The fabrication of a ceramic matrix composite generally consists of two major steps. The first is to incorporate the fibers into the matrix, which is still in an unconsolidated state. One of the more common ways this is done is to pass a fiber tow through a slurry tank and wind it on a drum. This is known as slurry infiltration. Once it

is dry the next step is to cut and stack the tows. Finally the ceramic matrix composite is consolidated by hot pressing at temperatures above 1200°C [1].

Test specimens for this investigation were cut from a two plates provided by Corning Glass. Each plate had a $[0/90]_{4S}$ lay-up. The plates were square, 15.3 cm on a side, with a thickness of 0.32 cm. Each individual ply was 0.2 mm thick and was approximately 40 percent fiber by volume.

In the interest of conserving material, the specimens cut from the plates were 5.08 mm wide. The cutting was done with a Buehler Isomet low speed saw. The saw had a 12.7 cm x 0.4 mm Buehler wafering blade and Buehler Isocut fluid was used as a lubricant. The saw was modified with a guide affixed to a swing arm to insure an even and level cut. This was necessary due to the disparity between the width of the plates and the diameter of the blade. A plate was mounted onto the sliding guide and aligned with the blade. A micrometer was then used to adjust the guide to produce the desired thickness of the specimen. A cut was made half way down the length of the plate and then the guide would slide forward, with the plate still attached, and the final cut was made. This provided the typical specimen with dimension of 153 cm x 5.08 mm x 3.175 mm. Table 1 gives the final values of thickness, width and area for each of the specimens after cutting, grinding, and polishing.

The next step in the preparation of the specimen was polishing one edge in order to be able to take replicas for documentation of the damage. A Buehler Ecomet 3 variable speed grinder-polisher was used for this operation. A series of Buehler Metadi waterbase diamond suspensions was employed to produce the necessary finish on the specimen.

Table I Specimen Dimensions

SPECIMEN	WIDTH (CM)	THICKNESS (CM)	AREA (CM^2)
6	0.466	0.318	0.1480
7	0.455	0.318	0.1445
8	0.454	0.318	0.1443
9	0.451	0.318	0.1432
11	0.448	0.318	0.1423
12	0.445	0.318	0.1446
14	0.464	0.316	0.1467
15	0.462	0.316	0.1459
16	0.456	0.316	0.1443
17	0.454	0.316	0.1433
18	0.465	0.316	0.1466
19	0.443	0.315	0.1396
20	0.461	0.316	0.1458
21	0.464	0.317	0.1472
22	0.454	0.318	0.1440
23	0.474	0.318	0.1507
5[1]	0.453	0.318	0.1439
6[1]	0.445	0.318	0.1413
13[1]	0.413	0.318	0.1310
15[1]	0.469	0.318	0.1490

[1]These were cut from the different plate that was also used by Grant [5]

After the oil from the cutting operation was removed, a 45 micron suspension was used for the initial grinding step. A perforated TEXMET polishing cloth with a chemically (MEK) activated adhesive was applied to a 20.3 cm polishing wheel. The cloth was impregnated with the 45 micron suspension and the specimen was polished for 20 minutes at 300 rpm. This leveled the surface that was being polished and gave it a smooth but somewhat grainy appearance. After the 45 micron suspension was used, a 15 micron suspension was used on the same type of polishing cloth. The specimen was polished for 20 minutes at 300 rpm. A visual inspection with an optical microscope at 30X was made, and if the surface had a good polished appearance with some scratches the next step was to move on to a 9 micron suspension. All the remaining suspensions were applied to a

non-perforated TEXMET polishing cloth. The 9 micron suspension was used for 10 minutes and then subsequent sessions of ten minutes with 6, 3, and 1 micron suspensions occurred. A visual inspection with an optical microscope at 30X was made between each of the steps. At the completion of this process the transverse fibers were clearly visible and the matrix appeared as smooth unblemished surface at 30X. A Buehler Metadi fluid extender for diamond abrasive was employed with all of the suspensions and a new TEXMET cloth was used for each of the suspensions.

The final step in the test preparation procedure was to affix tabs to the ends of each of the specimens. The tabs were used to protect the composite material from damage as the specimen was gripped. The tabs were cut from a sheet of Aluminum 2020-0 that was 1.6 mm thick. The dimensions of the tabs were 20 mm x 6 mm x 1.6 mm. The ends of the tabs were beveled with a bench grinder to try to minimize any stress concentrations that might occur in the specimen at the end of the tab. Four tabs were attached to each specimen with a two part epoxy resin. The tabs were clamped to the specimen with two inch binder clips after the epoxy was applied, then the specimen, tabs, and clips were put into an oven at 150°C and cured for 2 hours. The environment in the oven was air. A diagram of the prepared specimen can be seen in Appendix A.

D. Experimental Procedure

After the specimen preparation, the test was set up and conducted. The test set up consisted of mounting the specimen, attaching the thermocouples, attaching the extensometer, heating the specimen, and starting the test.

The first step was to install the cooling collars onto the hydraulic grips. Once this was accomplished the hydraulics were activated from the MTS microconsole. A warm up run of 10 minutes was accomplished before each of the tests. The warm up run consisted of cycling the MTS integral actuator for 10 minutes at a frequency of 1 Hz and a total stroke of 5 cm. This operation was obviously performed under displacement control. After the warm up run was completed, the actuator was adjusted so that the distance between the heads was long enough that the specimen tabs extended past the end of the grips by about 1 cm.

With the distance between the heads properly adjusted for the length of the specimen, the top grip was closed and the specimen gripped. The alignment of the specimen was checked with a machined aluminum alignment tool and a bubble level. If the specimen was not level it was ungripped, adjusted, and regripped until it was aligned with the actuator. The MTS microconsole was then switched from displacement control to load control and the lower grip was closed. A 1 kip load card was used in the load control module for all the tests. The set point of the load control module was adjusted so that there was no load on the specimen.

When the specimen was mounted and secured, three thermocouples were attached. Prior to the mounting of the specimen, points 1.27 cm to either side of the middle of the specimen were marked with small amounts of the thermocouple adhesive. These marks indicated the bounds of the 2.54 cm gauge length at the center of the specimen and indicated the location for thermocouple attachment. A thermocouple was attached to the front of the specimen at the top edge of the gauge length, one was attached to the back of

the specimen at the bottom of the gauge length, and one thermocouple was placed on the front of the specimen in the center of the gauge length. The two thermocouples at the top and bottom of the gauge length provided data to the lamp controllers and were used to control the temperature of the specimen. The purpose of offsetting the control thermocouples at the top and bottom, and front and back, of the specimen was to try and achieve a uniform temperature throughout the gauge length. The third thermocouple was used to monitor the temperature at the center of the gauge length and was not in any sort of feed back loop with a controller. This procedure has been used in a previous study by Tuznik [13]. The thermocouples used were K type thermocouples and were attached in the following manner. The thermocouple wire was adjusted in such a way that the thermocouple bead was firmly against the specimen in the desired location. A 36 gauge strand of alumel wire was then used secure the thermocouple wire to the specimen. The alumel wire was wrapped around the thermocouple wire where the insulation was still attached. This was to try to prevent a short across the thermocouple junction. When all three thermocouples had been attached in this manner 903 Green Ceramic Adhesive was applied to the thermocouples. The adhesive was applied until it covered the thermocouple junctions and any exposed thermocouple wire.

The next step was to position the quartz rods of the extensometer against the specimen. The extensometer was positioned so that there was only a moderate amount of pressure holding the rods against the specimen. If there was too much pressure there was the possibility of inducing small bending stresses into the specimen and if there was too little the rods would slip when the 10 Hz waveform was applied.

After the extensometer was positioned and zeroed the heat lamps were moved into position. The lamp housings were capable of holding four bulbs each but for these tests two bulbs in each lamp were sufficient. The front lamp was positioned so that the bulbs were aligned with the control thermocouple attached to the front of the specimen. The back lamp was positioned so that the bulbs were aligned with the control thermocouple attached to the back of the specimen. Both lamps were positioned 2.54 cm from the specimen and centered horizontally on the specimen.

The last step in preparing the specimen for testing was to cure the thermocouple adhesive. Before this could be done the cooling system was activated and checked to insure that both the air and the water were circulating as expected. This done, the MATE software was programmed to heat the lamps to 120°C for a period of two hours. The temperature was ramped up over a period of 3 minutes. This also served as a good opportunity to check the alignment of the lamps and the thermocouples by observing the output of the two lamps and insure that one was not working harder than the other. If the output of the two lamps was within two percent they were considered to be working at the same level. Another check was the output of the center thermocouple, which should read the same temperature as the two control thermocouples.

There were three different types of tests run. One monotonic tensile test and a series of fatigue tests were run at each of the two temperatures investigated. The fatigue tests were run at either 1 Hz or 10 Hz. The temperature ramp performed before each test was the same for all of the tests. The MATE software was programmed to heat the lamps to the desired temperatures in a period of 10 minutes. The specimen was then allowed to

soak at the target temperature for 10 additional minutes to insure that the lamps were stabilized and that the entire cross section of the gauge length had reached the target temperature.

The monotonic tensile tests were performed with the MATE MSNTEST software developed by George Hartman of the University of Dayton Research Institute. The load was increased at a rate of 4 MPa per second until failure. Instantaneous values of load and displacement were recorded for every 1 MPa increase in load. These data pairs were stored in a data file as they were recorded.

The fatigue tests were run a slightly differently. The first cycle of every test was run manually, to insure that data for the first cycle was recorded. This was accomplished by the using the BETASTAT.EXE program. This program recorded the load and displacement at user specified intervals as the load was manually increased, using the set point of the load control module, to achieve the desired maximum stress. After this first cycle was recorded, the MATE MSNTEST, MATE stress/life program was used to run the fatigue loading. All the tests were run with a triangular load input wave and an R value (σ_{min} / σ_{max}) of 0.1. The program calculated a maximum and minimum load based on the requested maximum stress and the area of the specimen which were input by the user. This program also recorded data in the form of load and strain numbers at the rate of 1000 per second with a data acquisition cycle automatically running at 1 Hz. This resulted in data in the form of 1000 pairs of load and strain data that ran from the minimum stress up to the maximum stress and back down to the minimum again. The data was collected every tenth cycle for the first 100 cycles and every 100 cycles up to 1000

cycles. After 1000 cycles the data was collected on a logarithmic basis at 10000, 1000000... etc.

Fatigue tests were run at temperature of 566°C and 1093°C. Frequencies of 1 Hz and 10 Hz were used at both of these temperatures. The monotonic tensile tests were also run at a 566°C and 1093°C.

IV. Results and Discussion

The objective of this study was to investigate the fatigue behavior and damage mechanisms of a Nicalon/MAS cross-ply ceramic matrix composite, and how they varied with frequency and temperature. For this purpose, experiments were performed at two elevated temperatures, 566°C and 1093°C, using triangular loading waveforms with two different frequencies, 1Hz and 10 Hz.

Damage mechanisms were evaluated using post-mortem microscopic evaluation of the failed specimens. Optical microscopes were used but the main tool for this effort was a scanning electron microscope (SEM). Another means used to evaluate the damage mechanisms was the indirect method of using the degradation of modulus of elasticity during cycling. The modulus of elasticity was calculated by dividing the difference between maximum stress and the minimum stress by the difference between the maximum and minimum strain at each cycle. This was done because the stress-strain curves after the first ten cycles were nearly linear for these tests. The stress-strain curves for selected cycles of these tests can be found in Appendix C. Both the modulus and the normalized modulus were plotted against the number of cycles. The normalized modulus was calculated by dividing the instantaneous modulus at each cycle by the modulus at the first cycle.

This chapter is divided into six sections dealing with the different methods used to evaluate the fatigue behavior and the damage mechanisms. Section A is a discussion of

the results of the monotonic tensile tests. Section B is a discussion of the fatigue life curves. The fatigue life is evaluated in terms of both cycles and time. Section C is a discussion of the modulus degradation during cycling. Section D covers the comparisons of the maximum, minimum, and strain difference trends during cycling. Section E is an evaluation of the trends in the loop hysteretic energy and Section F is the results of the fractographic analysis.

Table II gives a synopsis of all the tests that were conducted in this investigation. The tests are grouped by the test temperature and the frequency of the cyclic loading. Some of the tests were conducted on a horizontal test machine [5]. These tests were also conducted with material cut from a different plate and are indicated by the superscript 1 on the specimen number. Both plates used in this study exhibited the same properties in the form of initial moduli, ultimate strength, and strain at failure at the two different test temperatures. A comparison of these properties can be seen in Table III.

Not all of the tests were run to failure and those specimens that did not break after the indicated number of cycles are denoted by the superscript 2 on the number of cycles in Table I. All tests were run with an R value of 0.1 and a triangular waveform.

A. Monotonic Test Results

Monotonic tensile tests were conducted with this material at the two different temperatures used in this study, 566°C and 1093°C. These tests were conducted at a constant rate of 4 MPa per second until the specimen failed. The measured stress-strain response for each of the two temperatures can be seen in Figures 1 and 2. These figures

Table II Test Matrix

SPECIMEN NUMBER	TYPE OF TEST	LOADING FREQUENCY (Hz)	TEMP (°C)	MAX STRESS (MPa)	FATIGUE LIFE
19	**STATIC**			**292.41**	
6	**FATIGUE**	**10**	**566**	**137.90**	**10,256**
9	**FATIGUE**	**10**	**566**	**120.66**	**109,713**
7	**FATIGUE**	**10**	**566**	**103.43**	**518,724**
11	**FATIGUE**	**10**	**566**	**98.25**	**3,803,158**[2]
8	**FATIGUE**	**10**	**566**	**86.19**	**5,080,401**[2]
18	**STATIC**			**209.26**	
12	**FATIGUE**	**10**	**1093**	**137.90**	**351**
14	**FATIGUE**	**10**	**1093**	**103.43**	**48,166**
15	**FATIGUE**	**10**	**1093**	**96.53**	**193,600**
17	**FATIGUE**	**10**	**1093**	**94.81**	**947,562**
16	**FATIGUE**	**10**	**1093**	**86.19**	**3,177,985**[2]
5[1]	**FATIGUE**	**1**	**566**	**137.90**	**472**
20	**FATIGUE**	**1**	**566**	**120.66**	**8,906**
6[1]	**FATIGUE**	**1**	**566**	**103.43**	**10,251**
22	**FATIGUE**	**1**	**566**	**99.98**	**390,555**[2]
15[1]	**FATIGUE**	**1**	**1093**	**137.90**	**25**
21	**FATIGUE**	**1**	**1093**	**120.66**	**88**
13[1]	**FATIGUE**	**1**	**1093**	**103.43**	**20,444**
23	**FATIGUE**	**1**	**1093**	**96.53**	**33,968**
24	**FATIGUE**	**1**	**1093**	**86.19**	**503,826**[2]

[1] Specimen was from a different plate and test was run on the horizontal test stand [5].

[2] Specimen was unbroken after the indicated number of cycles.

show that the material had a similar response at both temperatures. In both cases there was an initially linear response, a knee, another linear portion, and then a nonlinear region up to failure.

A.1. Monotonic Test 566°C. Figure 1 shows the stress strain response of the monotonic tensile test at 566°C. This figure shows that the material exhibits a knee at 50 MPa at this temperature. This knee is indicative of the proportional limit of the material where permanent damage of the 90° plies occurs. The material then displays a linear response up to a stress of 280 MPa, at which point the stress-strain response is nonlinear up to failure. The ultimate strength of the material at 566°C is 292.41 MPa and the

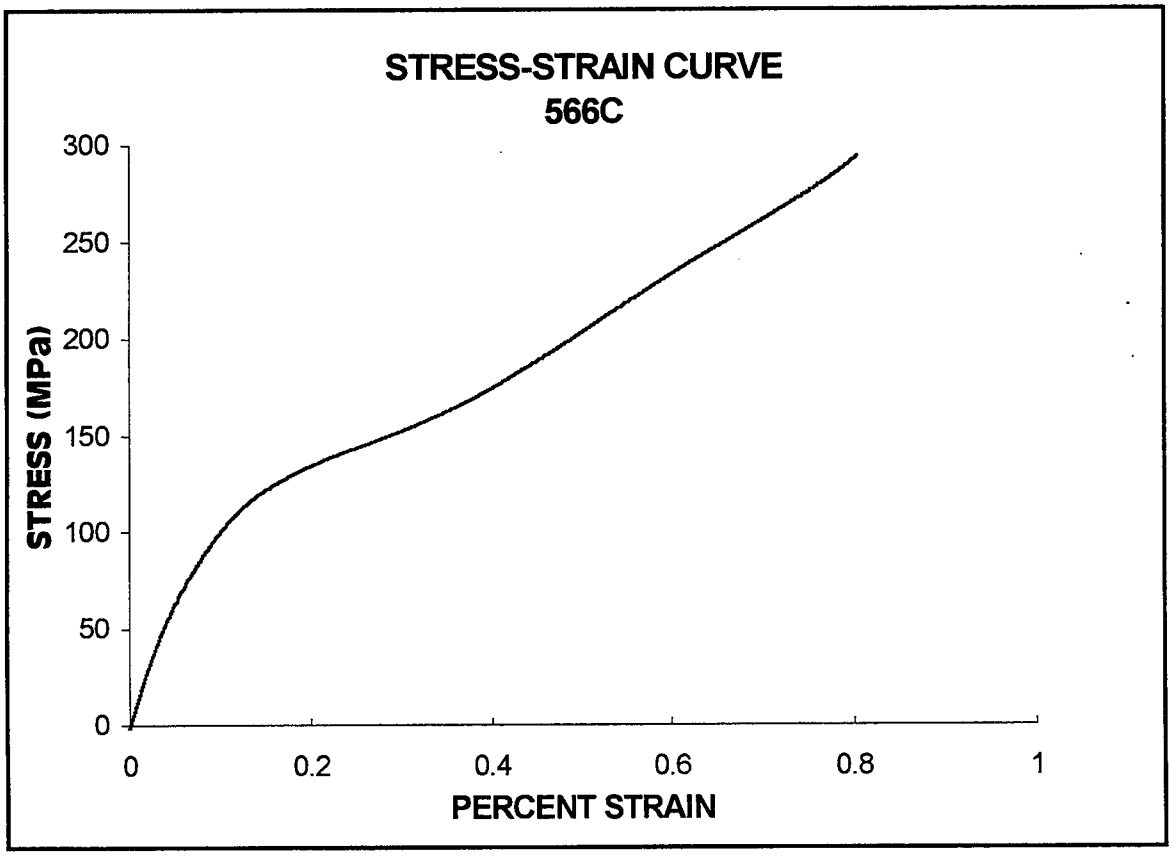

Figure 1. Stress Strain Curve for 566°C

ultimate strain is 0.8 percent. The slope of the initial linear region was 117.99 GPa which is the initial modulus of elasticity of the material at 566°C. These values compare well with the values reported by Larsen which were 270 MPa for ultimate strength, 0.7 percent strain at failure, and an initial modulus of 124 GPa [7]. A comparison between the tensile stress-strain responses at this temperature, from this study and from the work done by Larson, can be found in the Appendix.

A.2. Monotonic Test 1093°C. Figure 2 shows the stress strain response of the monotonic tensile test at 1093°C. This figure shows that the material exhibits a knee at 30 MPa at this temperature. This is similar to previous work done by Larsen which shows a knee at 34 MPa.[7] The material then displays a linear response up to a stress of 195 MPa, at which time the stress-strain response is nonlinear up to failure. The ultimate

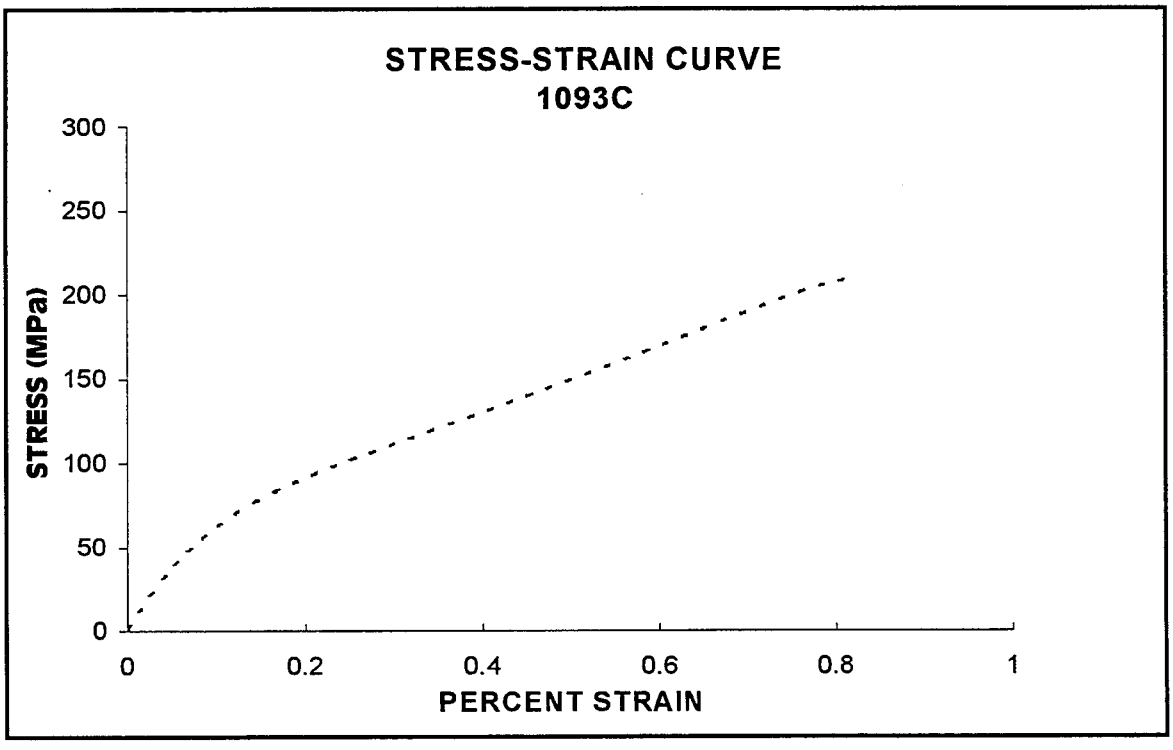

Figure 2. Stress Strain Curve for 1093°C

strength of the material at 1093°C is 209.26 MPa and the strain at failure is 0.82 percent. The slope of the initial linear region was 96.19 GPa which is the initial modulus of elasticity of the material at 1093°C . These values compare well with the values reported by Larsen which were 230 MPa for the ultimate strength, 0.73 percent strain at failure, and 96.5 GPa for the initial modulus[7]. A comparison between the tensile stress-strain responses at this temperature, from this study and from the work done by Larson, can be found in Appendix B.

A.3. Monotonic Test Comparison 566°C vs 1093 °C. Figure 3 shows a comparison of the stress-strain curves at two temperatures, 566°C and 1093°C. It can be seen from this figure that the two curves are similar in shape. The material stress-strain response remains linear up to a higher stress level at 566°C than it does at 1093°C. The

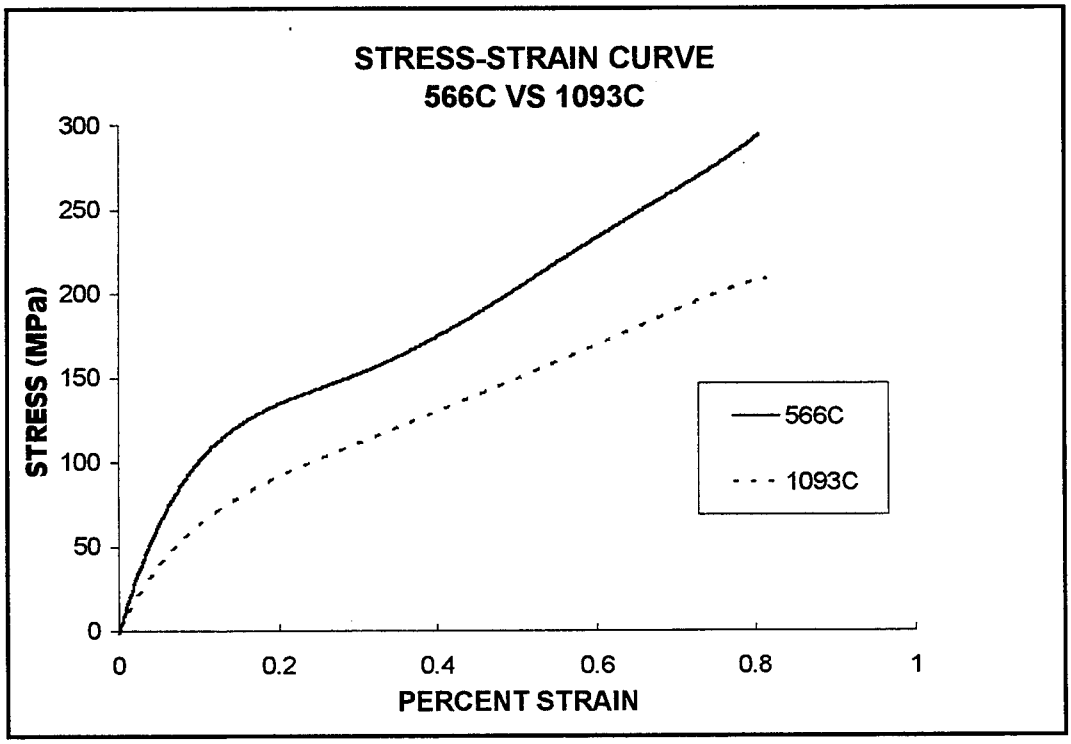

Figure 3. Stress Strain Curve Comparison 566°C vs 1093°C

ultimate strength is higher and the strain at failure is lower for the test conducted at 566°C than for the test conducted at 1093°C. This is consistent with the results obtained by Larsen which showed that the strain at failure was slightly higher at 1093°C than it was at 566°C.

Table III provides a comparison of the material properties at the two different temperatures at which tests were conducted, the properties that were determined by Larsen, and the material properties of the other plate, but from the same batch of material, which was used by Grant [5]. It can be seen that the initial modulus of elasticity and the ultimate strength are reduced as the temperature increases, while the strain at failure increases. However, there is only a small increase in the strain at failure for 1093°C in

Table III Material Properties

MATERIAL PROPERTY	TEMP	PRESENT STUDY	GRANT [5]	LARSEN [7]
ULTIMATE STRENGTH	566°C	292.41 MPa	282.70 MPa	270 MPa
	1093°C	209.26 MPa		230 MPa
STRAIN AT FAILURE	566°C	0.80 %	0.77 %	0.70 %
	1093°C	0.82 %		0.73 %
INITIAL MODULUS	566°C	117.99 GPa	123.4 GPa	124.1 GPa
	1093°C	96.19 GPa		96.53 GPa

comparison to 566°C. This is expected since materials generally exhibit longer strain at elevated temperature either due to decreased stiffness or more creep. These trends are consistent for the tests conducted by Grant [5], Larsen [7] and the author. The values of ultimate stress, strain at failure, and modulus are also consistent between all three studies.

B. Fatigue Life

The fatigue life curves were developed using data from both the monotonic tensile tests and the tension-tension fatigue tests. As can be seen in Table I five tension-tension fatigue tests were conducted at 566°C with an R value of 0.1 and a frequency of 10 Hz. These tests had maximum stress values of 137.9 MPa, 120.66 MPa, 103.43 MPa, 98.25 MPa, and 86.19 MPa. The two tests conducted at 98.25 MPa, and 86.19 MPa were terminated before the specimen failed because it was considered that these tests had reached cycle runout. There were also four tension-tension fatigue tests conducted at 566°C with an R value of 0.1 and a frequency of 1 Hz. These tests had maximum stress values of 137.9 MPa, 120.66 MPa, 103.43 MPa, and 99.98 MPa. The test conducted at 99.98 MPa was terminated before the specimen failed because it was again considered that this test had reached cycle runout.

There were five tension-tension fatigue tests which were conducted at 1093°C with an R value of 0.1 and a frequency of 10 Hz. These tests had maximum stress values of 137.9 MPa, 103.43 MPa, 96.53 MPa, 94.81 MPa, and 86.19 MPa. The test conducted at 86.19 MPa was terminated before the specimen failed because it was considered that this test had reached cycle runout. There were also four tension-tension fatigue tests conducted at 1093°C with an R value of 0.1 and a frequency of 1 Hz. These tests had maximum stress values of 137.9 MPa, 120.66 MPa, 103.43 MPa, and 96.53 MPa

B.1. Fatigue Tests 10 Hz. Figure 4 uses the monotonic tensile and fatigue test data to show fatigue- life curves for the SiC/MAS material at 566°C/1050°F and 1093°C/2000°F for the cycling frequency of 10 Hz. These curves show that the ultimate

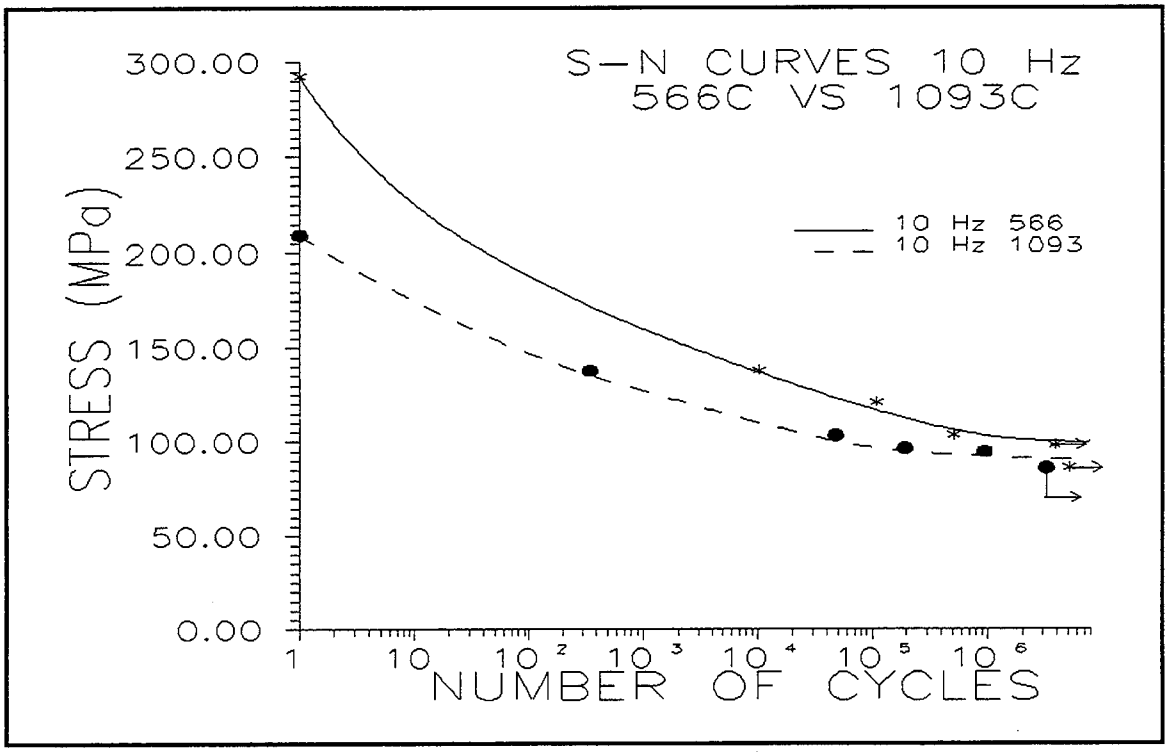

Figure 4. Fatigue Life Curves 10 Hz 566°C vs 1093°C

strength, as well as the ability of this material to withstand tension-tension fatigue, is reduced as the temperature increases. Figure 5 is a magnified view of a portion of Figure 4 and gives a much clearer picture of the dependence of the fatigue life upon the temperature at 10 Hz. Figure 6 shows the normalized fatigue life curves for the 10 Hz waveform at 566°C/1050°F and 1093°C/2000°F. These curves were normalized with respect to their ultimate strengths obtained from the monotonic tensile tests at their respective temperatures. These curves show that for a given percentage of ultimate strength, the SiC/MAS material performs better at the higher temperature of 1093°C/2000°F than it does at the lower temperature of 566°C/1050°F.

These curves compare favorably with a similar material, SiC/CAS, which was investigated by Tuznik [12]. Figure 7 compares the fatigue-life curves of the SiC/MAS

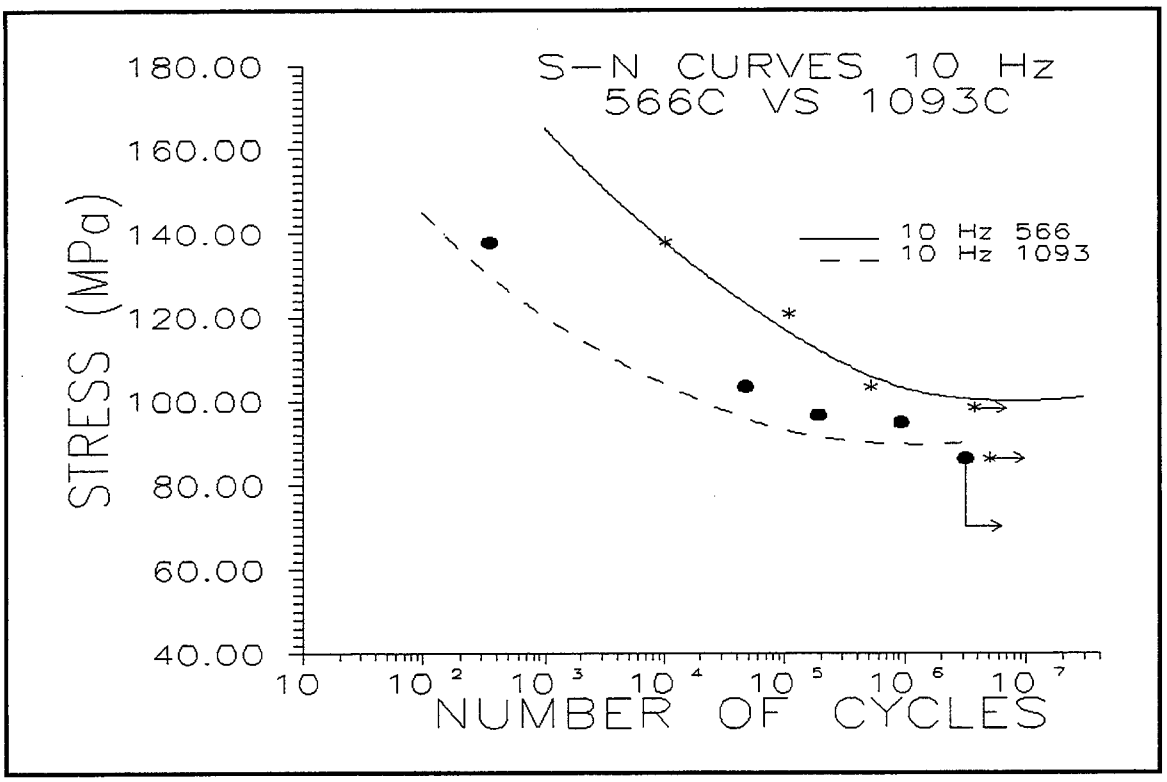

Figure 5. Fatigue Life Curves 10 Hz 566°C vs 1093°C Magnified

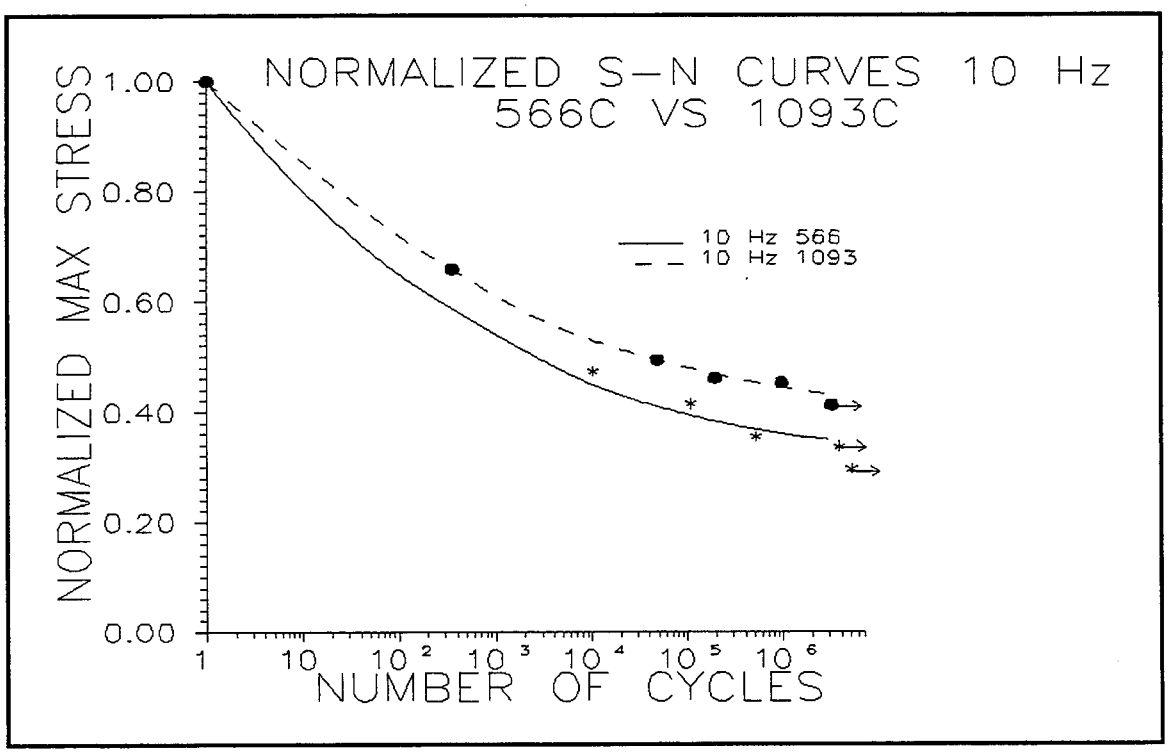

Figure 6. Normalized Fatigue Life Curves 10 Hz 566°C vs 1093°C

material against the SiC/CAS material at a frequency of 10 Hz for the low temperature tests. Figure 8 compares the fatigue-life curves for the high temperature tests. The only difference between the fatigue-life curves of the two materials is that the SiC/MAS exhibits an improved fatigue life and ultimate tensile strength at both temperatures in comparison with SiC/CAS. Because the temperatures used in these two studies are not the same, a more legitimate comparison is to look at the normalized fatigue life curves for the two studies. Figure 9 is a comparison of the normalized fatigue life curves for the tests conducted at 10 Hz in these two studies. This chart shows that, when evaluated on the basis of a percentage of ultimate strength, there is very little difference in the fatigue life of these two systems.

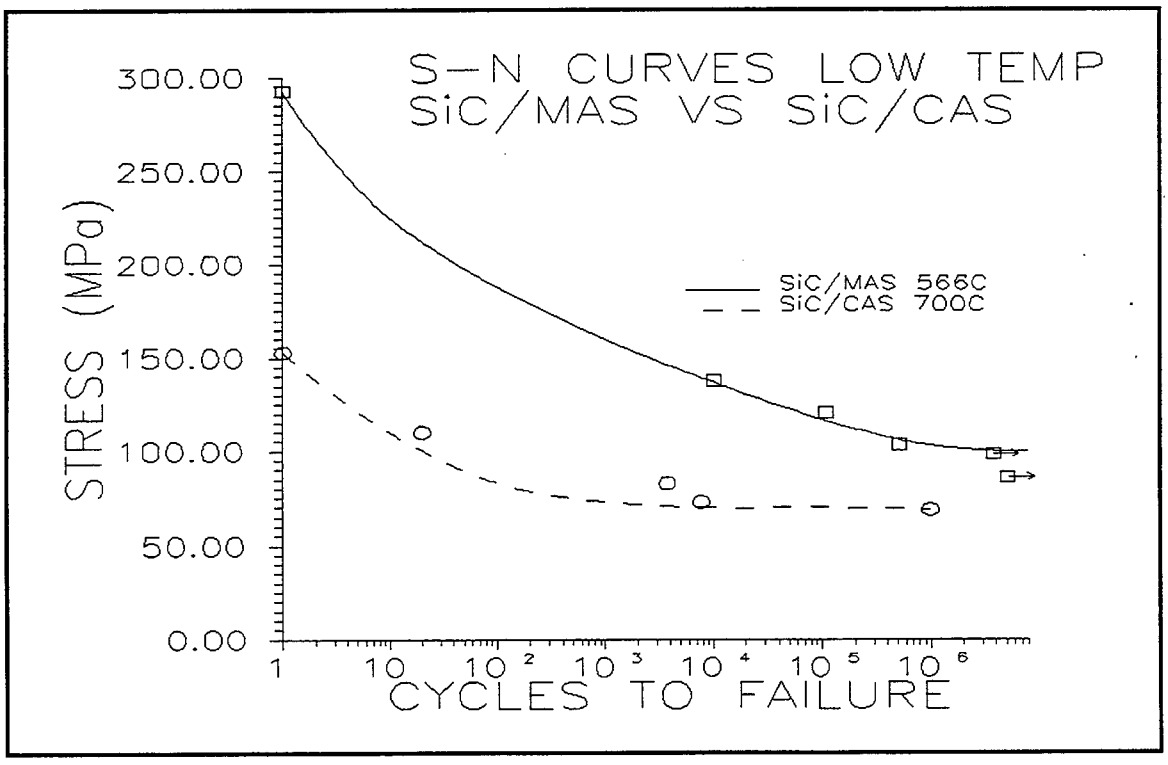

Figure 7. Fatigue Life Curves SiC/MAS vs SiC/CAS Low Temperature

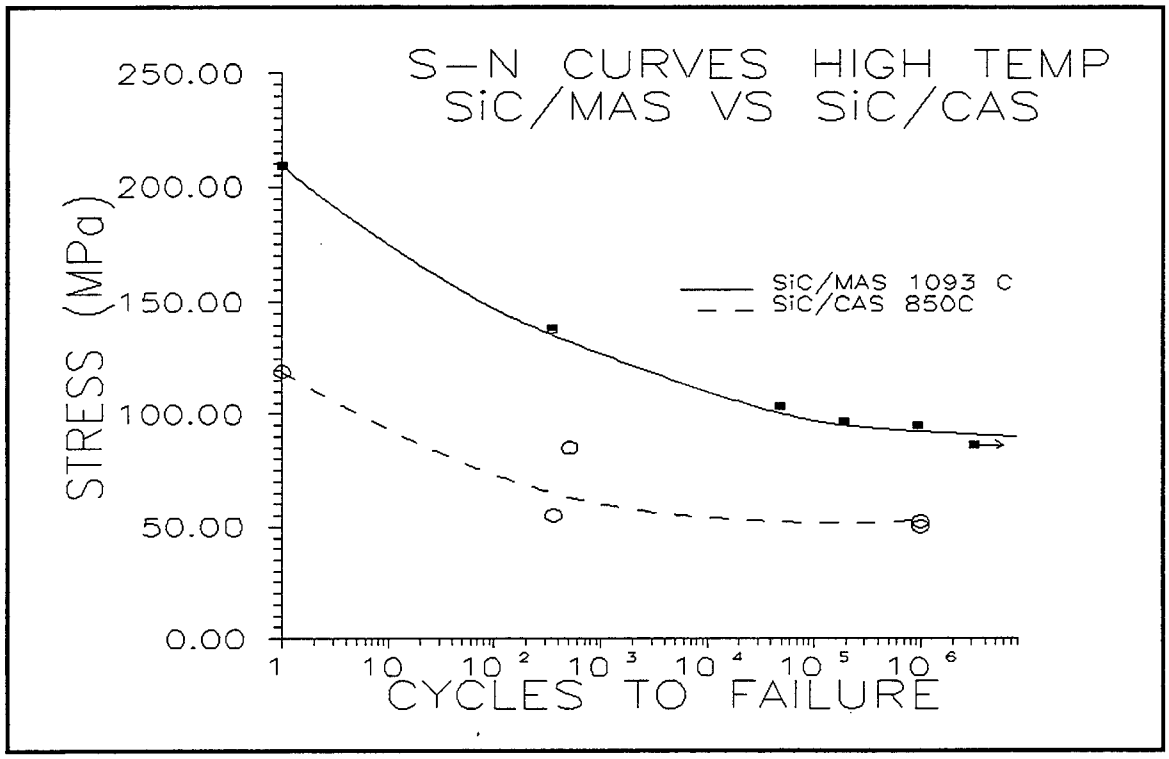

Figure 8. Fatigue Life Curves SiC/MAS vs SiC/CAS High Temperature

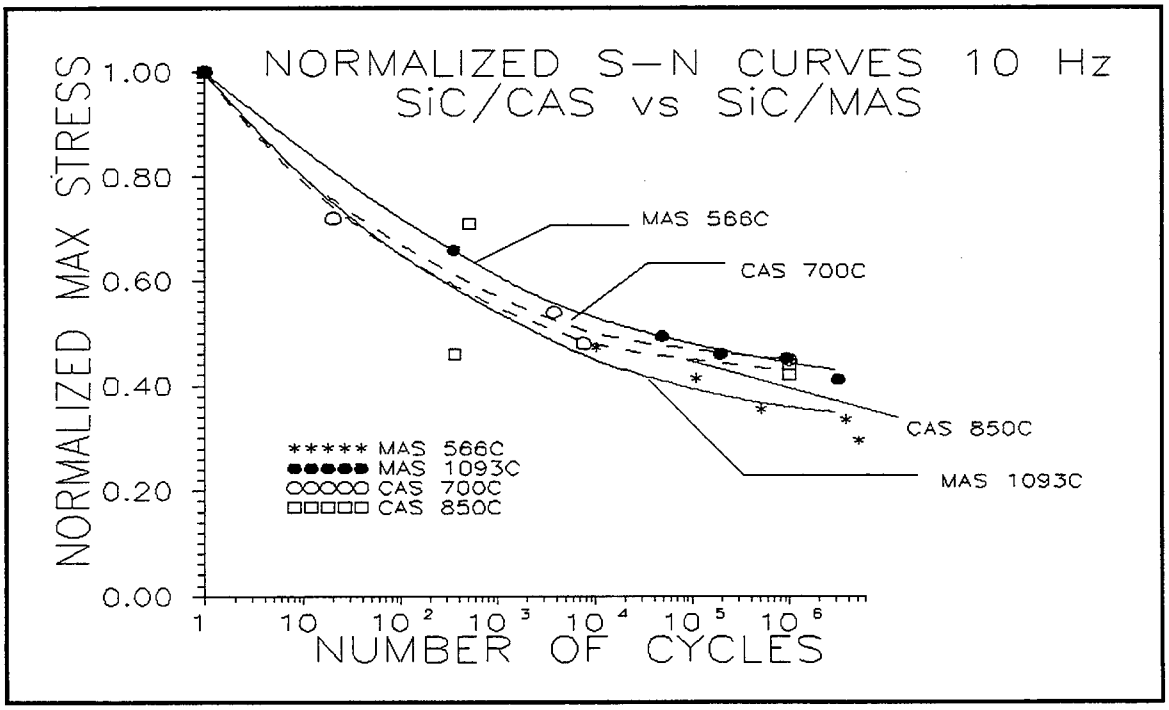

Figure 9. Normalized Fatigue Life Curves SiC/MAS vs SiC/CAS

B.2. Fatigue Tests 1 Hz. Figure 10 uses the tensile and fatigue test data to show fatigue life curves for the SiC/MAS material at 566°C/1050°F and 1093°C/2000°F when the cyclic loading was conducted at 1 Hz. These curves show that the ultimate strength, as well as the ability of this material to withstand tensile fatigue, is reduced as the temperature increases at this frequency, as in the case of the 10 Hz loading. Figure 11 is a magnified view of a portion of Figure 10 and gives a much clearer picture of the dependence of the fatigue life upon the temperature at 1 Hz. Figure 12 shows the normalized fatigue life curves for the 1 Hz waveform at 566°C/1050°F and 1093°C/2000°F. These curves were normalized with respect to the ultimate strengths recorded in the monotonic tensile tests. The curves show that for a given percentage of

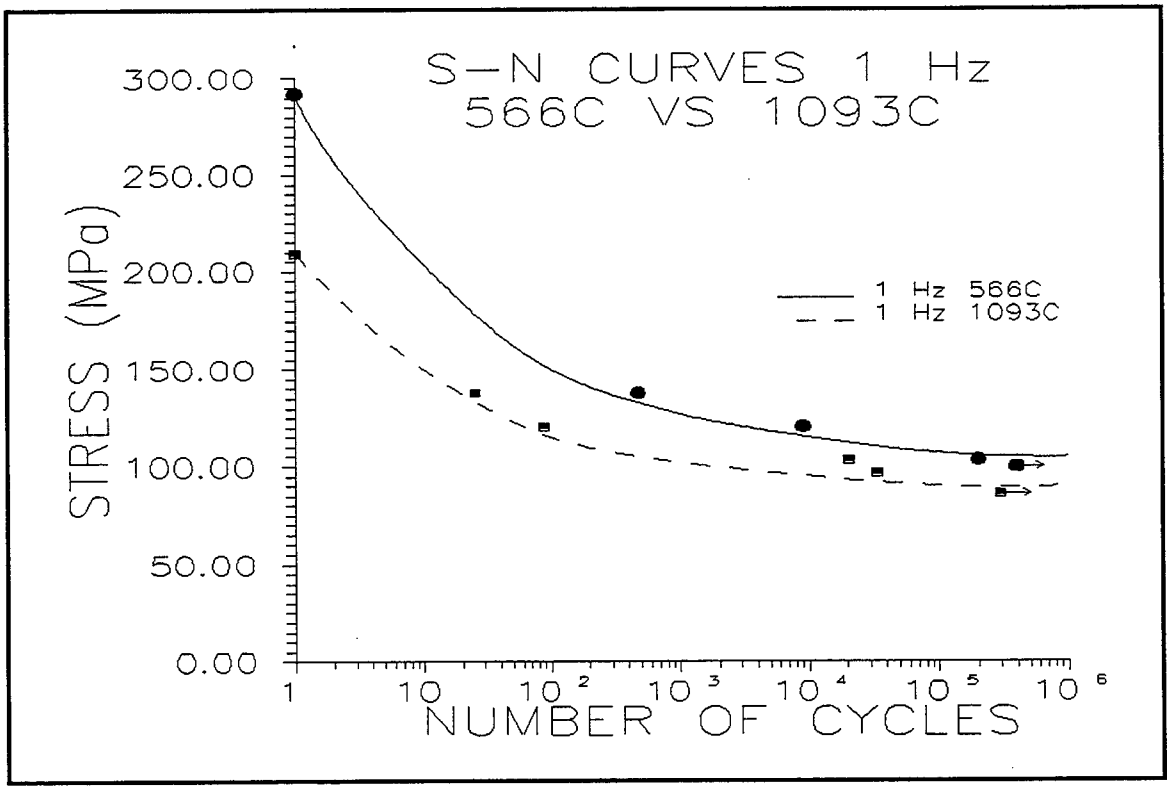

Figure 10. Fatigue Life Curves 1 Hz 566°C vs 1093°C

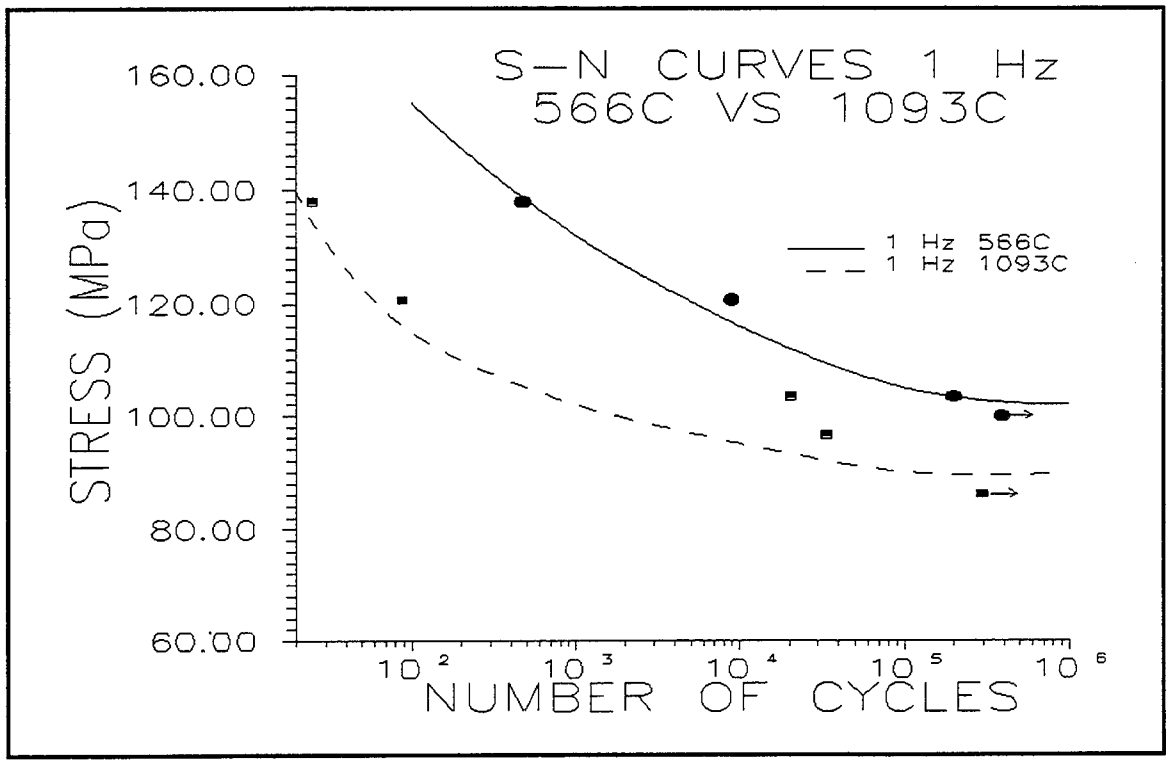

Figure 11. Fatigue Life Curves 1 Hz 566°C vs 1093°C Magnified

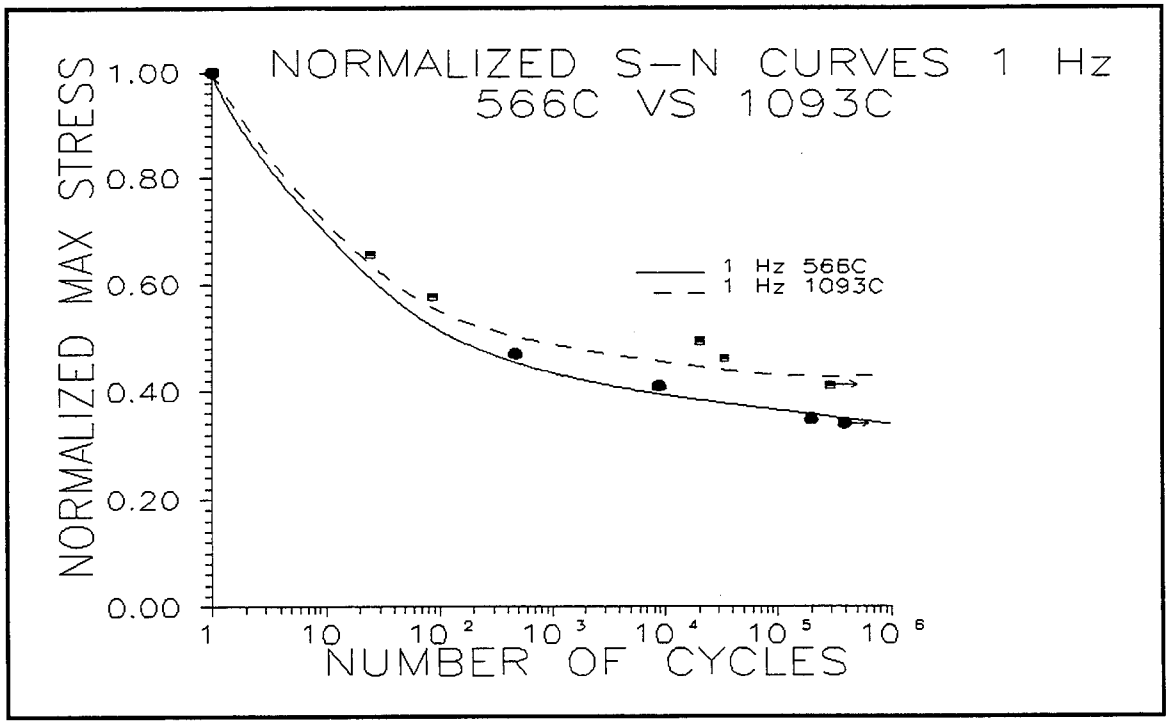

Figure 12. Normalized Fatigue Life Curves 1 Hz 566°C vs 1093°C

ultimate strength, the SiC/MAS material performs better at the higher temperature of 1093°C/2000°F than it does at the lower temperature of 566°C/1050°F. This is the same observation as was made in the case of the higher frequency, 10 Hz.

B.3. Fatigue Tests 566°C. Figure 13 shows the comparison of the fatigue life curves for the SiC/MAS material at 566°C/1050°F for the 10 Hz and 1 Hz cyclic frequencies. This figure shows that the material has a greater fatigue life expectancy, in terms of cycles, with the 10 Hz frequency than with the 1 Hz frequency. Both fatigue life curves show basically the same shape.

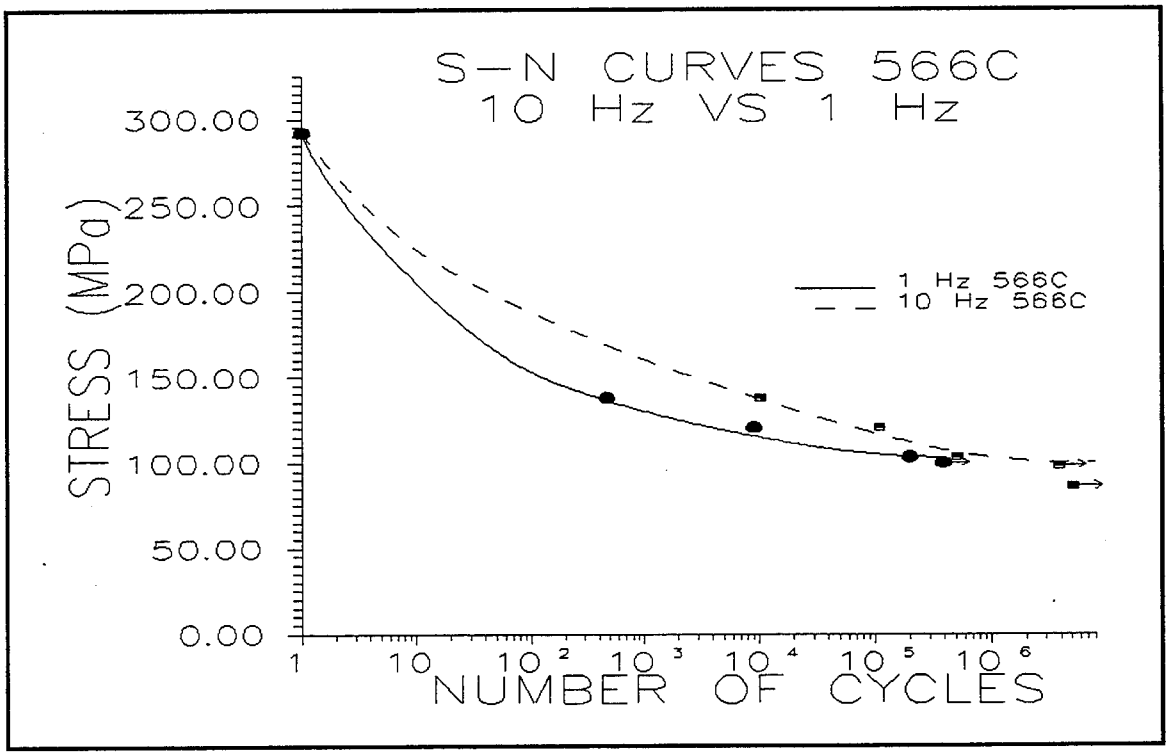

Figure 13. Fatigue Life Curves 566°C 1 Hz vs 10 Hz

For the same two frequencies, at the same temperature, if the maximum stress in the fatigue test is plotted against the length of time from the start of the cyclic loading

until failure, it can be seen that the curves collapse upon one another. This can be seen in Figure 14. This indicates that, at this temperature, the frequency is not as important a factor as the length of exposure at a given maximum stress level in determining the life of the specimen.

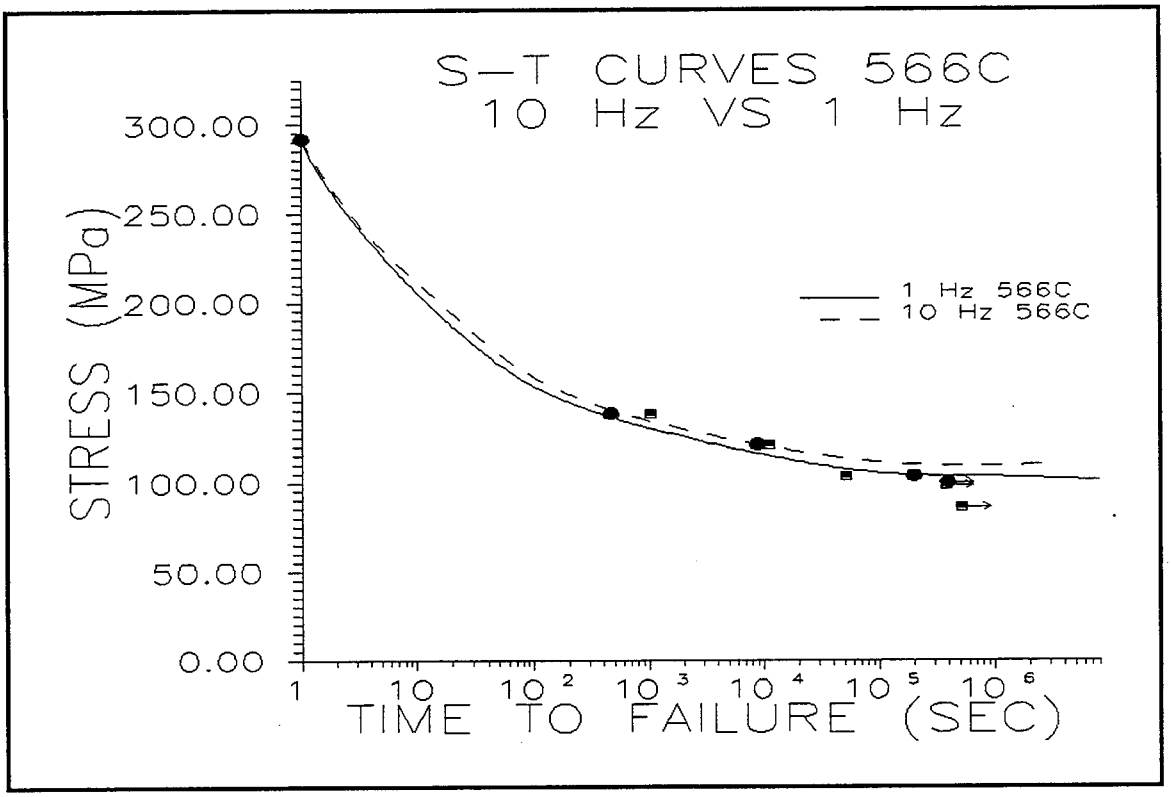

Figure 14. Fatigue Life Curves 566°C 1 Hz vs 10 Hz

B.4. Fatigue Tests 1093°C. Figure 15 shows a comparison between the fatigue life curves for the SiC/MAS material at 1093°C/2000°F for both a 10 Hz frequency and a 1 Hz frequency. This figure shows that the material has a greater fatigue life expectancy, in terms of cycles, with the 10 Hz frequency than with the 1 Hz frequency at this temperature. Both fatigue life curves have basically the same shape. This is the same

relationship that was observed at the lower temperature. The similarity in shape can be attributed to the similarity of the failure mechanisms at the two frequencies.

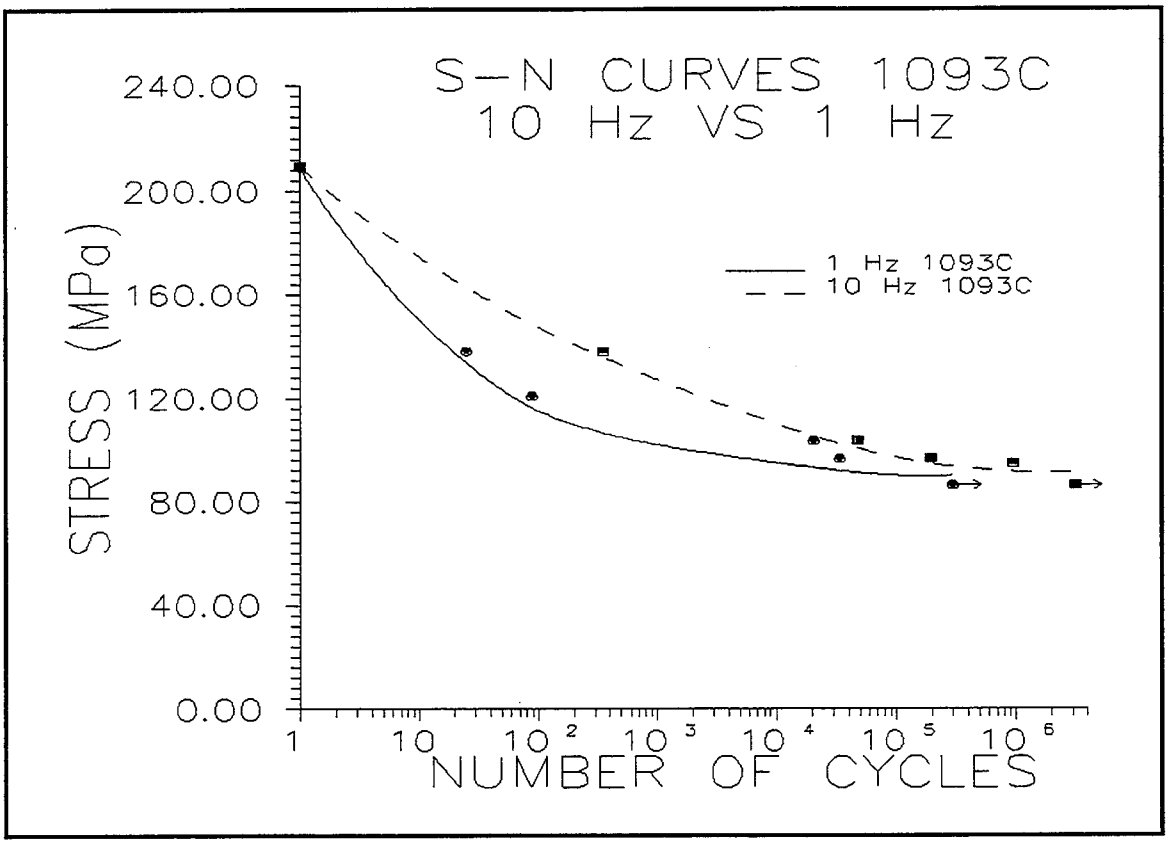

Figure 15. Fatigue Life Curves 1093°C 1 Hz vs 10 Hz

For the same two frequencies and the same temperature, if the maximum stress in the fatigue test is plotted versus the length of time from the start of cyclic loading until failure it can be seen that the curves collapse upon one another. This can be seen in Figure 16. This indicates that, at this temperature too, the frequency of the cycling is not as important a factor as the length of exposure or the maximum stress level in determining the life of the specimen. To complete this comparison it is helpful to look at another plot of the fatigue life in terms of time. Figure 17 is a plot of the two curves derived from all

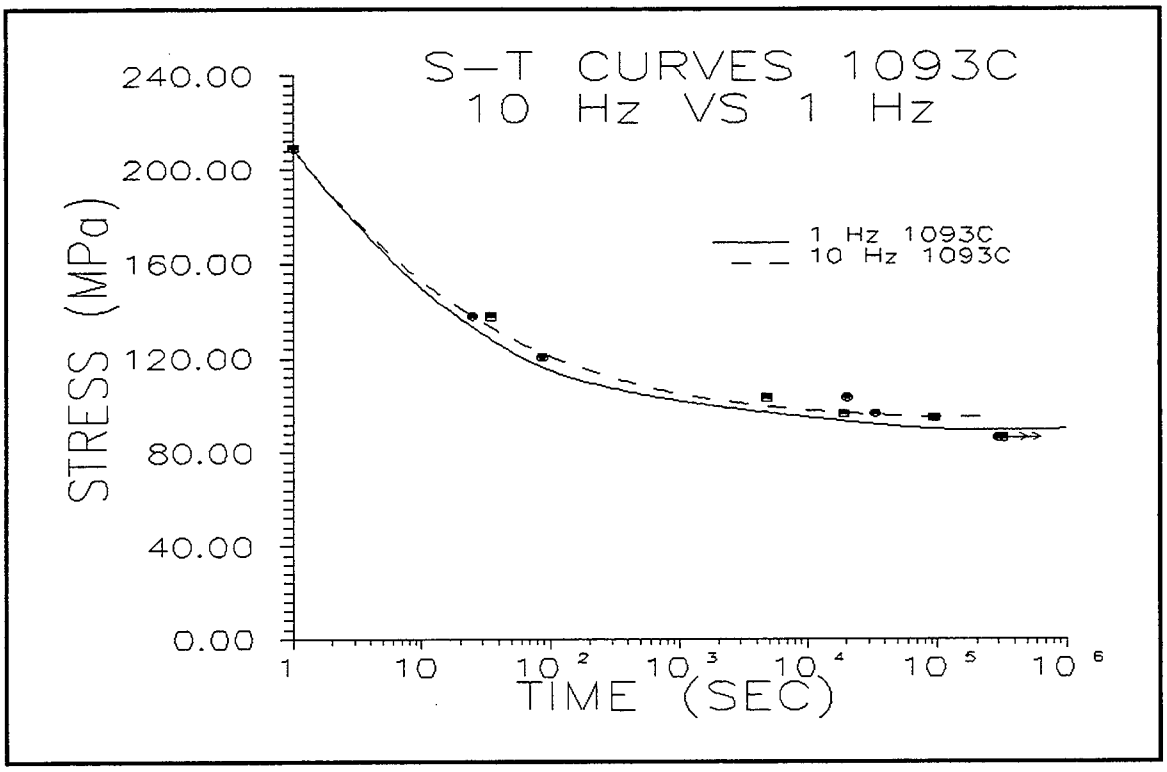

Figure 16. Fatigue Life Curves 1093°C 1 Hz vs 10 Hz

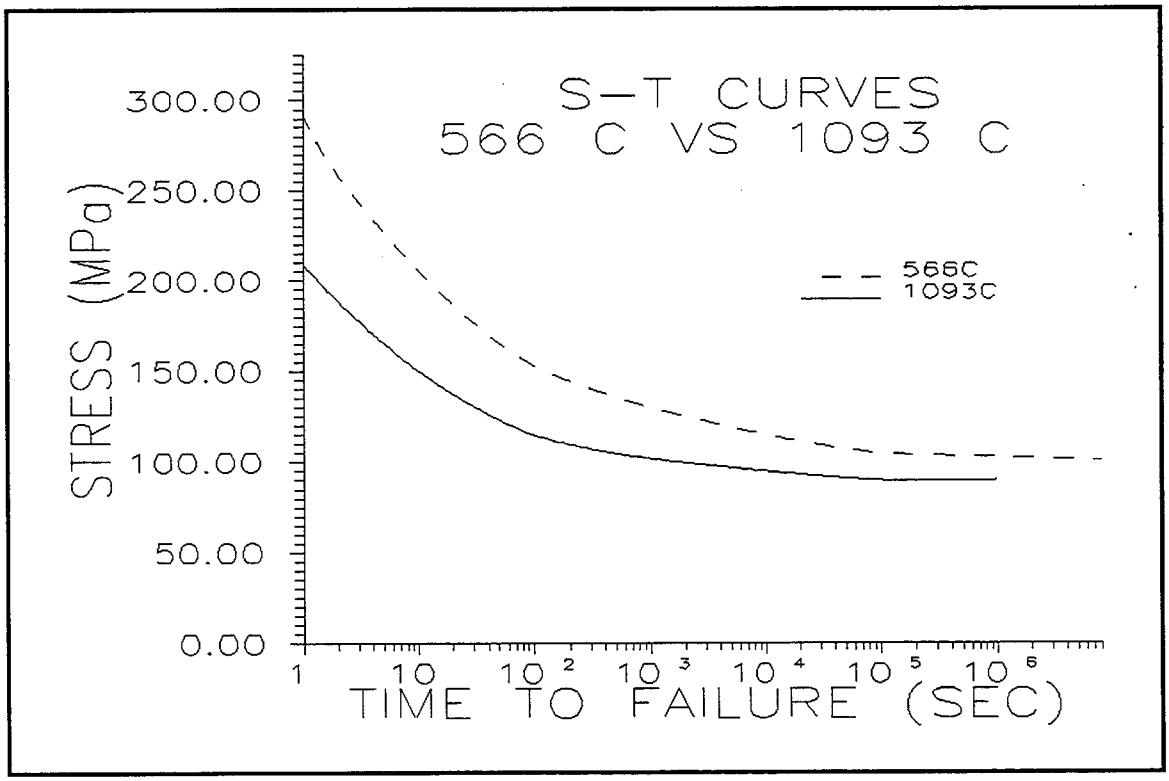

Figure 17. Fatigue Life Curves 1093°C vs 566°C

of the 1 Hz and 10 Hz fatigue life curves at the two different temperatures. It is a combination of the two curves seen in Figures 14 and 16. Figure 17 shows that the temperature or the environment will effect the fatigue life of the material. For a given stress level, the higher the temperature of the environment is, the shorter the fatigue life will be.

In summary, there are a number of things that can be observed from the fatigue life curves generated from this data. The first observation is that the fatigue life of the SiC/MAS system is reduced at the higher temperature. On the basis of a percentage of ultimate strength, it performs better at the higher temperature. This is true for both 1 Hz, as can be seen in Figures 10 and 12, and 10 Hz, as can be seen in Figures 4 and 6. The next observation is that, for a given temperature, the fatigue life of this material is unaffected by the frequency of the cycling. This is true for both of the temperatures used in this investigation and can be seen in Figure 14 for 566°C and Figure 16 for 1093°C. The caveat is that only two frequencies and two temperatures were investigated. One more temperature, say room temperature, and one more frequency, say 0.1 Hz would help to complete this picture.

C. Modulus Degradation

One of the methods of assessing the damage progression is to look at the effective modulus of elasticity and, more to the point, how that modulus degrades during cycling. Characterizing the damage progression in a ceramic matrix composite with the degradation of the modulus of elasticity is a common practice. There are numerous ways

to measure the modulus, given the stress-strain hystereses that were generated in these tests. The method used for the following discussion was to divide the stress difference by the strain difference in each cycle to get an instantaneous measure of the modulus of elasticity. Some of the discussion is based on normalized moduli. The modulus in each of these cases was normalized with the average of the initial moduli, as measured in the monotonic tensile tests and the first cycle of each fatigue test, for each of the temperatures evaluated. For the low temperature of 566°C/1050°F the initial modulus was 117.99 GPa (17.11 Msi). For the high temperature test at 1093°C/2000°F the initial modulus was 96.19 GPa (13.95 Msi).

C.1. Modulus Degradation 566°C. Figure 18 shows the modulus degradation of the tests conducted at 566°C/1050°F with a frequency of 10 Hz. This figure shows that,

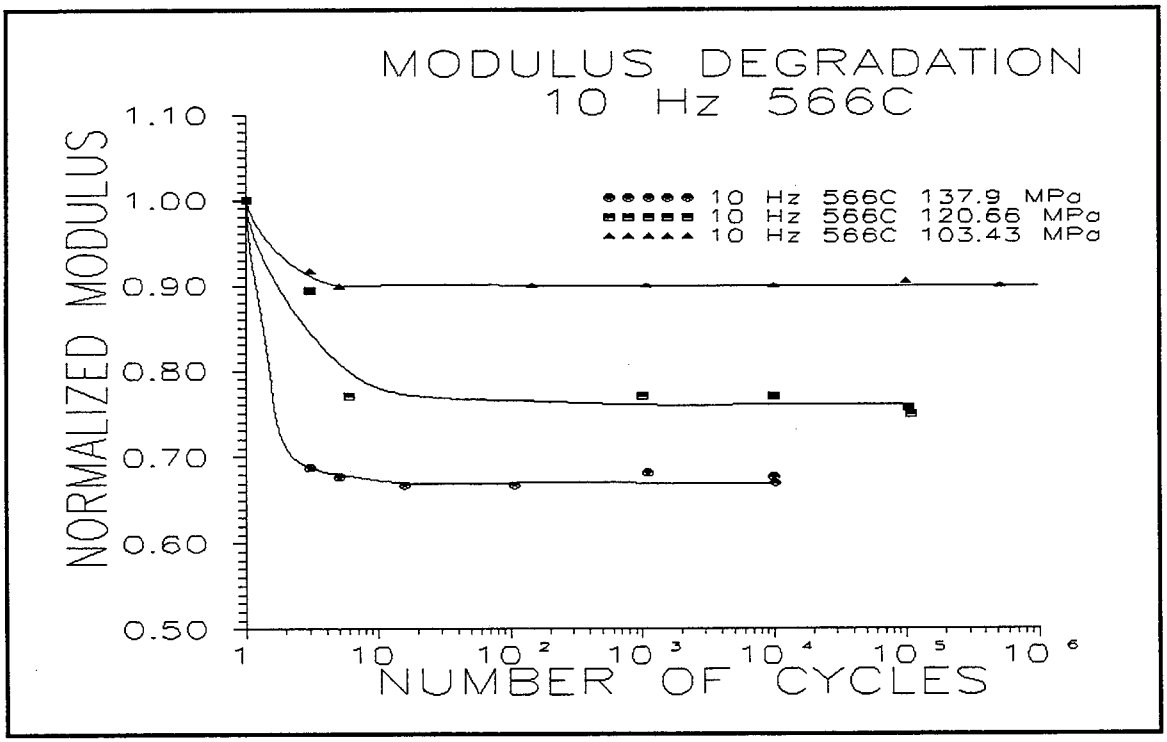

Figure 18. Modulus Degradation 566°C 10 Hz

for each of these tests, there is a large initial reduction in modulus over the first five cycles and then the modulus remains almost constant until failure. The large initial reduction of the modulus is obviously due to the creation and propagation of large numbers of microcracks in the matrix of the 90° plies. The lack of decay of the modulus after the first few cycles would then be due to the fact that the specimen is undergoing a time-dependent environmentally assisted crack growth caused by a combination of stress and the environment. This time dependent, creep type mechanism, is discussed in greater detail in section D of this chapter. There is a definite trend, as expected, that the higher stress tests result in a greater reduction in modulus. The test conducted at a maximum stress of 137.9 MPa had a reduction in modulus of about 30 percent which is fairly close to the 40 percent predicted by the total discount method. This would indicate that, after the first five cycles, a large portion of the load was being supported by the 0° plies.

In Figure 19 the same information can be seen for the tests conducted at a temperature of 566°C/1050°F with a 1 Hz frequency. The same trends can be seen here as were seen in the modulus degradation for the 10 Hz tests.

It can be seen that, for a given stress level at this temperature, the specimens tested at 1 Hz have a greater modulus degradation than those cycled at 10 Hz. For example, the 137.9 GPa test at 1 Hz degraded to about 65 percent of the initial value which is close to the value predicted by the total discount method and about five percent more than the test conducted at 10 Hz.

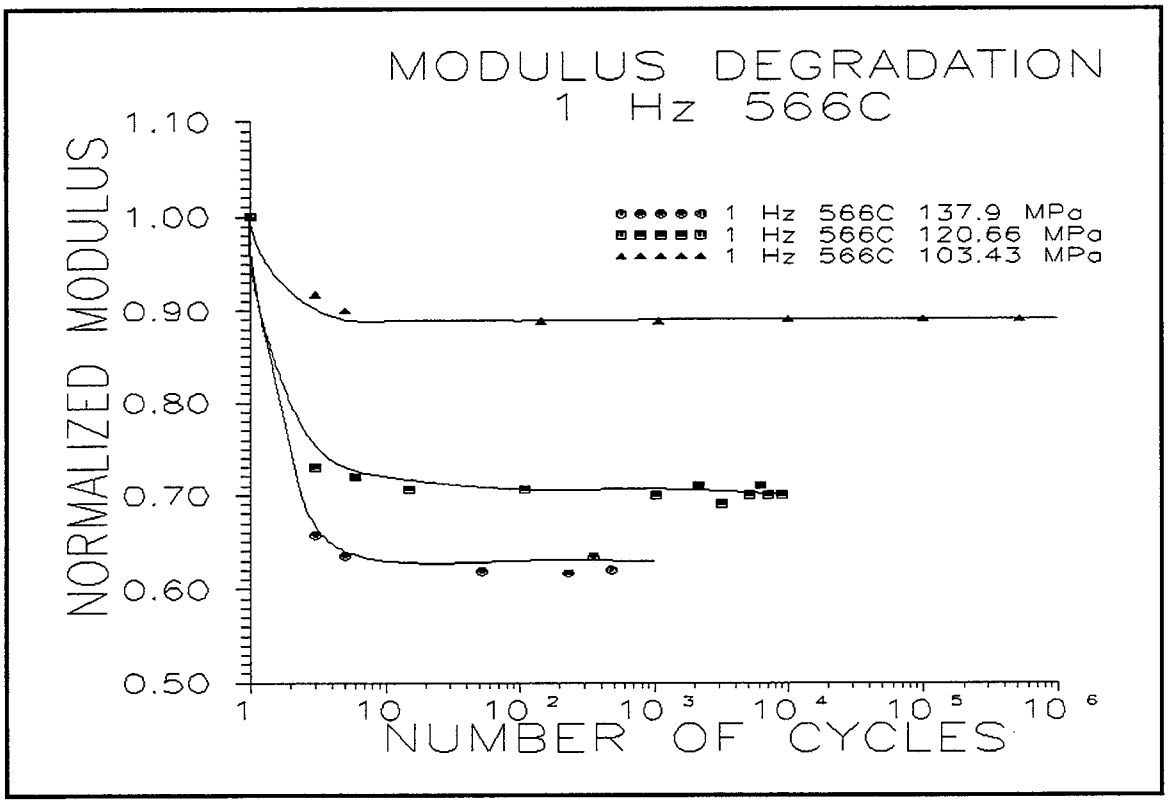

Figure 19. Modulus Degradation 566°C 1 Hz

Figures 20, 21, and 22 show that, for maximum stress levels of 137.9 MPa, 120.66 MPa, and 103.43 MPa at a temperature of 566°C/1050°F, specimens tested at a 1 Hz frequency exhibit about 5 percent more degradation in modulus than the those that were tested at the 10 Hz frequency. This indicates that, at this temperature, the rate at which the specimen was cycled will have a small effect on the amount of modulus degradation. This can be attributed to the greater amount of time spent at the highest load levels during the first ten cycles for the specimens tested at 1 Hz than for those tested at 10 Hz. This additional time corresponds to more environmentally assisted crack growth due to more exposure to the environment.

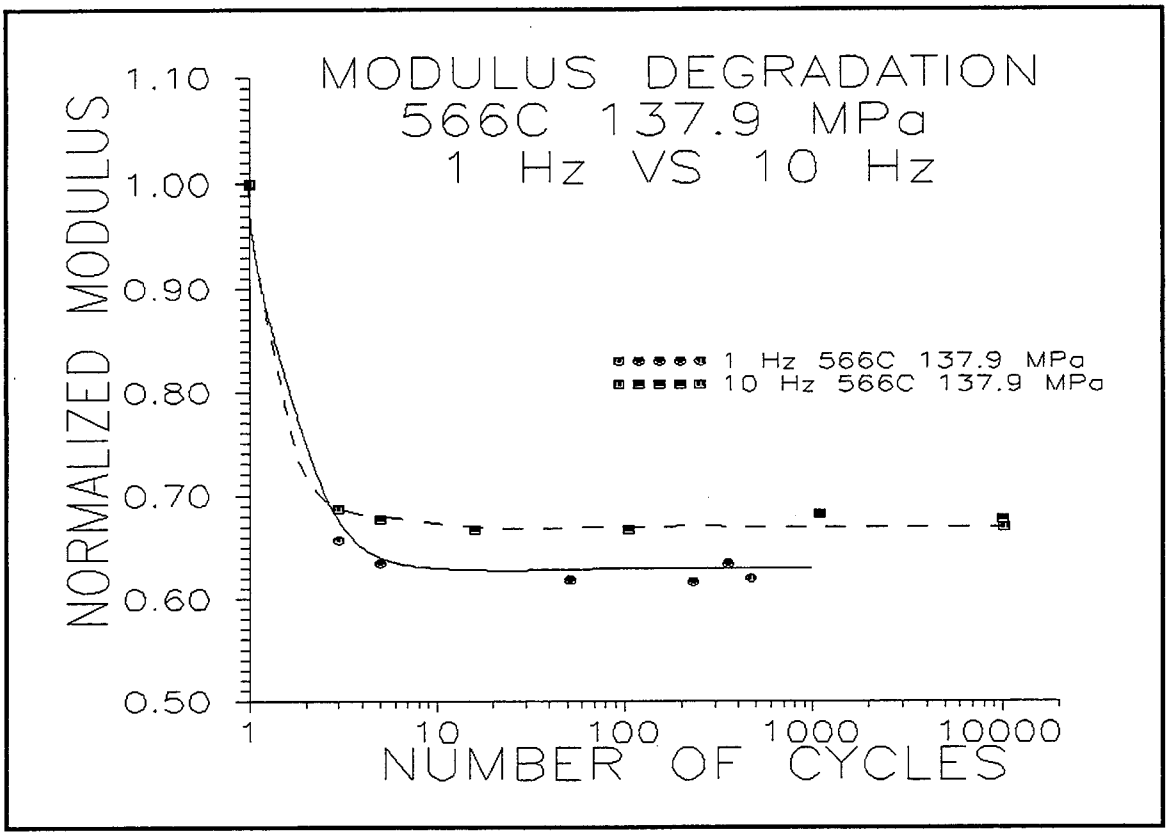

Figure 20. Modulus Degradation 566°C 137.9 MPa

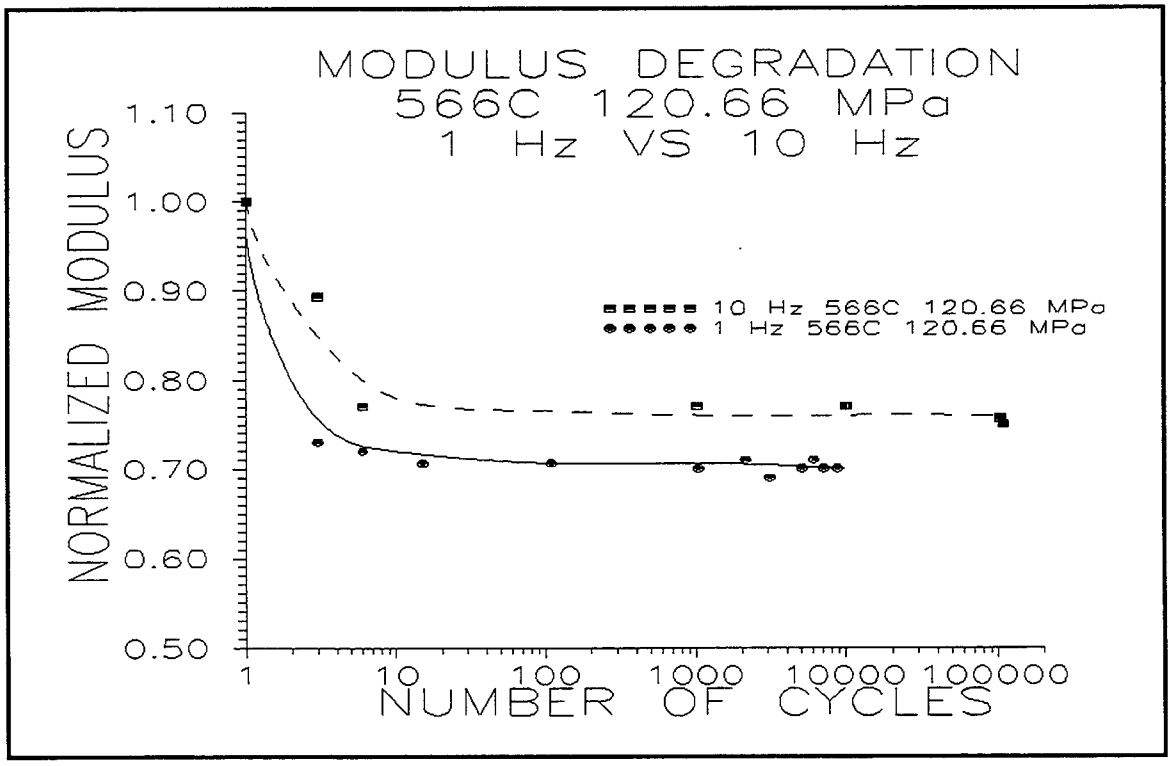

Figure 21. Modulus Degradation 566°C 120.66 Mpa

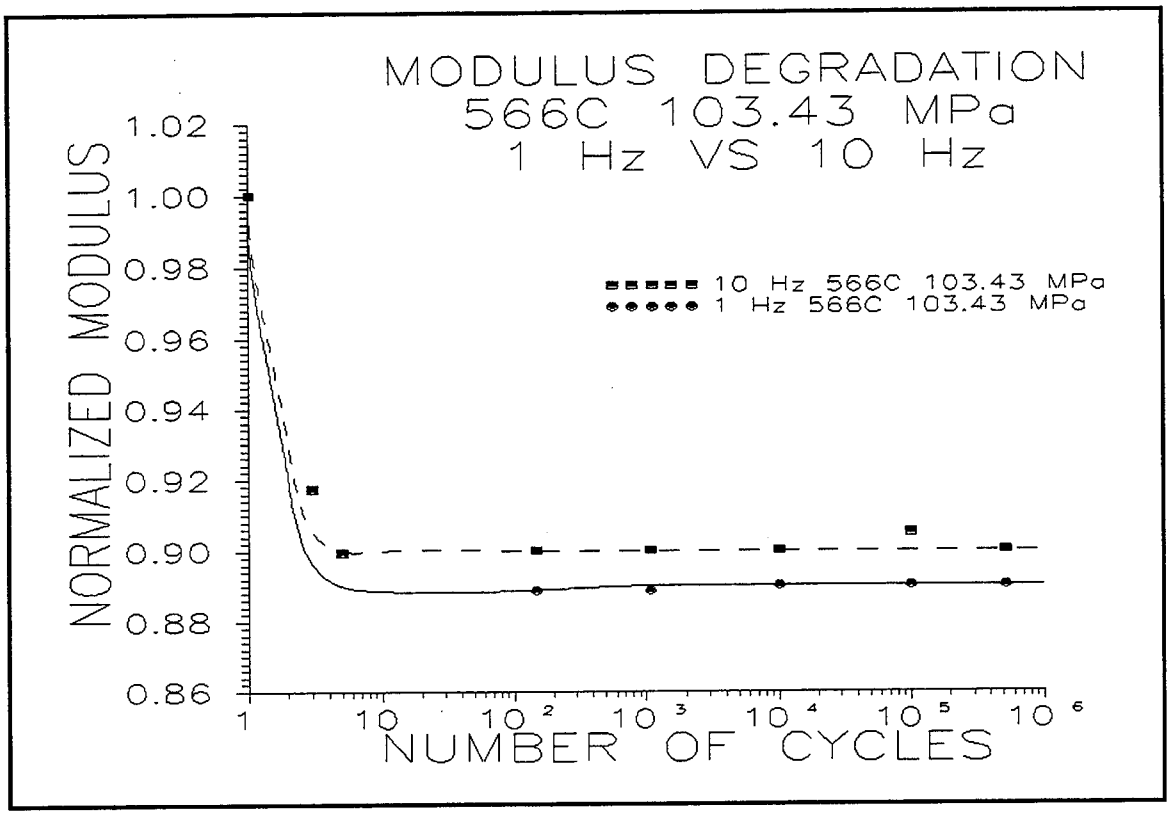

Figure 22. Modulus Degradation 566°C 103.43 MPa

C.2. Modulus Degradation 1093°C. Figure 23 shows the modulus degradation for the tests conducted at a temperature of 1093°C/2000°F with a frequency of 10 Hz. This figure shows that for each of these tests there is a large initial reduction in modulus over the first ten cycles and then the modulus remains constant until failure. There is a definite trend, as expected, that the higher stress tests result in a greater reduction in modulus due to the creation of more matrix cracks. The test conducted at a maximum stress of 137.9 MPa had a reduction in modulus of about 40 percent which is nearly exactly that predicted by the total discount method. This indicates that the entire load is being supported by the fibers of the 0° plies after the first ten cycles. The other tests at lower stress levels show a much smaller initial degradation in modulus.

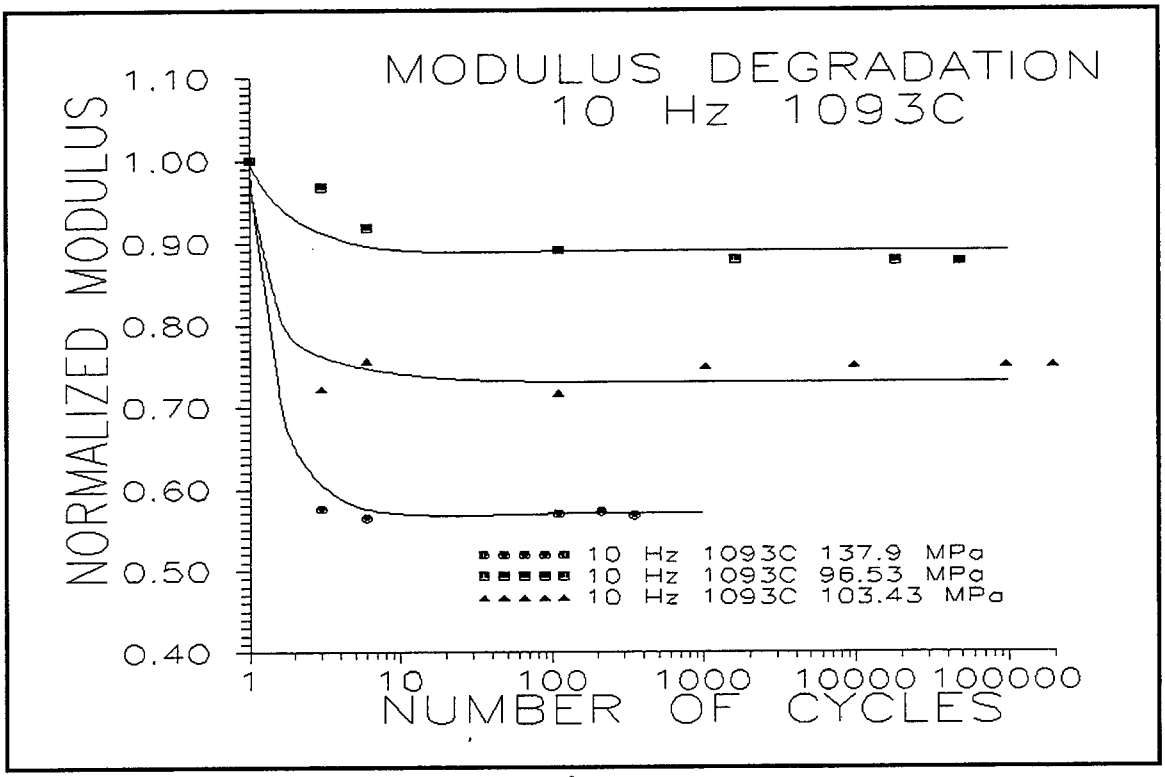

Figure 23. Modulus Degradation 1093°C 10 Hz

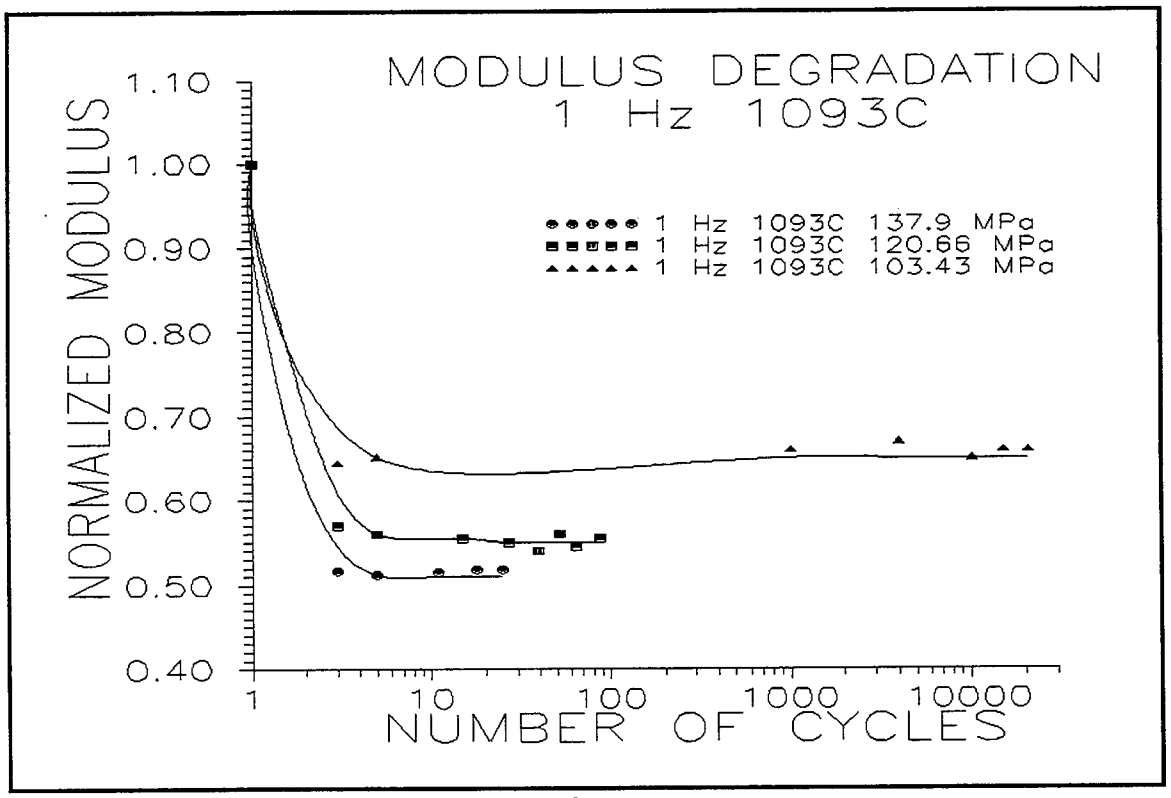

Figure 24. Modulus Degradation 1093°C 1 Hz

Figure 24 analyzes the same information for the tests conducted at 1093°C/2000°F with a frequency of 1Hz. The same trends can be seen here as were seen in the modulus degradation for the tests conducted at 10 Hz.

It can be seen that, for a given stress level at this temperature, the specimens tested at 1 Hz have more modulus degradation than those cycled at 10 Hz. Figure 25 shows that, for the tests conducted at a maximum stress level of 137.9 MPa at a temperature of 1093°C/2000°F, the specimen cycled at a 1 Hz frequency exhibits 5 percent more degradation in modulus than the specimen cycled at the 10 Hz frequency. Figure 26 shows that the same trend holds true for the specimens tested at a maximum stress of 103.43 MPa. This is the same observation as was made for the specimens tested at the lower temperature.

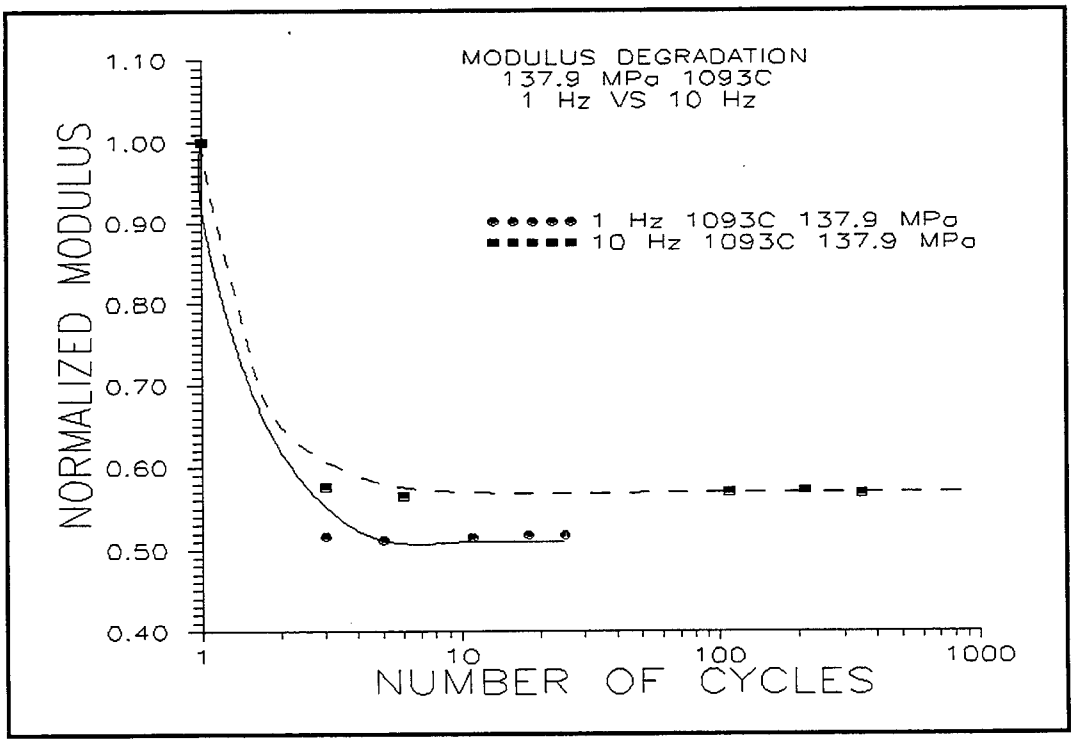

Figure 25. Modulus Degradation 1093°C 137.9 MPa 10 Hz vs 1 Hz

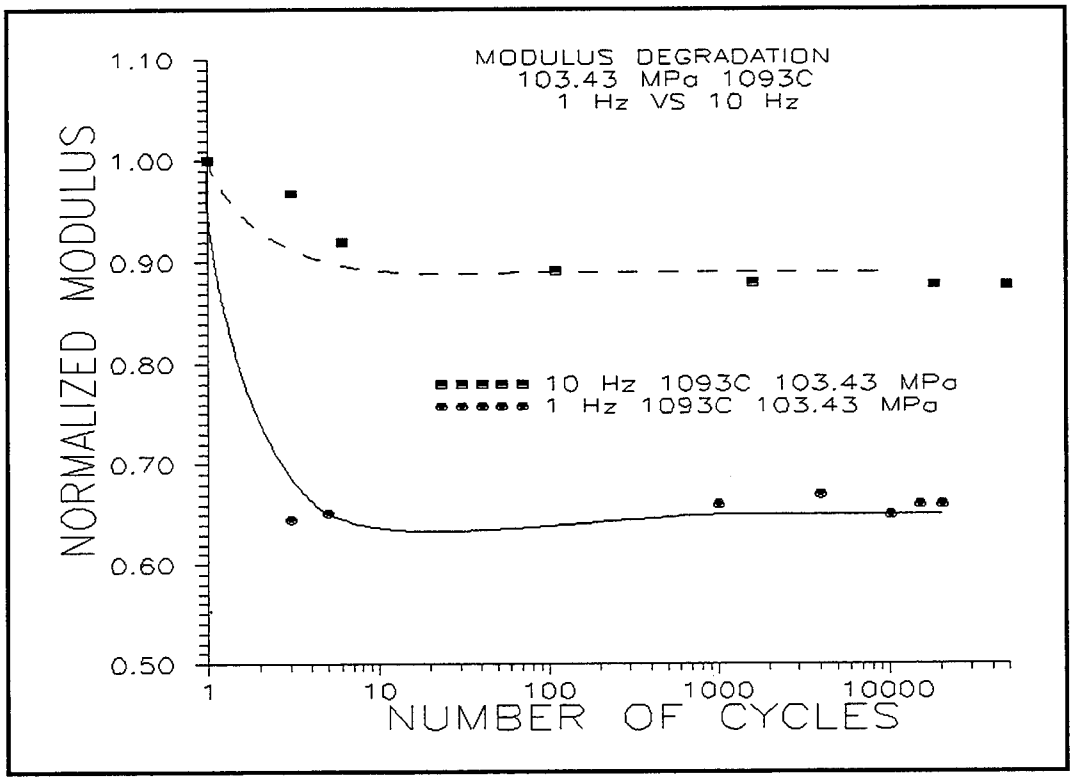

Figure 26. Modulus Degradation 1093°C 103.43 MPa 10 Hz vs 1 Hz

C.3. Modulus Degradation 10 Hz. It has been shown that the frequency of the loading will have an effect on the amount of modulus reduction, with the lower frequency resulting in a slightly increased reduction of modulus. Along the same lines it can be seen that the temperature of the test environment will also have an effect on the amount of modulus reduction.

In Figure 27 it can be seen that for the tests conducted at a frequency of 10 Hz and with a maximum stress of 137.9 MPa, the modulus reduction at a temperature of 1093°C is greater than the reduction at 566°C. In Figure 28 it can be seen that the same trend holds true for the tests conducted with a maximum stress level of 103.43 Mpa.

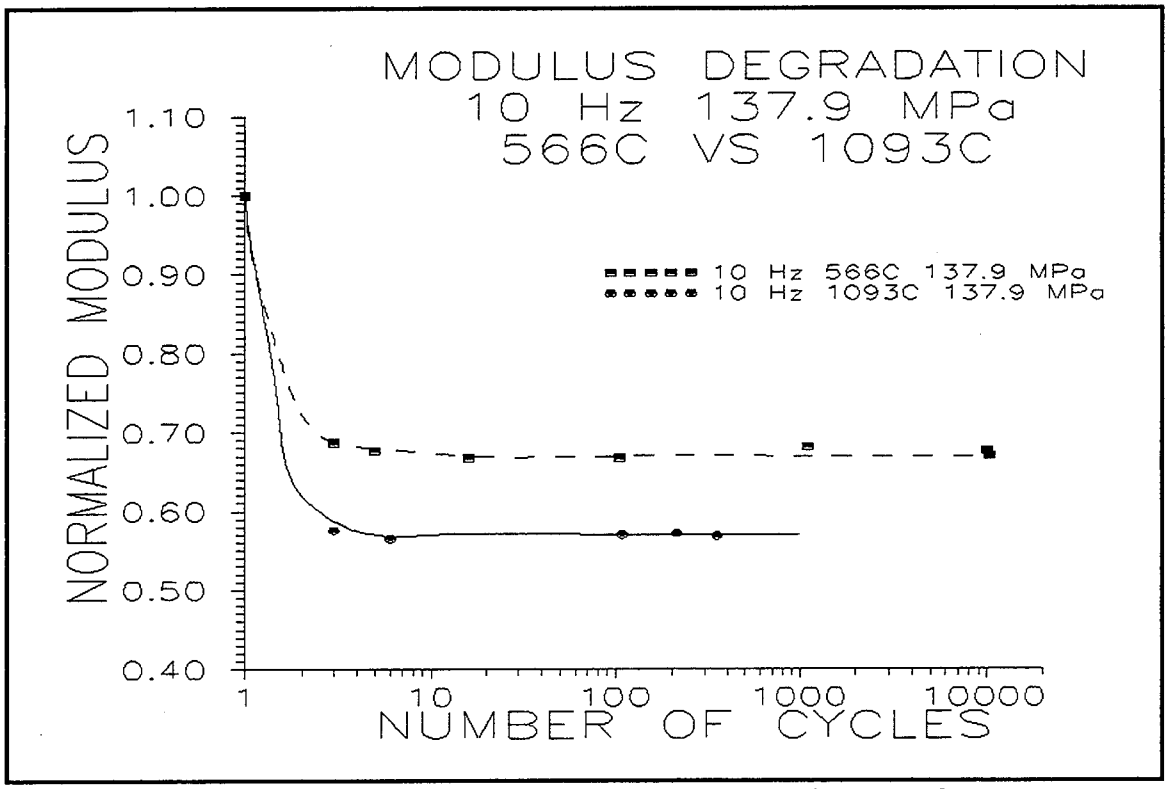

Figure 27. Modulus Degradation 10 Hz 137.9 MPa 1093°C vs 566°C

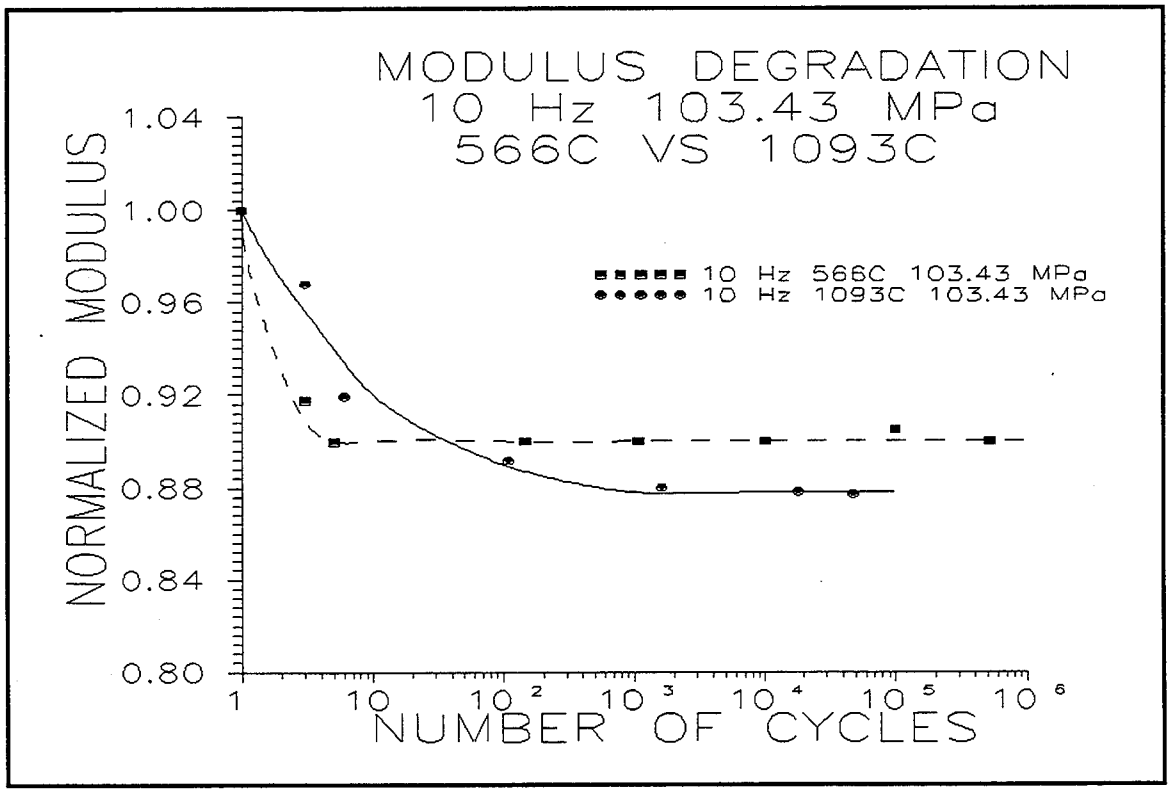

Figure 28. Modulus Degradation 10 Hz 103.43 MPa 1093°C vs 566°C

C.4. Modulus Degradation 1 Hz. It can also be shown that the same trends seen at 10 Hz are seen at 1 Hz. In Figure 29 it can be seen that, for the specimens tested at a frequency of 1 Hz and a maximum stress level of 137.9 MPa, the modulus reduction at a temperature of 1093°C is greater than the reduction at 566°C. In Figure 30 it can be seen that the same trend holds true for the tests conducted with a maximum stress level of 103.43 MPa.

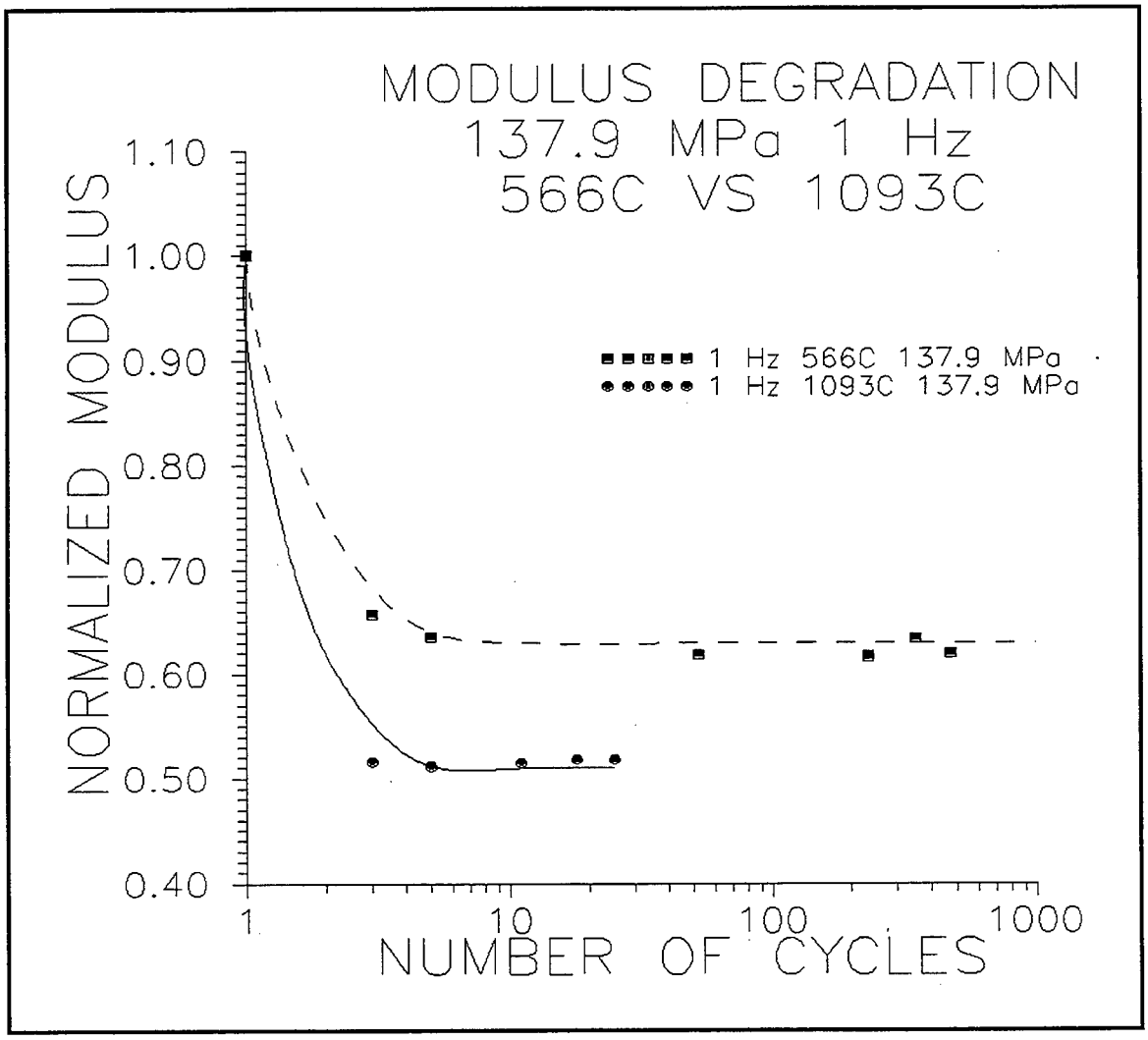

Figure 29. Modulus Degradation 1 Hz 137.9 MPa 1093°C vs 566°C

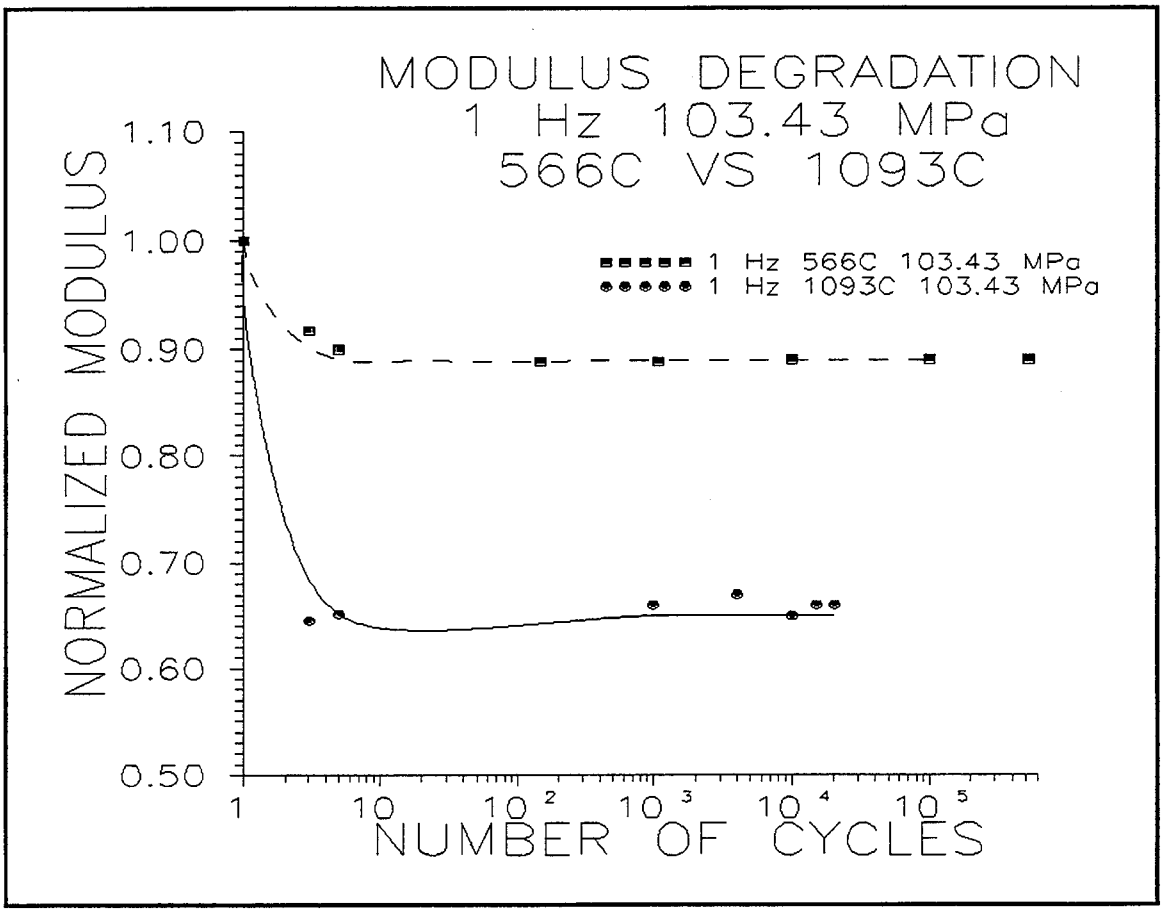

Figure 30. Modulus Degradation 1 Hz 103.43 MPa 1093°C vs 566°C

In summary, the plots in this section show that the degradation of modulus is dependent on both the frequency of the loading and the temperature of the environment. The lower frequency will cause more degradation, as will the higher temperature. They also show that, regardless of the temperature of the environment or the frequency of the loading, the same behavior is being demonstrated. The modulus of elasticity is decaying over the first ten cycles due to the development of matrix cracks. After the tenth cycle the modulus stabilizes and remains constant which indicates that stress and the environment is causing a time dependent environmentally assisted crack growth to occur. This could be thought of as a form of the phenomenon of creep.

D. Strain Data

Another way to monitor and analyze the damage progression throughout these tests is to look at the strain data. The strain was measured with an extensometer with a one inch gauge length. The maximum, minimum, and difference between maximum and minimum strains is plotted to provide comparisons between the tests conducted at different temperatures and different cyclic loading frequencies. These plots are created from the same strain data that was used to create the modulus degradation plots in the previous section and thus it is expected that they will lead to the same conclusions, that there is a greater amount of strain at higher temperatures, a greater amount of strain at lower frequencies, and creep occurs from after the tenth cycle until failure. In this context, creep is a time dependent damage mechanism induced by a combination of stress and environmental effect (temperature). The first cycle indicated on the following plots corresponds to the first cycle of the fatigue loading due to the fact that the actual first cycle of every test was performed manually at an approximate rate of 0.2 Hz and, for a given temperature and stress level, will not change. The reason the first cycle was performed manually was that the data acquisition software used in this study did not collect data during the first cycle.

D.1. Strain Data 566°C 10 Hz. Figures 31 through 33 show the plots of maximum strain, minimum strain, and the difference between the maximum and minimum strain for the tests conducted at 566°C with a frequency of 10 Hz. Figure 31, the plot of the maximum strain, shows that after the damage from the initial cycle there is some small steady increase of the maximum strain. In Figure 32 it can be seen that the minimum

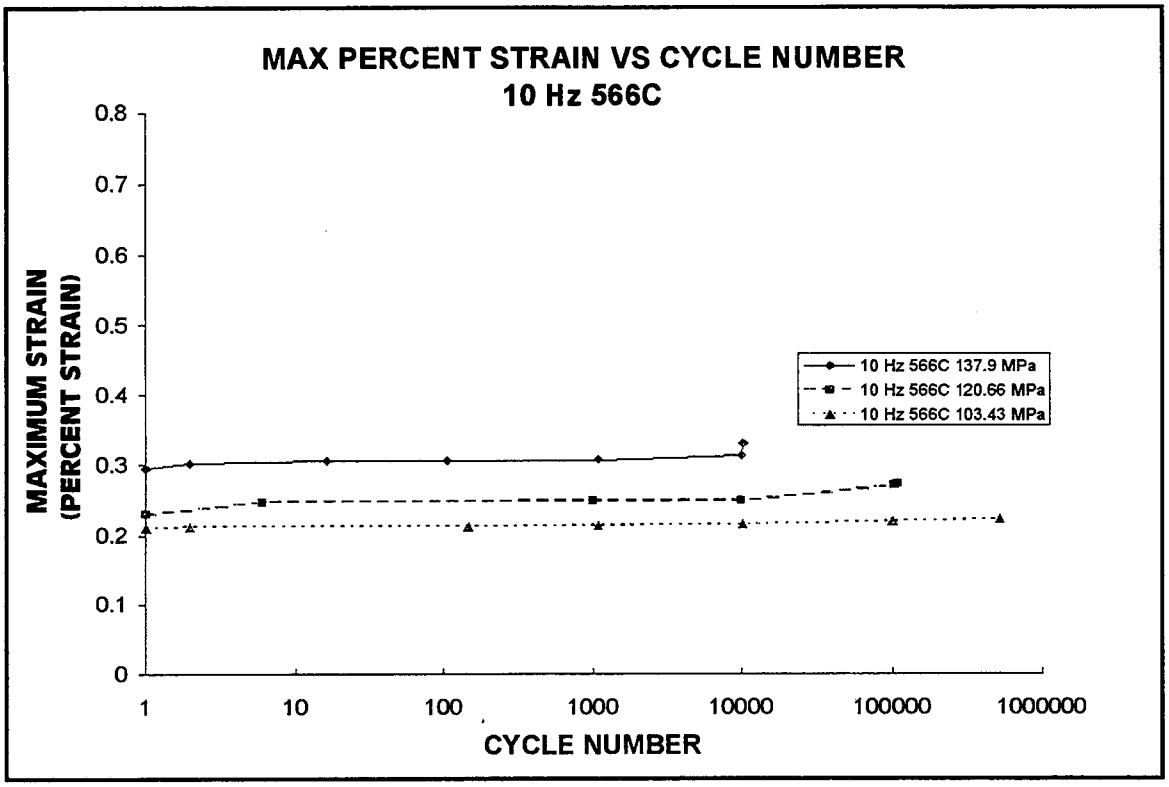

Figure 31. Maximum Strain 10 Hz 566°C

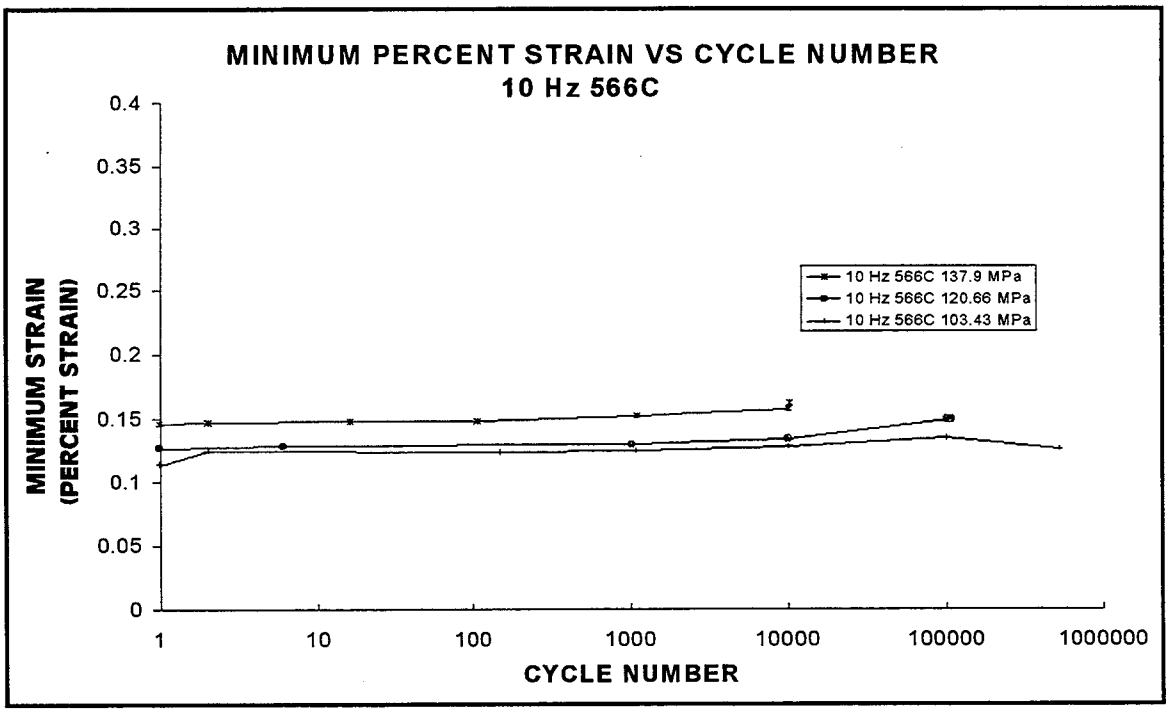

Figure 32. Minimum Strain 10 Hz 566°C

strains also increase a small amount over the duration of the test. Figure 33 shows that the strain difference remained almost constant throughout each of the tests at 566°C and 10 Hz. This indicates that the maximum strain and the minimum strain increased steadily at the same rate and that there was a time dependent environmentally assisted crack growth occurring in these tests. This corresponds well with the modulus degradation plots for this series of tests which indicated that there is very little modulus degradation after the damage incurred during the initial cycles. It can also be seen that there is a sharp increase in the strain difference at the very end of some of the tests. This increase in strain corresponds to a decrease in the modulus of elasticity at the very end of those tests. This can be seen in the section on modulus degradation, Section C.

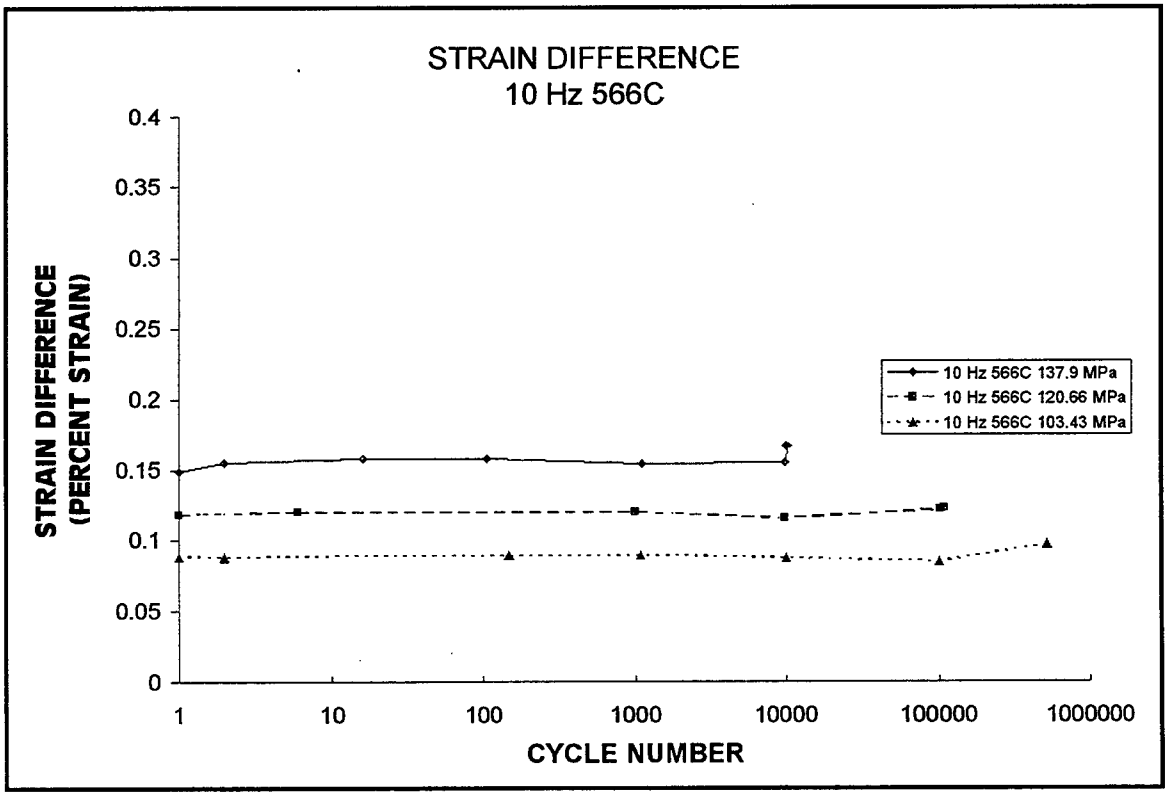

Figure 33. Strain Difference 10 Hz 566°C

D.2. Strain Data 566°C 1 Hz. Figures 34 through 36 show the plots of maximum strain, minimum strain, and strain difference for the tests conducted at 566°C with a frequency of 1 Hz. Figure 34, the plot of the maximum strain, shows that after the damage from the initial cycle there is an additional increase in the maximum strain. In Figure 35 it can be seen that the minimum strains also increase over the duration of the test. Figure 36 shows that the strain difference remained almost constant throughout each of the tests at 566°C and 1 Hz. This indicates that there was a time dependent environmentally assisted crack growth occurring in these tests as well. This corresponds well with modulus degradation plots for the material at this temperature and frequency which showed very little change in the modulus after the initial damage.

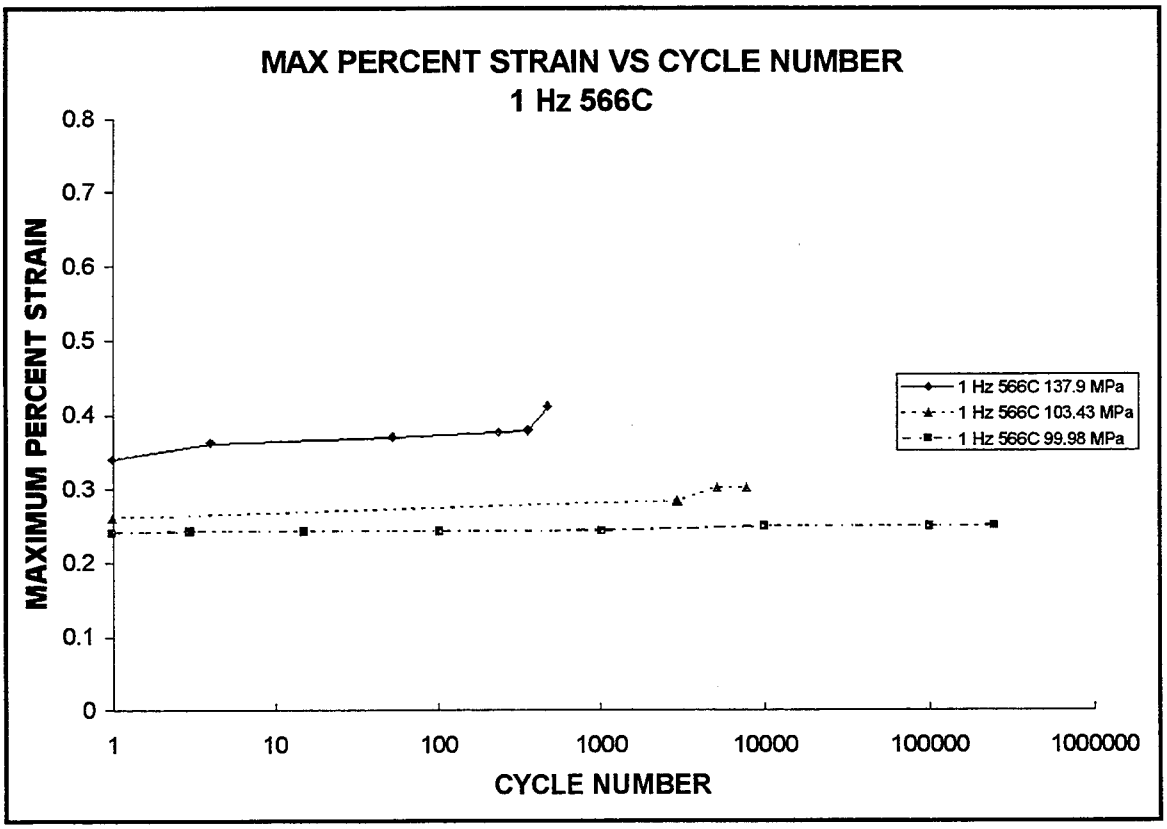

Figure 34. Maximum Strain 1 Hz 566°C

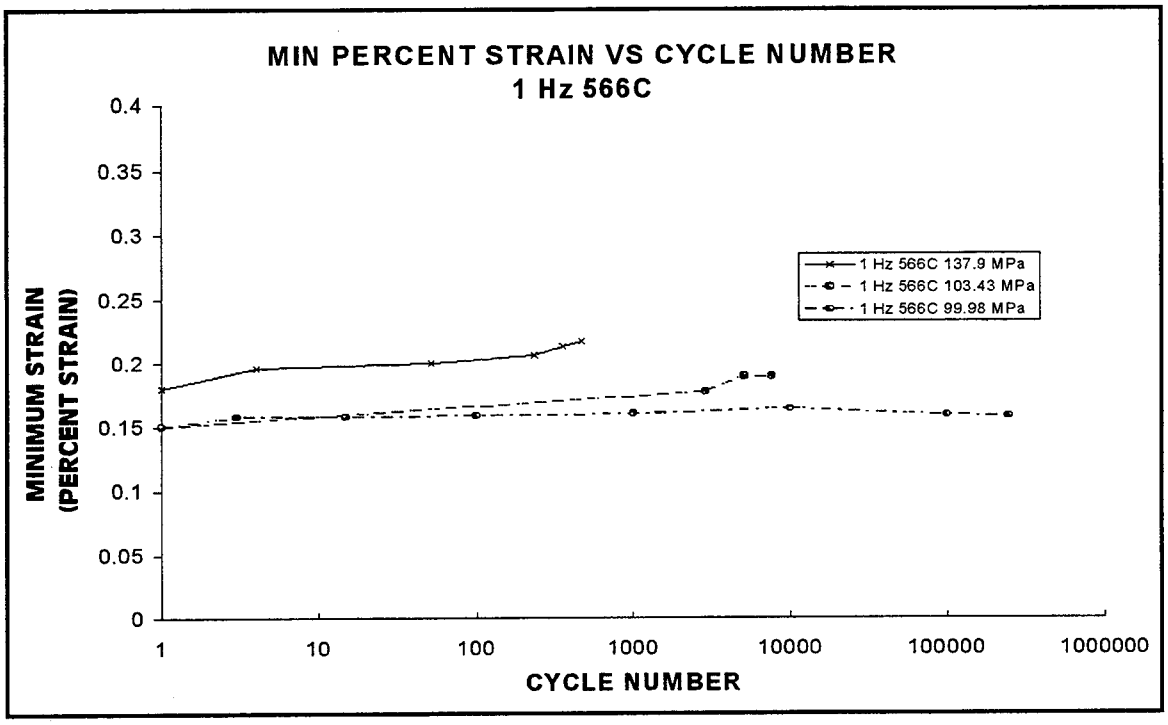

Figure 35. Minimum Strain 1 Hz 566°C

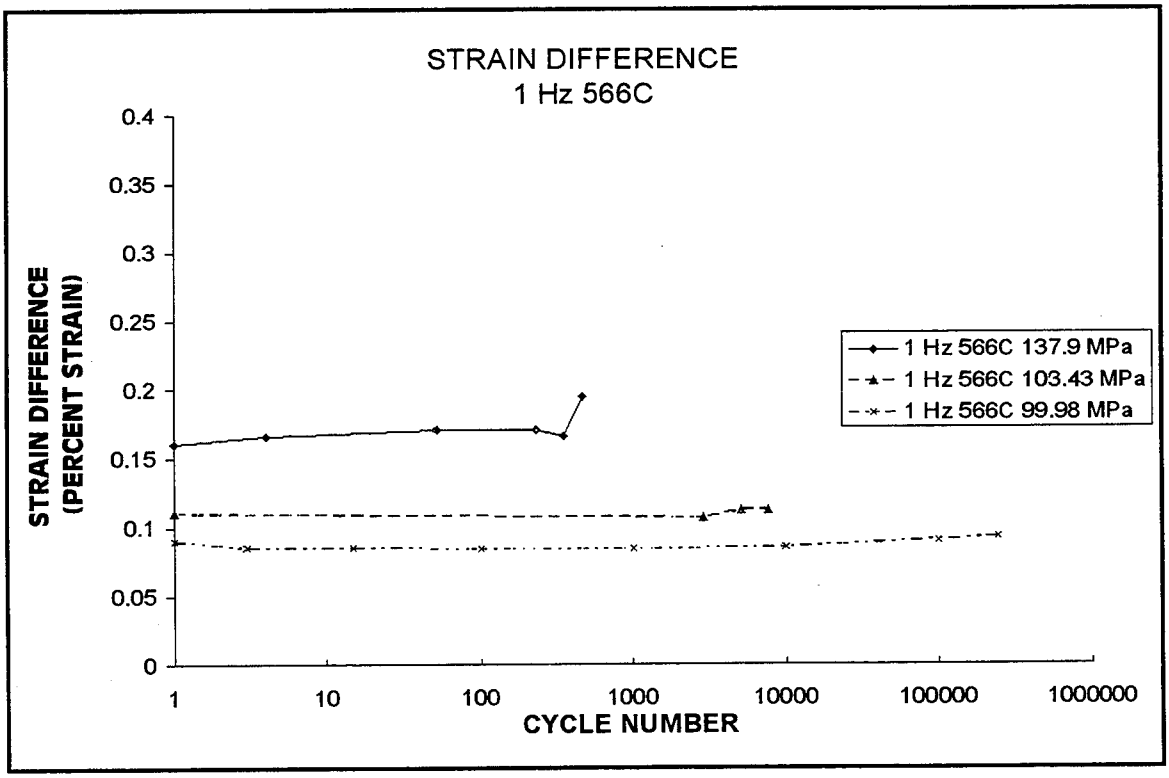

Figure 36. Strain Difference 1 Hz 566°C

D.3. Strain Data 10 Hz vs 1 Hz at 566°C. Figures 37 through 41 compare the cycle and time history of the maximum strain and the strain difference for tests conducted at frequencies of 1 Hz and 10 Hz at a temperature of 566°C. Figure 37 compares the maximum strains for the tests conducted at 137.9 MPa. It can be seen that the test conducted at 1 Hz has a greater maximum strain from the initial cycle of the fatigue loading until failure. The lower frequency test allows for more environmentally assisted crack growth to occur because it causes the specimen to be at the highest stress level for the greatest amount of time. It can also be seen that the test conducted at 1 Hz exhibits a notably higher rate of increase of maximum strain than the test conducted at 10 Hz. In Figure 38 it can be seen that the difference between the maximum and minimum strain for each of the tests is constant but that the difference is greater for the 1 Hz test than for the

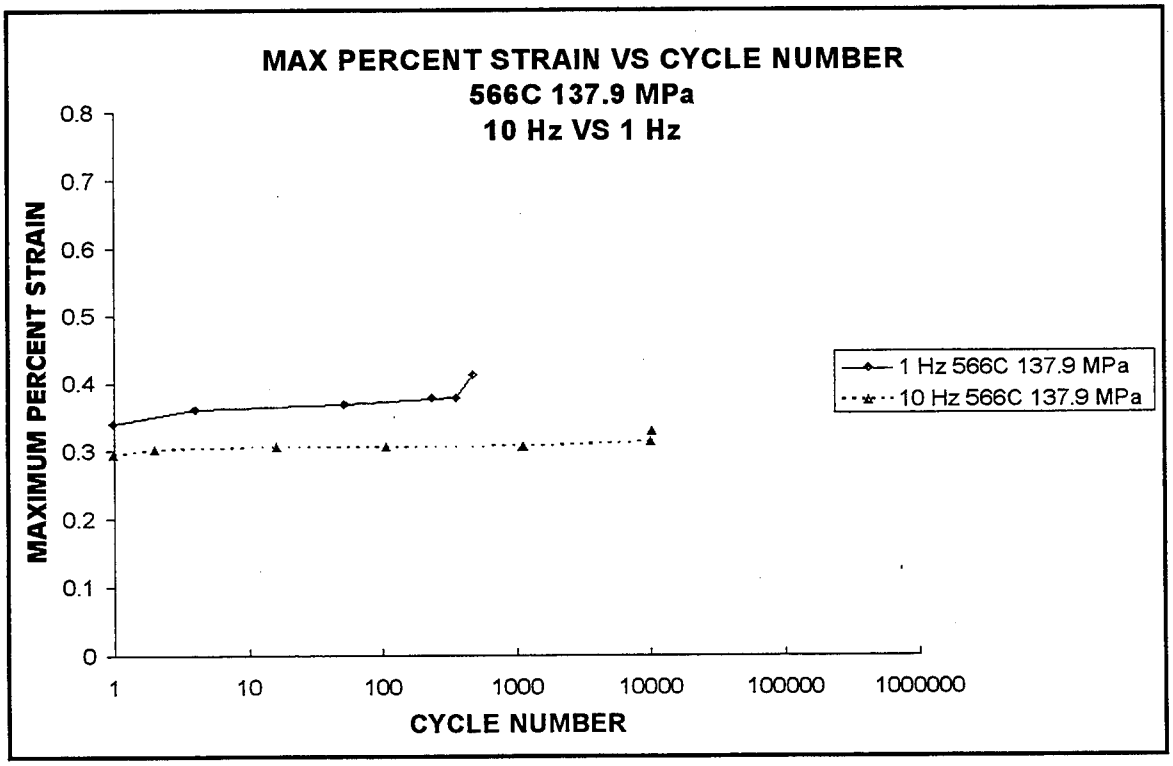

Figure 37. Maximum Strain 566°C 137.9 MPa 10 Hz vs 1 Hz

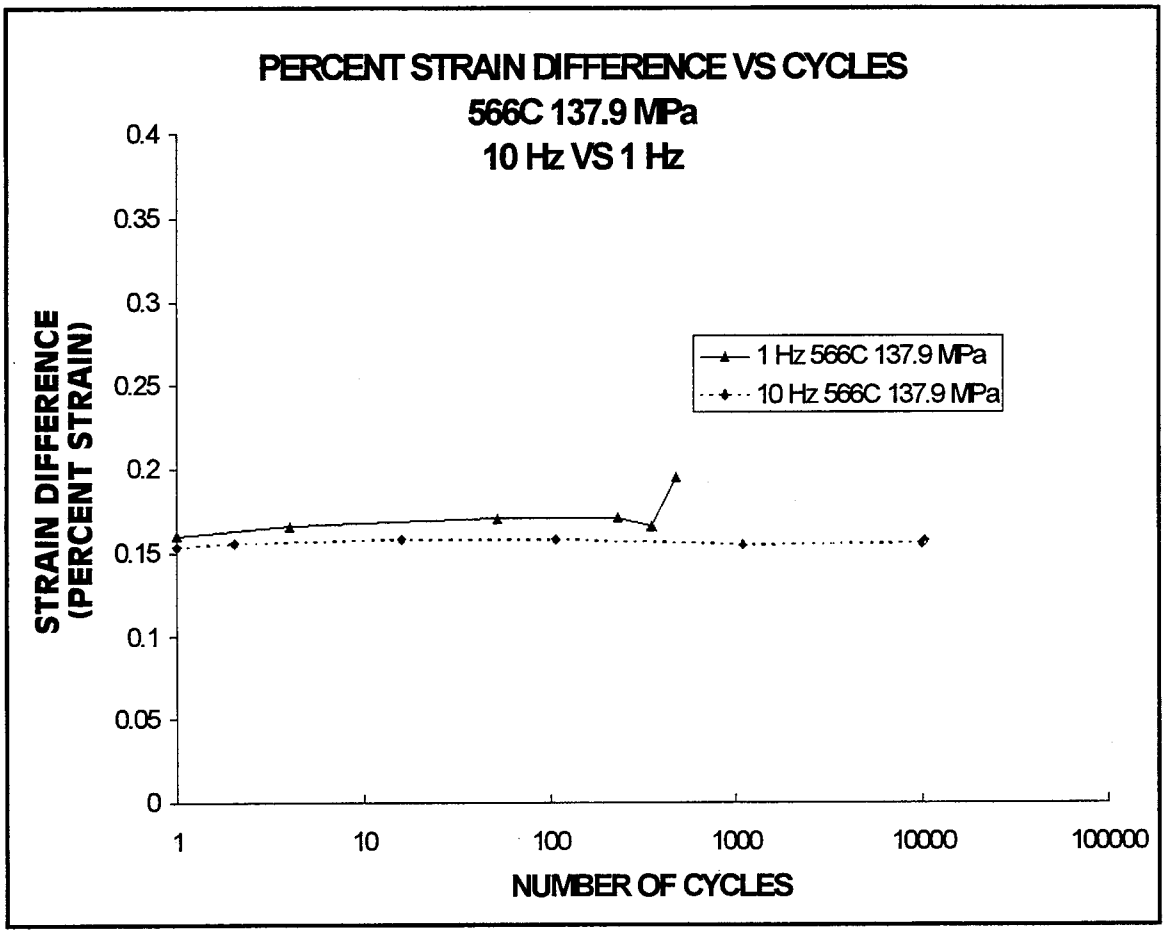

Figure 38. Strain Difference 566°C 137.9 MPa 10 Hz vs 1 Hz

10 Hz test. This would again indicate that the main phenomenon in both tests is creep-like, time dependent, environmentally assisted crack growth but that the amount of creep is greater at the lower frequency. The same trends are exhibited in Figures 40 and 41 for a maximum stress of 103.43 MPa. In addition, when the maximum strain is plotted against the time to failure, it can be seen that the frequency of the loading is not a factor in the life of the specimen. This is demonstrated in Figure 39 for the tests conducted at 566°C and a maximum stress of 137.9 Mpa.

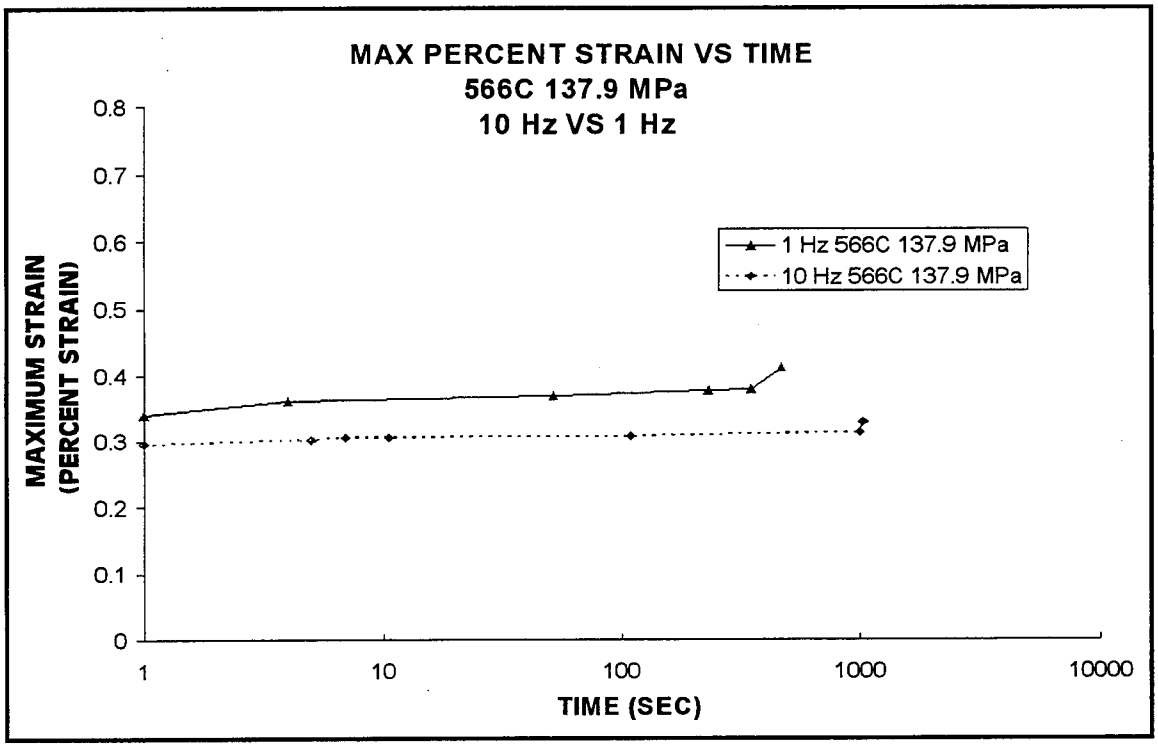

Figure 39. Maximum Strain vs Time 566°C 137.9 MPa 10 Hz vs 1 Hz

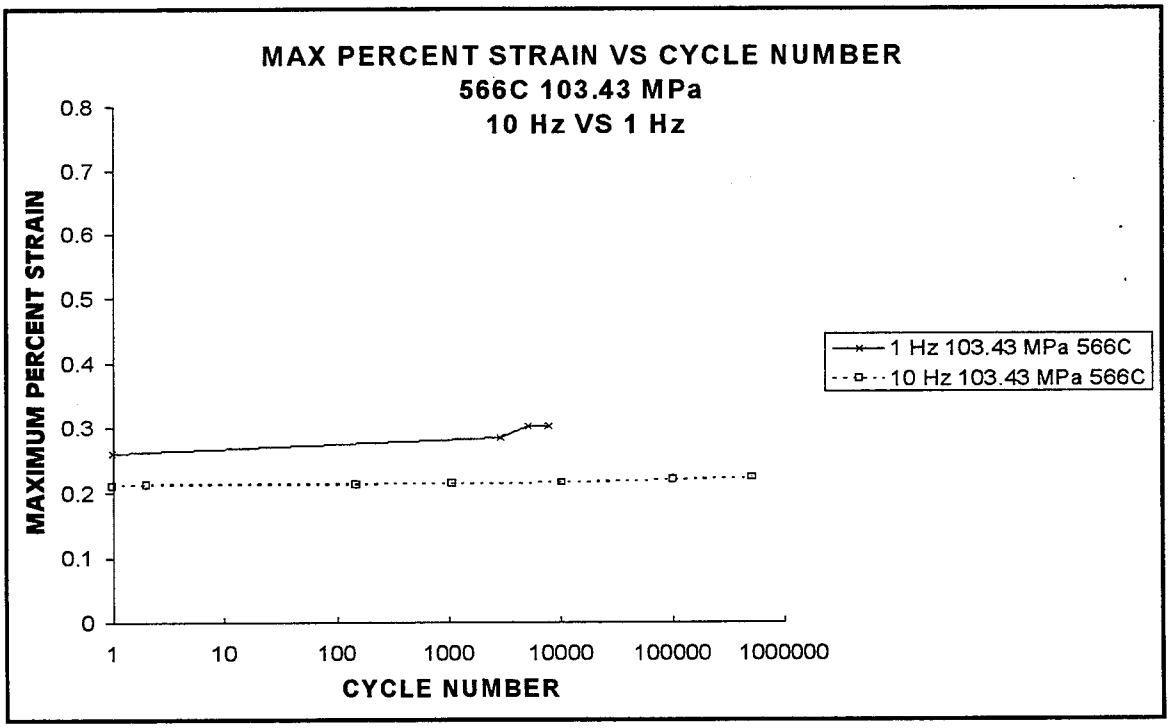

Figure 40. Maximum Strain 566°C 103.43 MPa 10 Hz vs 1 Hz

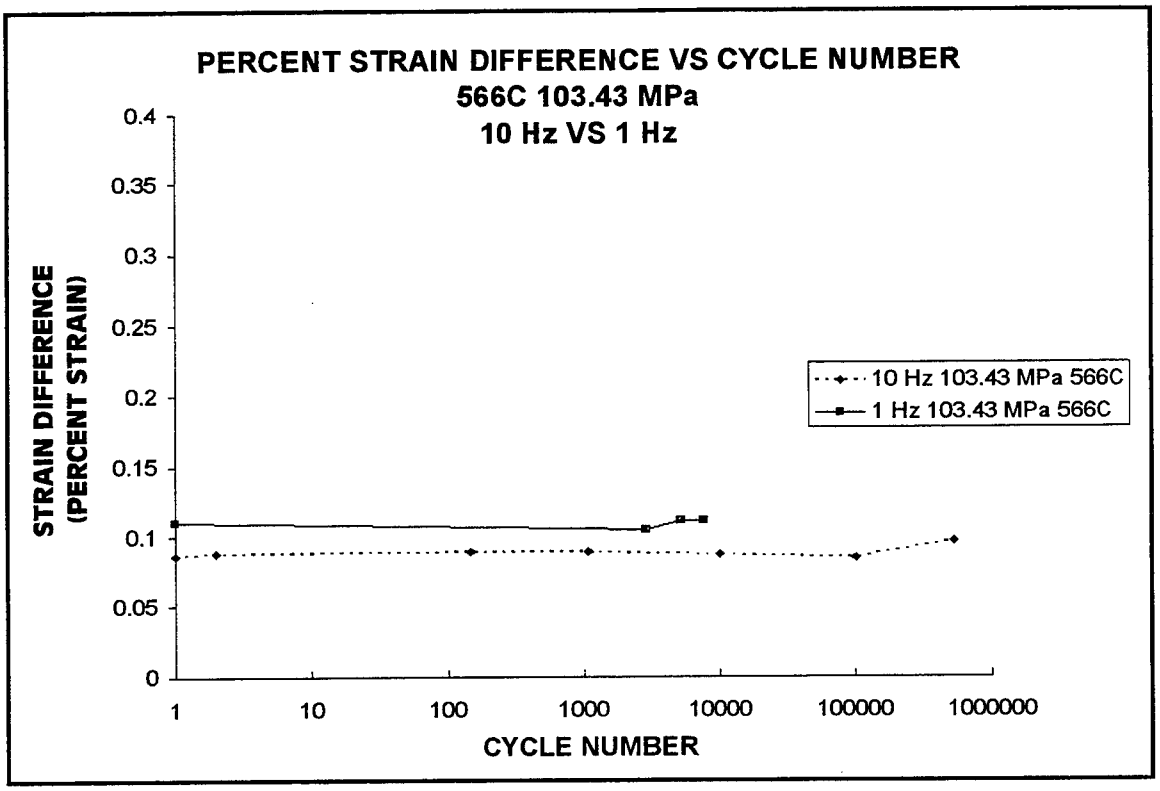

Figure 41. Strain Difference 566°C 103.43 MPa 10 Hz vs 1 Hz

D.4. Strain Data 1093°C 10 Hz. Figures 42 through 44 show the maximum percent strain, minimum percent strain, and the strain difference plotted against cycle number for the tests conducted at a temperature of 1093°C/2000°F and a frequency of 10 Hz. Figure 42 shows that the maximum percent strain increases slowly at a constant rate after the initial damage of the first couple of cycles. This is the same observation as was made for the specimens tested at a temperature of 566°C/1050°F and a frequency of 10 Hz. Figure 43 shows the minimum percent strain plotted against the cycle number for all the tests conducted at a temperature of 1093°C/2000°F and a frequency of 10 Hz. This chart shows that the minimum strain increases steadily throughout the test for all of the specimens.

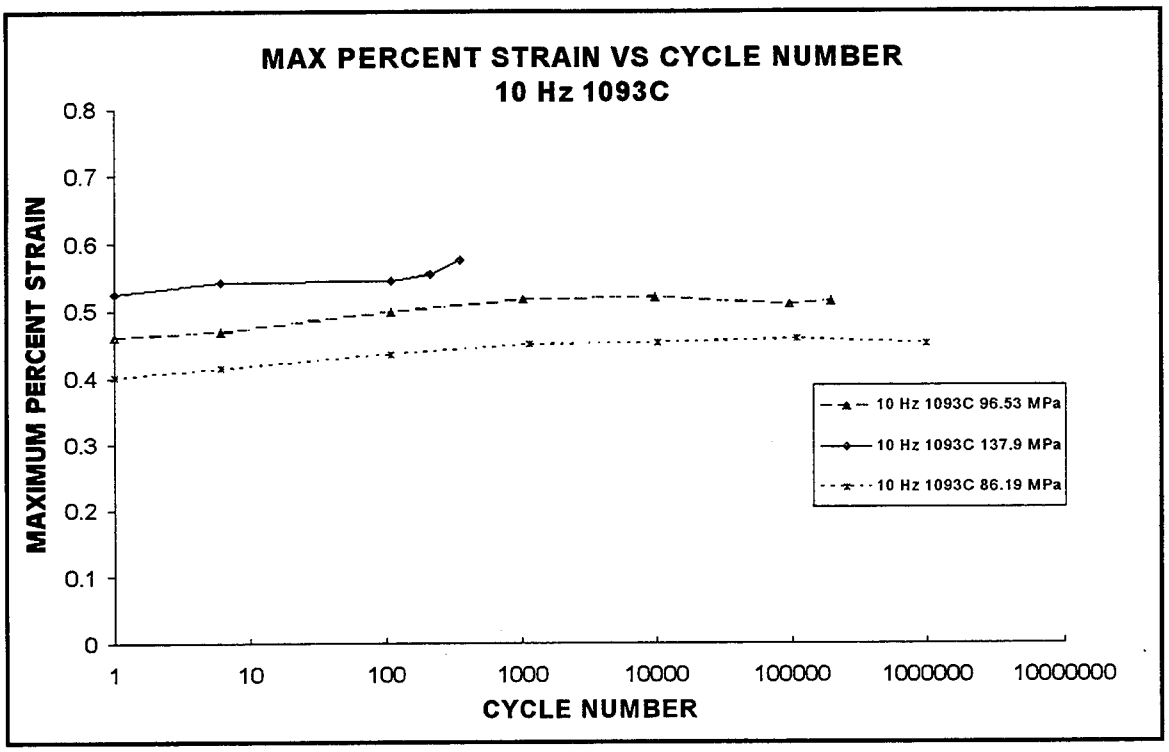

Figure 42. Maximum Strain 10 Hz 1093°C

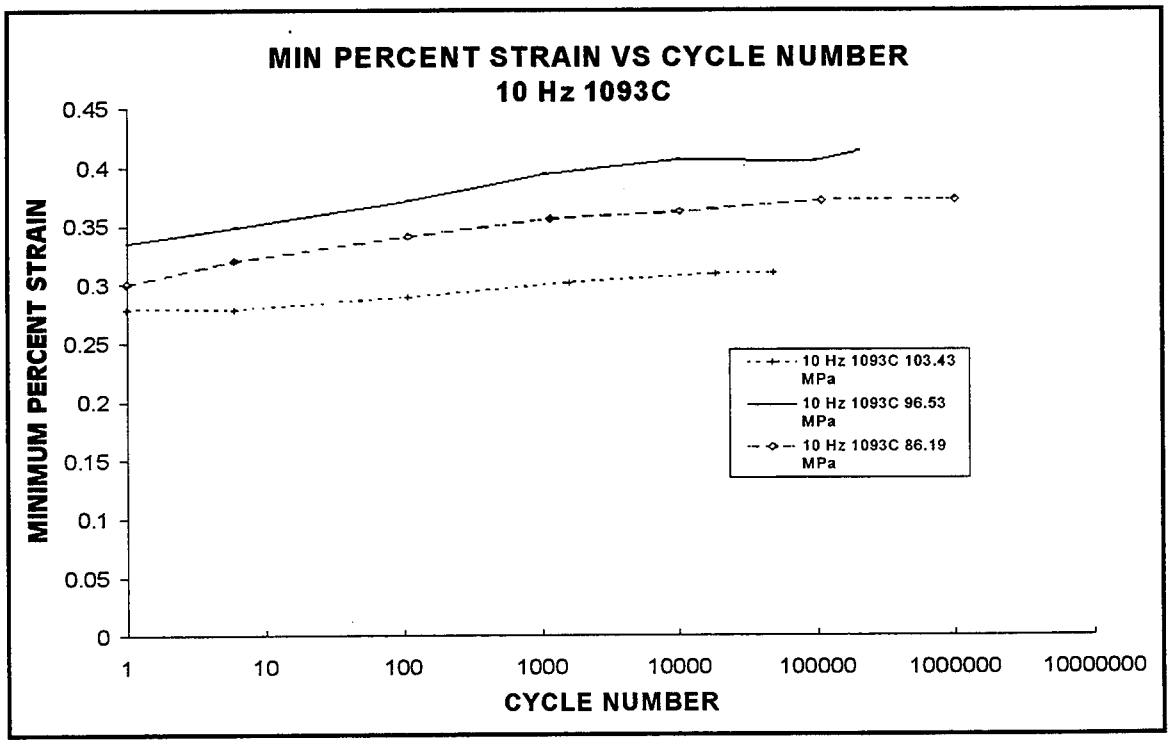

Figure 43. Minimum Strain 10 Hz 1093°C

Figure 44 shows that the strain difference remains constant for the duration of these tests. This indicates that, as was seen in the tests conducted at 566°C/1050°F, the main phenomenon occurring in all of these tests was a time dependent environmentally assisted crack growth. The data also support the results from the analysis of the modulus degradation plots for this series of tests which showed very little degradation after the initial cycles.

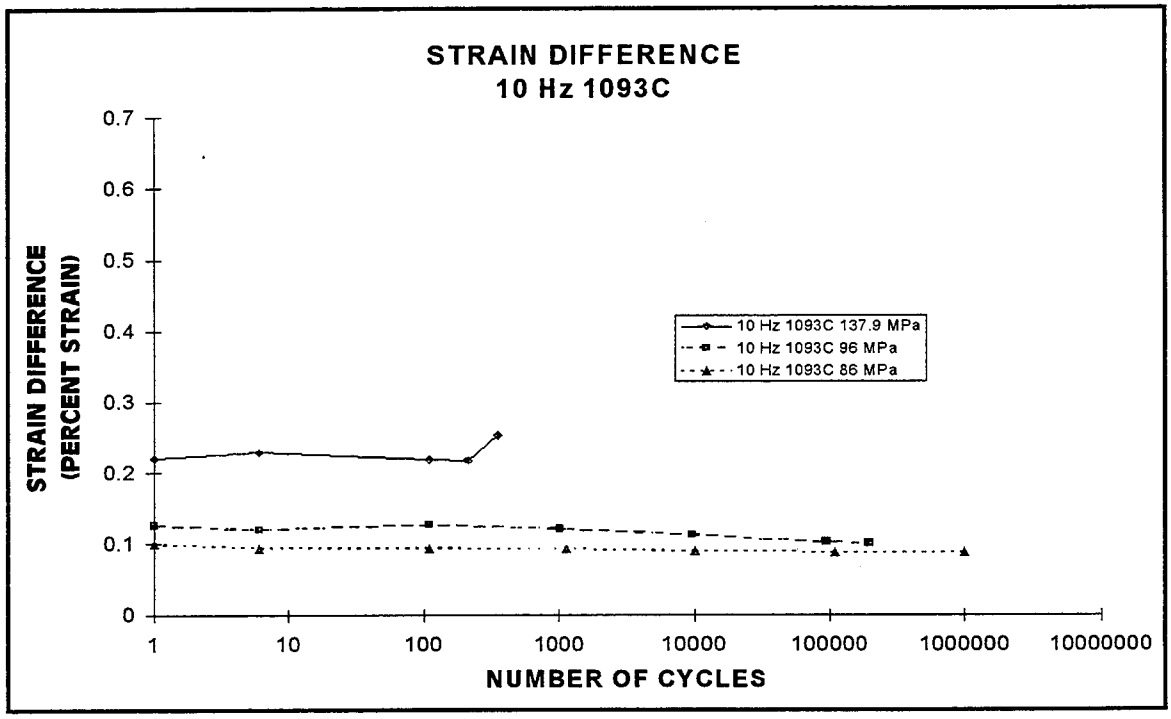

Figure 44. Strain Difference 10 Hz 1093°C

D.5. Strain Data 1093°C 1 Hz. Figures 45 through 47 show the maximum percent strain, minimum percent strain, and the strain difference plotted against cycle number for all the tests conducted at a temperature of 1093°C/2000°F and a frequency of 1 Hz. Figure 45 shows that there is an increase in the maximum percent strain

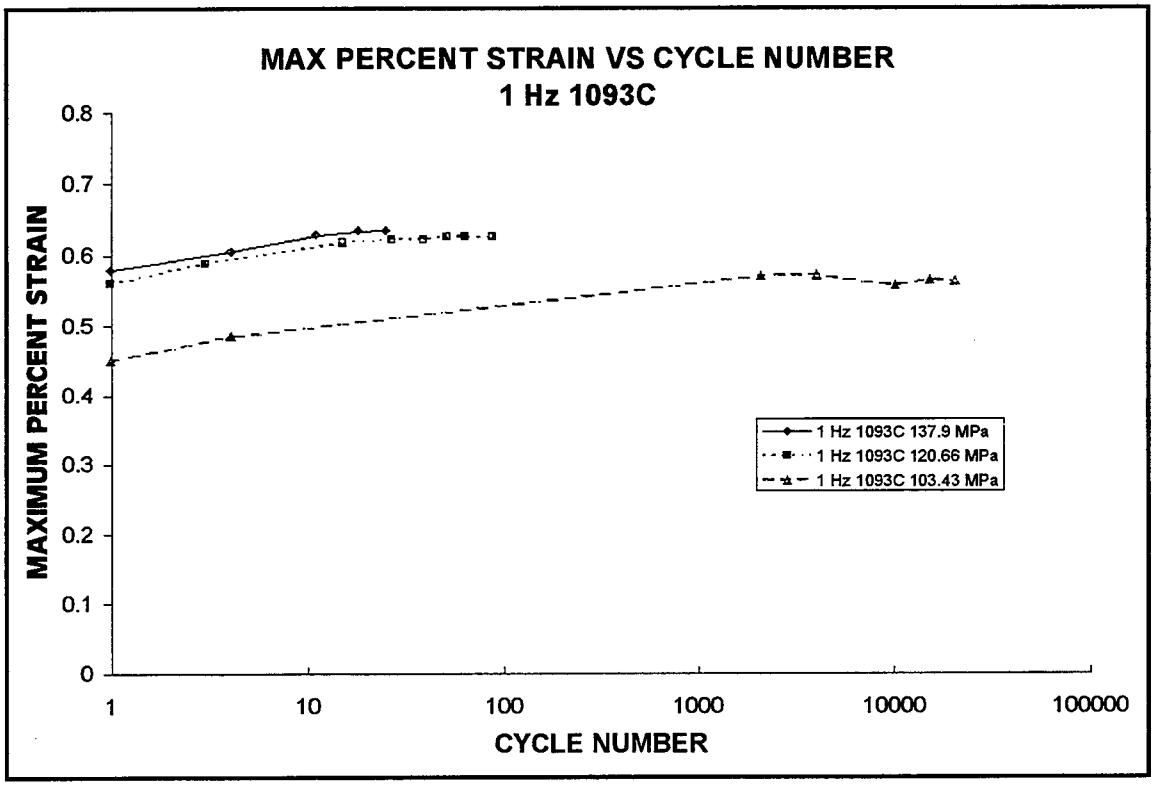

Figure 45. Maximum Strain 1 Hz 1093°C

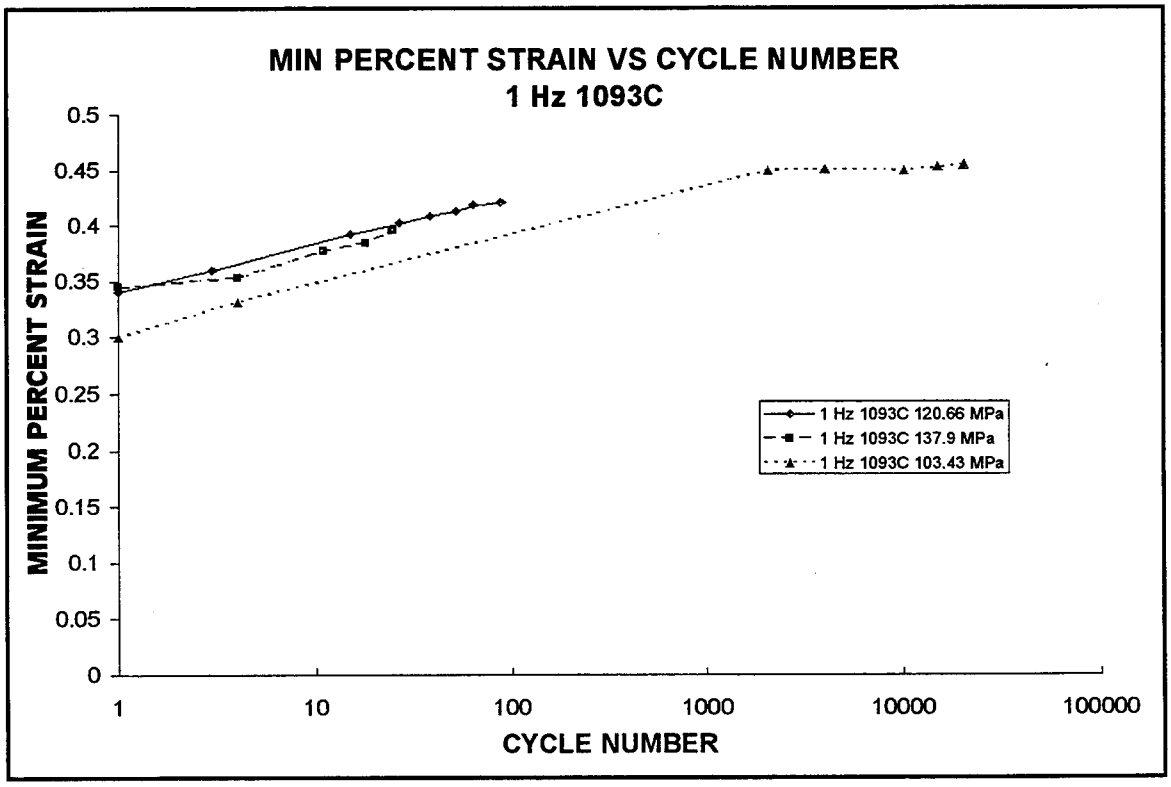

Figure 46. Minimum Strain 1 Hz 1093°C

after the initial damage of the first couple of cycles. This is the same observation as was made for the specimens tested at a temperature of 566°C/1050°F and a frequency of 1 Hz.

Figure 46 shows the minimum percent strain plotted against the cycle number for all the tests conducted at a temperature of 1093°C/2000°F and a frequency of 1 Hz. This chart shows that the minimum strain increases significantly, at a constant rate, throughout the test for all of the specimens.

Figure 47 shows that the strain difference remained constant for the duration of all the tests. The constant strain difference is a result of the maximum and minimum strains increasing at the same rate. This indicates that, as was the case for the tests conducted at 566°C/1050°F, there was a time dependent damage mechanism occurring in all of the tests

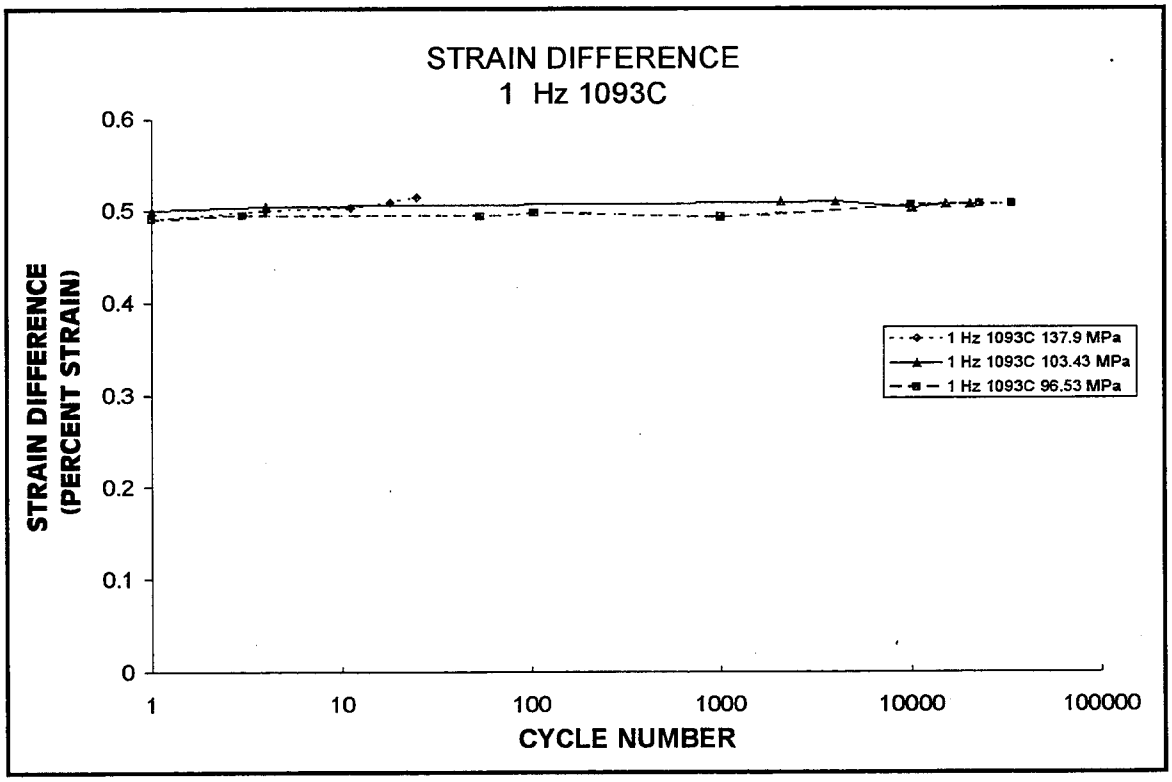

Figure 47. Strain Difference 1 Hz 1093°C

conducted at 1 Hz. This corresponds well with the modulus degradation plots for this series of tests which indicate that, after the damage of the initial cycles, there is no appreciable reduction in modulus.

D.6. Strain Data 10 Hz vs 1 Hz at 1093°C. Figures 48 through 52 examine the difference between the strains induced when the tests are conducted at the two different frequencies of 10 Hz and 1 Hz at a temperature of 1093°C/2000°F. Figure 48 shows the maximum strains of the two tests that were conducted at a maximum stress level of 137.9 MPa and Figure 49 shows the strain differences of the same two tests. The test conducted at 1 Hz had a consistently higher percent strain than that conducted at 10 Hz. Figure 49 shows that the strain difference for both tests was constant, which indicates that both tests exhibited the previously observed time dependent damage mechanism. Figures 50 and 51

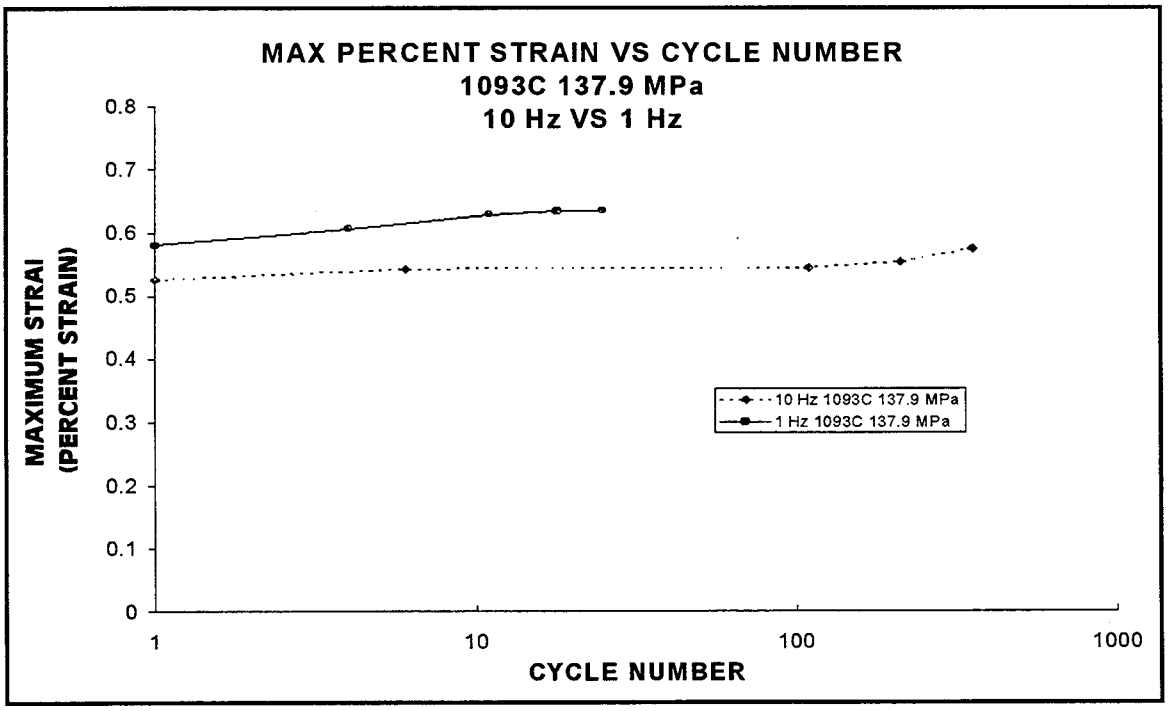

Figure 48. Maximum Strain 1093°C 137.9 MPa 1 Hz vs 10 Hz

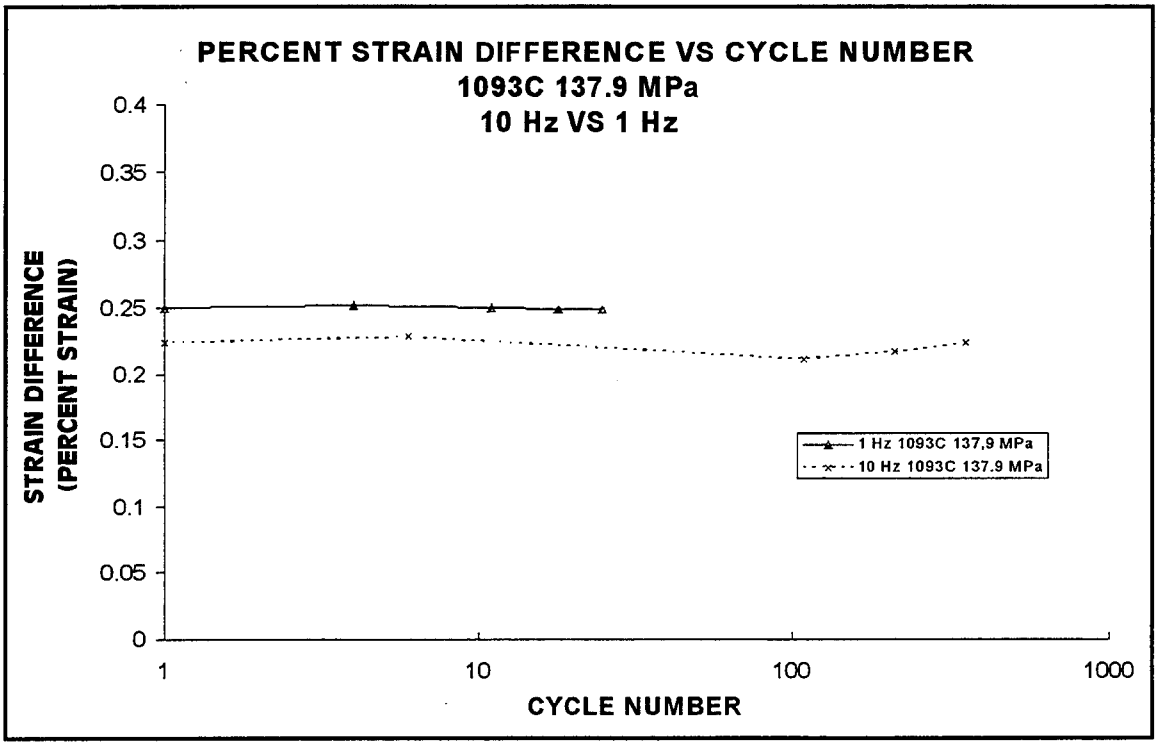

Figure 49. Strain Difference 1093°C 137.9 MPa 1 Hz vs 10 Hz

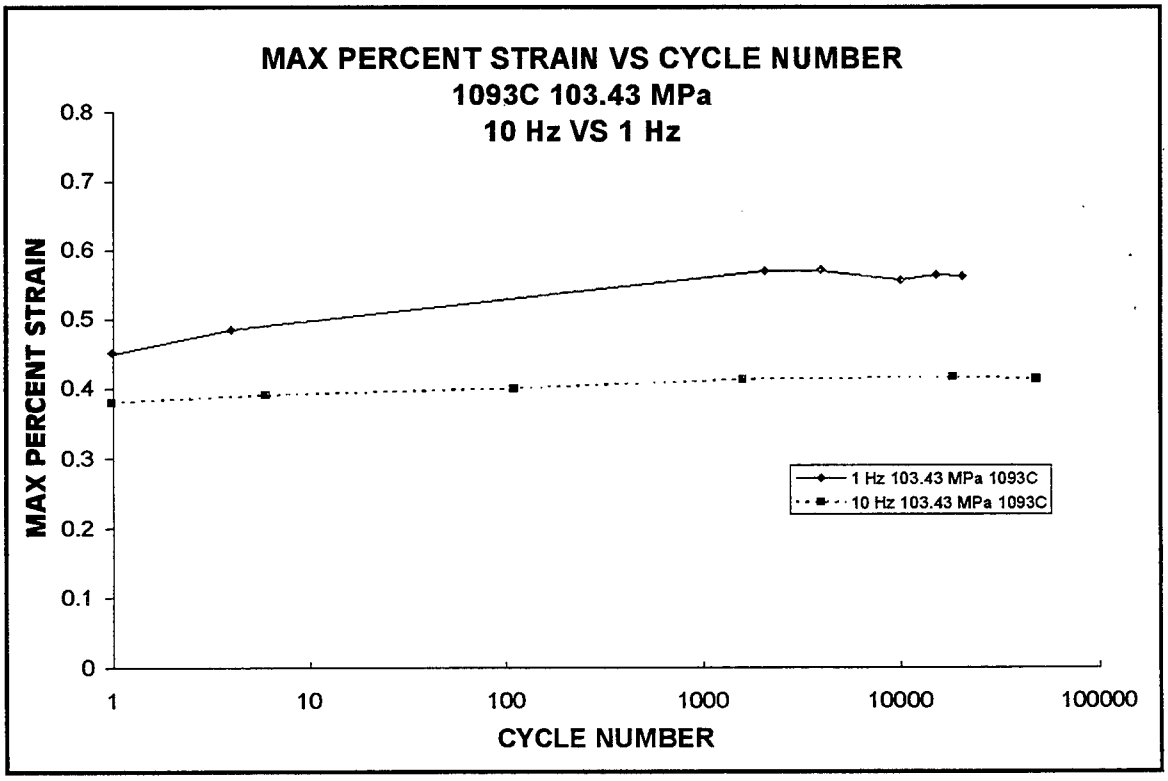

Figure 50. Maximum Strain 1093°C 103.43 MPa 1 Hz vs 10 Hz

show the same phenomenon and trend for the tests conducted at a maximum stress level of 103.43 MPa and a temperature of 1093°C. These are the same observations as were made for the tests that were conducted at the lower temperature. The reason for the strains being higher in the lower frequency tests at this temperature is the same as was discussed for the lower temperature tests.

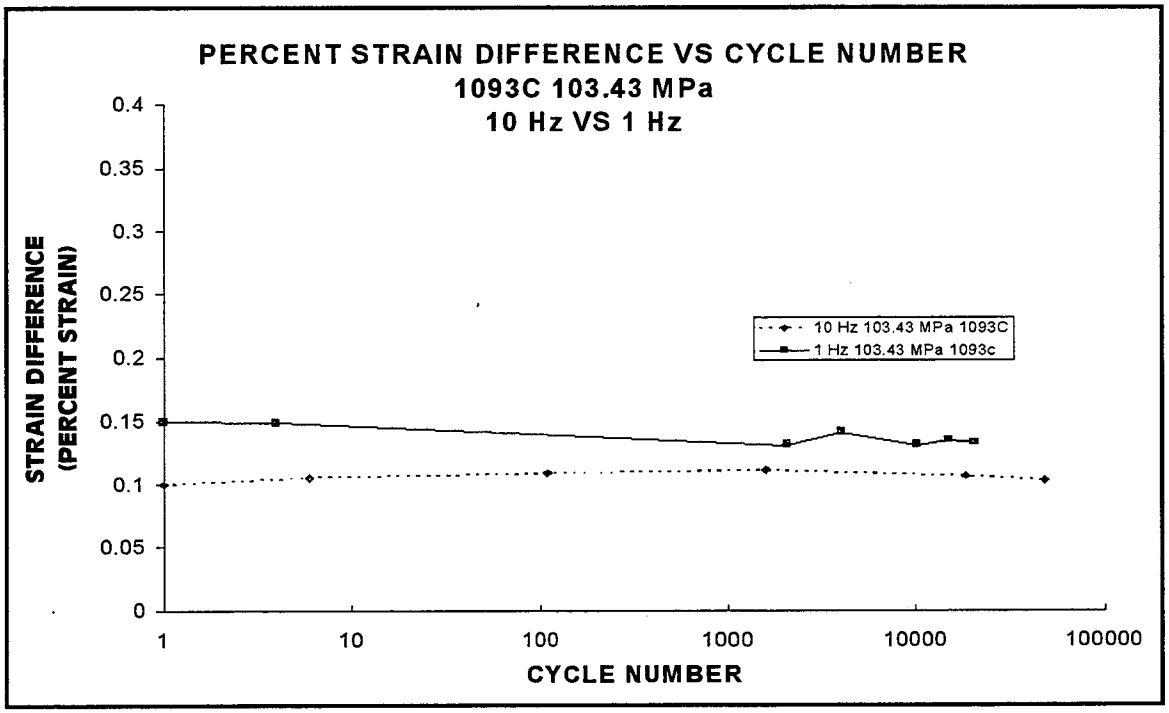

Figure 51. Strain Difference 1093°C 103.43 MPa 1 Hz vs 10 Hz

Figure 52 shows the strain difference for the test conducted at a frequency of 1 Hz, a temperature of 1093°C, and a maximum stress of 137.9 MPa plotted against the strain difference of the same test conducted at 10 Hz. The strain difference is plotted against time and shows that the fatigue life of the specimen is independent of the loading frequency. This is the same as was seen for the tests conducted at 566°C in Figure 39.

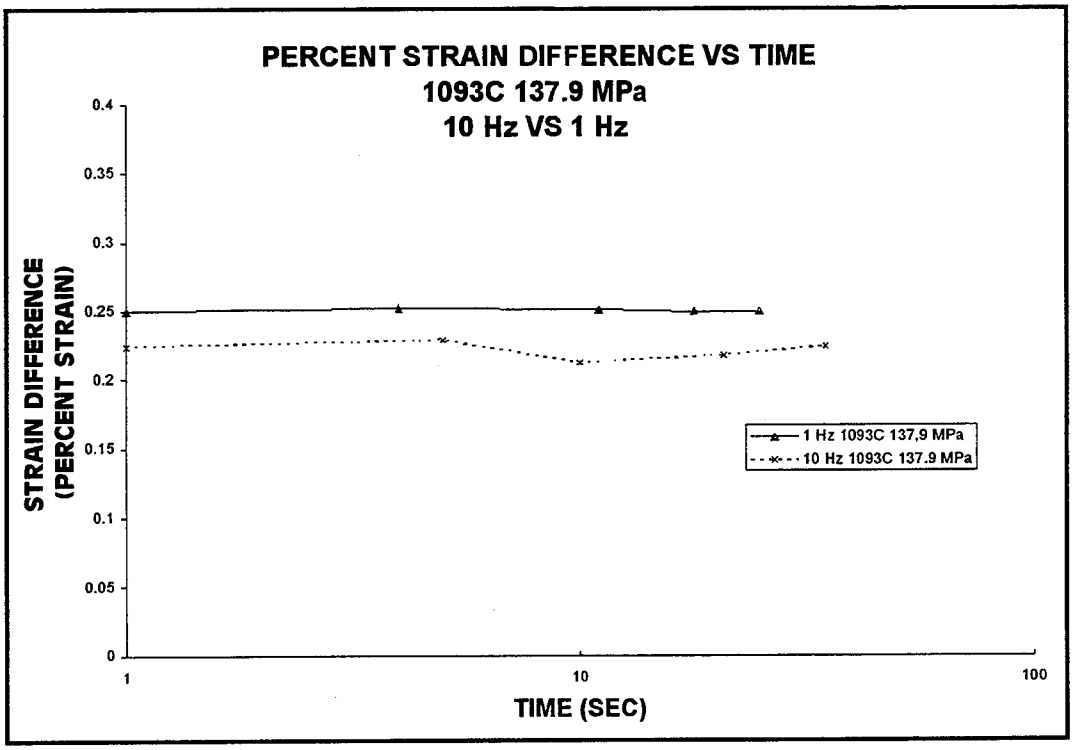

Figure 52. Strain Difference vs Time 1093°C 137.9 MPa 1 Hz vs 10 Hz

In summary, it has been shown that all of the specimens tested displayed a time dependent damage mechanism that was a result of the combination of stress and environmental influences, regardless of temperature or frequency. This can be seen in the strain difference plots of all the tests. These plots showed that for every test the difference between the maximum and minimum strain remained almost constant throughout the duration of the test.

It has also been seen that the tests conducted at a lower frequency induced a higher strain. This can be seen in Figures 37 through 41 and Figures 48 through 51. This can be attributed to the greater amount of time spent at the highest stress levels for the specimens tested at the lower frequencies. An illustration of this can be seen in Figure 53.

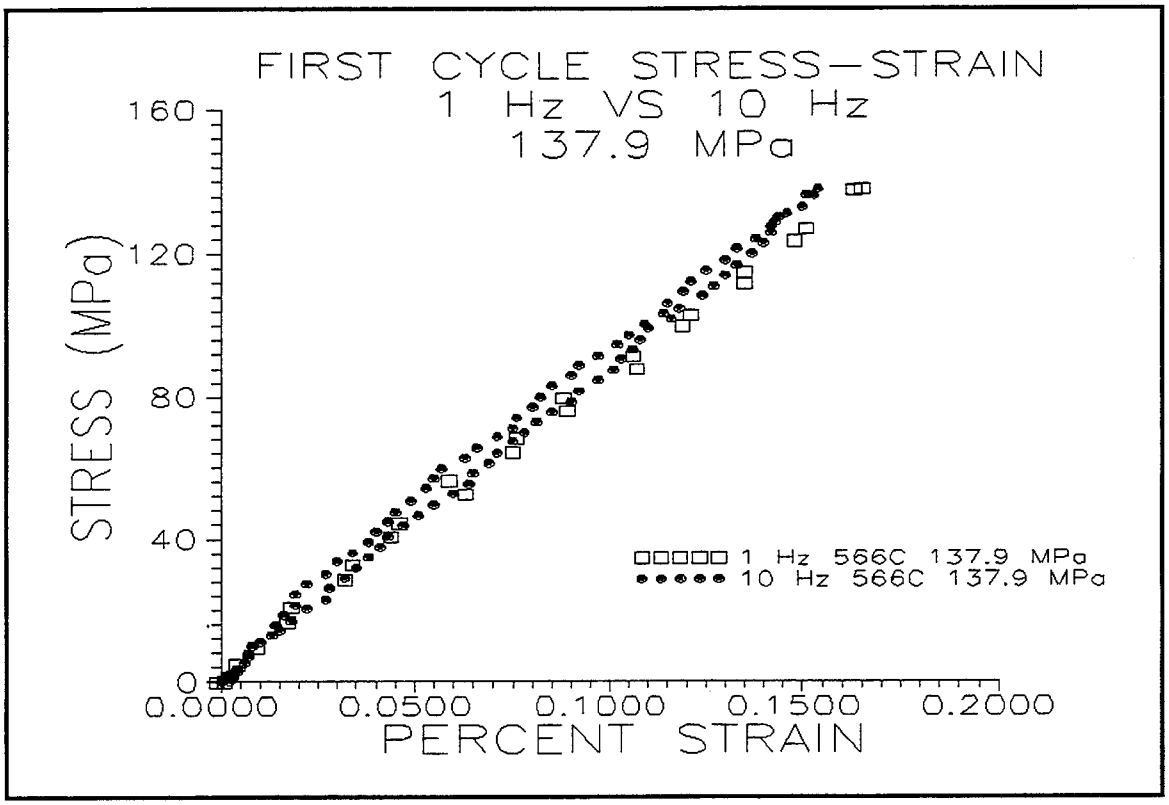

Figure 53. First Cycle Stress Strain 566°C 1 Hz vs 10 Hz

This figure shows that for the first cycle of fatigue loading at 137.9 MPa and a temperature of 566°C there was more strain in the test conducted at 1 Hz than there was for the test conducted at 10 Hz.

In the same manner it can be shown that, all things being equal, the higher the temperature, the higher the maximum strain. The specimens tested at higher temperatures showed more strain in the first cycle and then showed a greater tendency to creep under the subsequent fatigue loading at both frequencies. The difference in the strain between tests conducted at the two temperatures can be seen in Figure 54. This figure shows the first cycle stress-strain relationships for two of the tests conducted at 103.43 MPa. The

test conducted at 1093°C has both a lower initial modulus and a higher maximum strain for this first cycle.

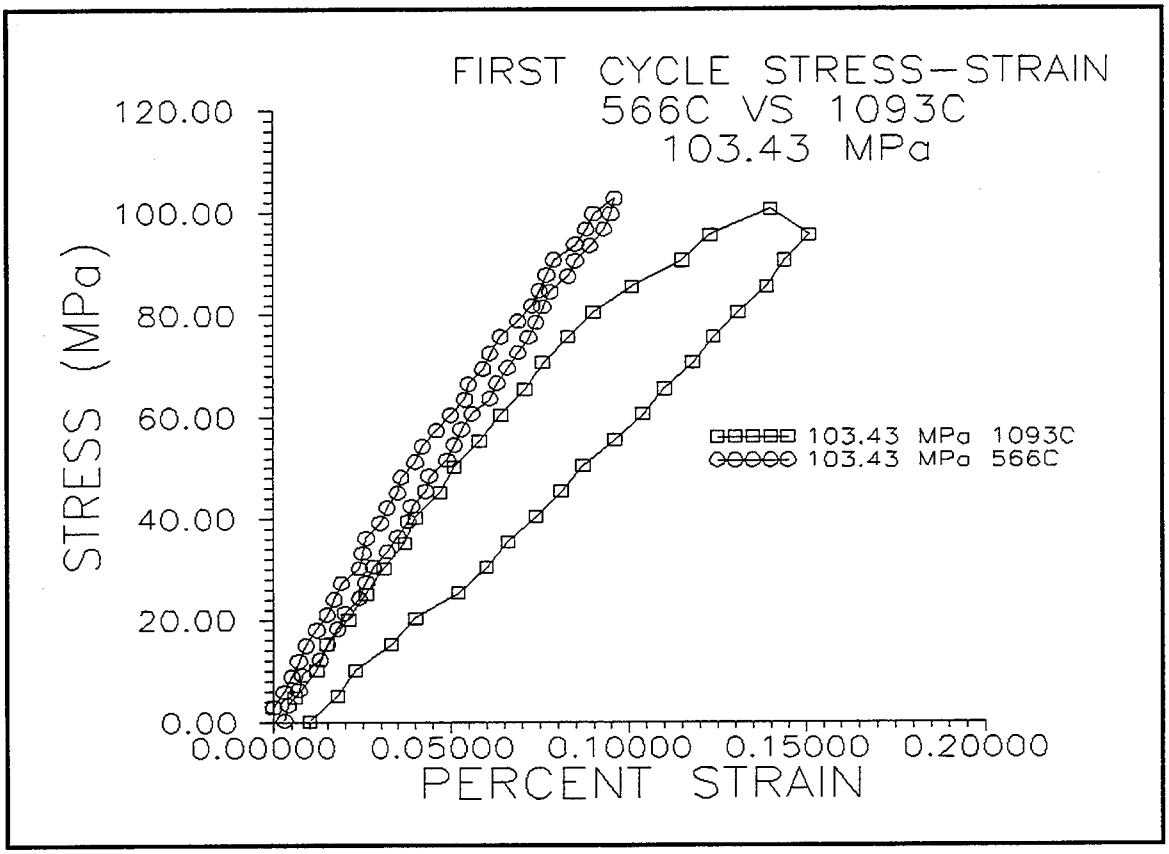

Figure 54. First Cycle Stress Strain 103.43 MPa 566°C vs 1093 °C

D.7. Strain Data 566°C vs 1093°C at 10 Hz. The greater amount of strain and tendency to creep at higher temperatures under cyclic loading is illustrated in Figures 55 through 62. Figure 55 shows that the maximum strain for the test conducted at 10 Hz and 1093°C/2000°F with a maximum stress level of 137.9 MPa is higher than that of the test conducted at 10 Hz and 566°C/1050°F at the same stress level. Figure 56 confirms that both of the tests were exhibiting a time dependent damage mechanism by showing that the

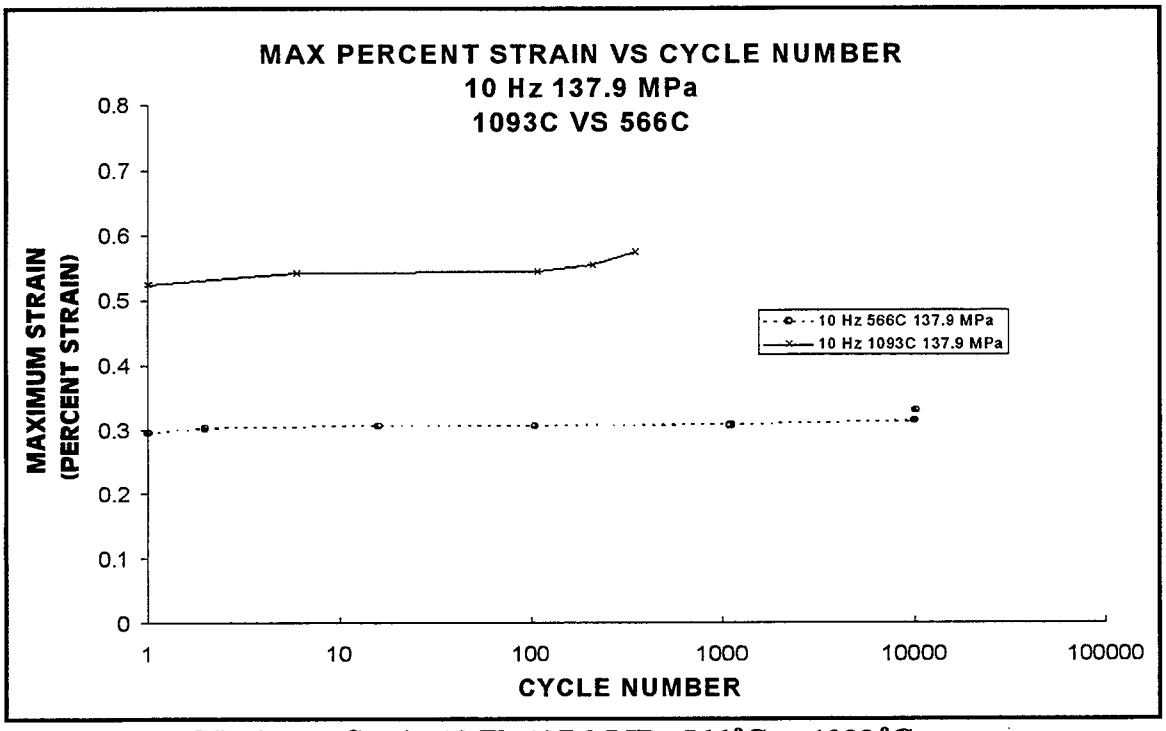

Figure 55. Maximum Strain 10 Hz 137.9 MPa 566 °C vs 1093 °C

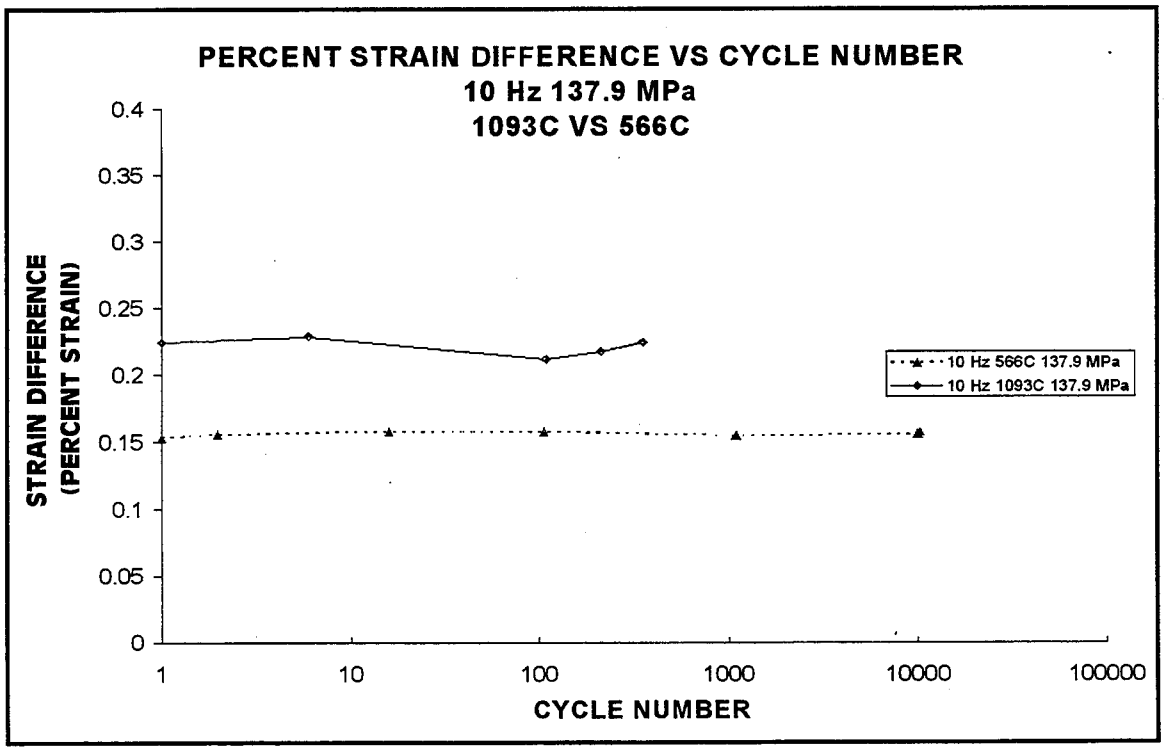

Figure 56. Strain Difference 10 Hz 137.9 MPa 566 °C vs 1093 °C

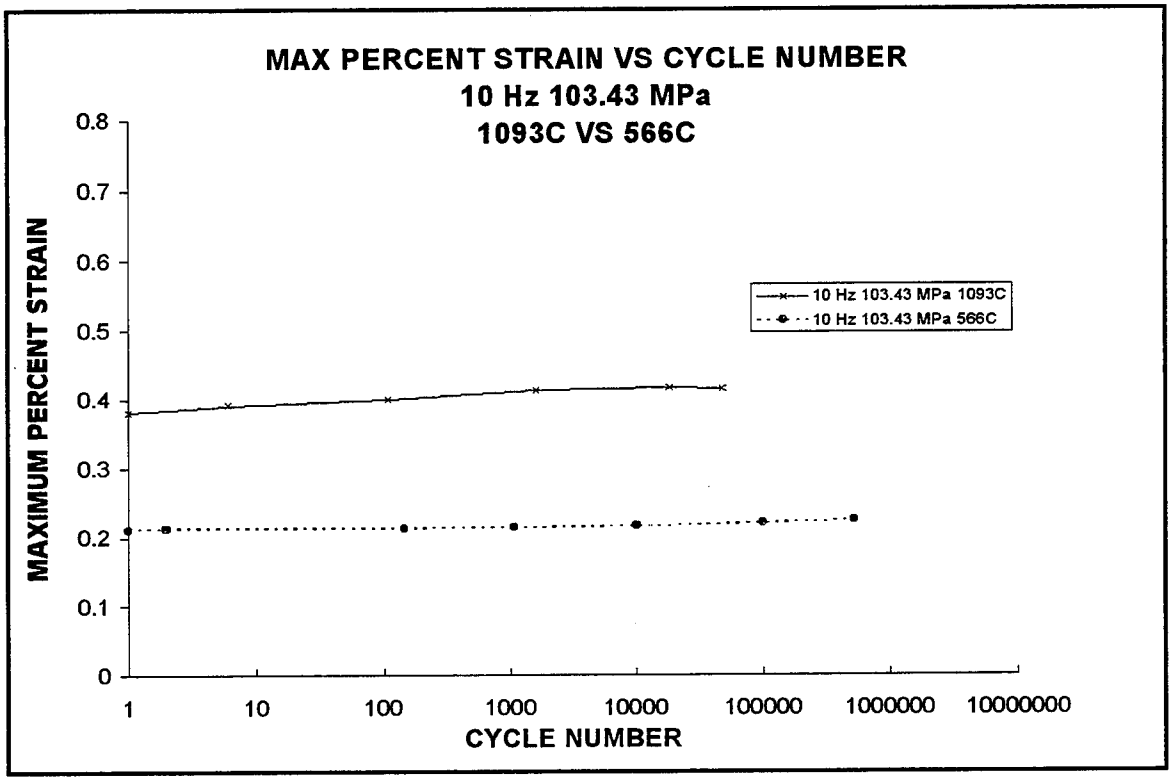

Figure 57. Maximum Strain 10 Hz 103.43 MPa 566 °C vs 1093 °C

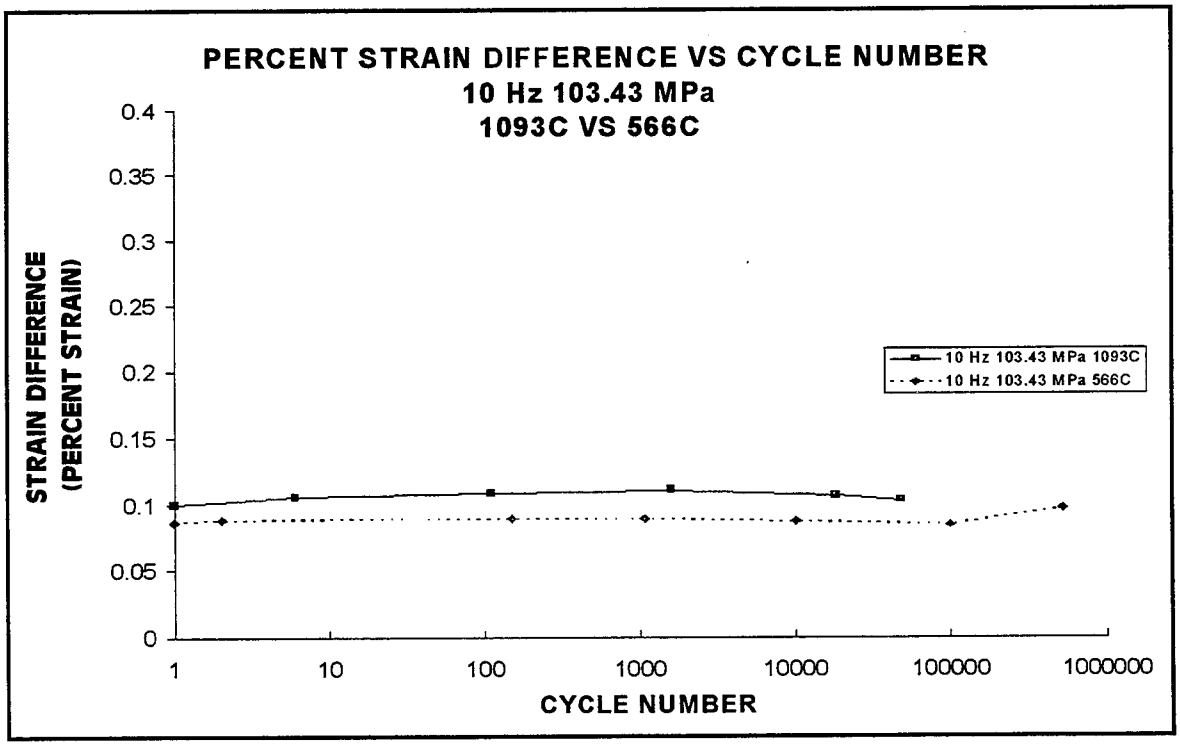

Figure 58. Strain Difference 10 Hz 103.43 MPa 566 °C vs 1093 °C

strain differences remain constant. Figures 57 and 58 show the same results for the tests conducted with a maximum stress level of 103.43 MPa and a frequency of 10 Hz.

D.8. Strain Data 566°C vs 1093°C at 1 Hz. Figure 59 shows that the test conducted at 1 Hz and 1093°C/2000°F with a maximum stress level of 137.9 MPa reaches a greater maximum strain than the test conducted at 1 Hz and 566°C/1050°F with the same stress level. Figure 60 confirms that both of the tests were exhibiting the time dependent damage mechanism by showing that the strain differences remain constant. Figures 61 and 62 show the same thing for the tests conducted with a maximum stress level of 103.43 MPa and a frequency of 1 Hz.

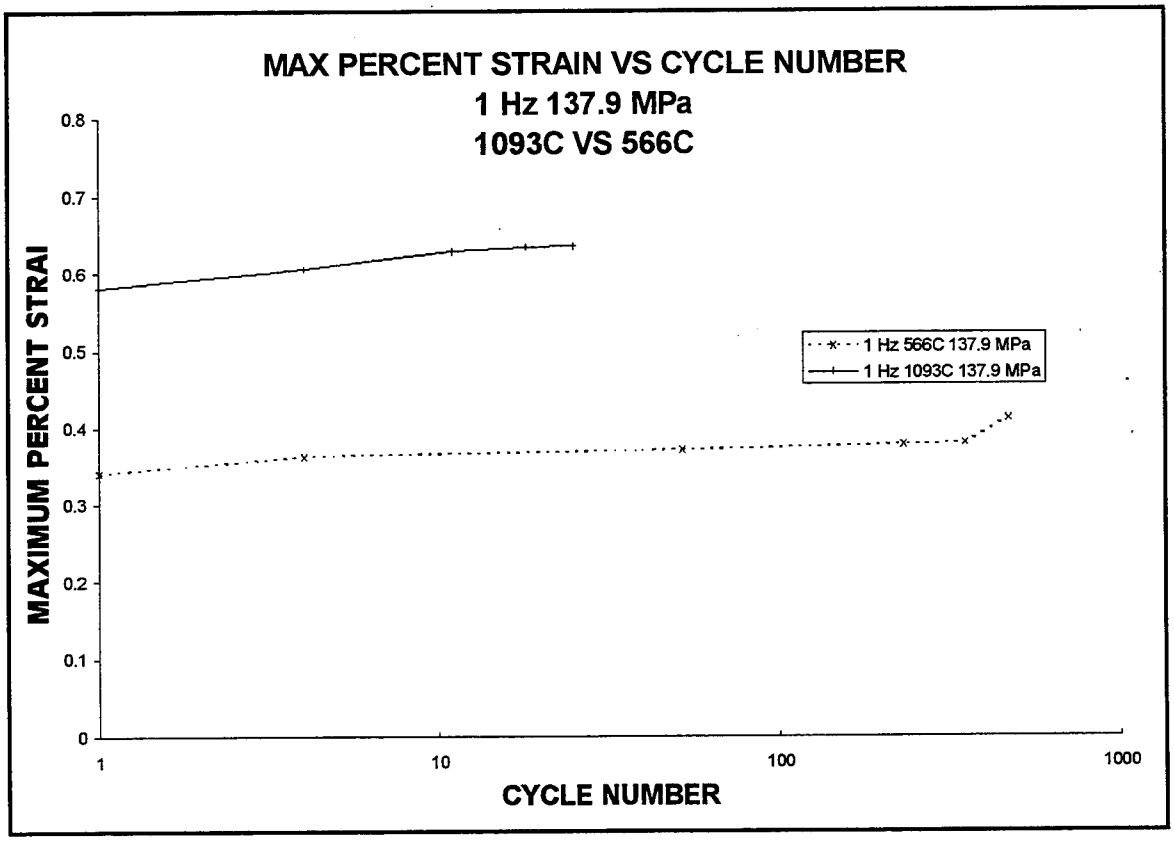

Figure 59. Maximum Strain 1 Hz 137.9 MPa 566°C vs 1093°C

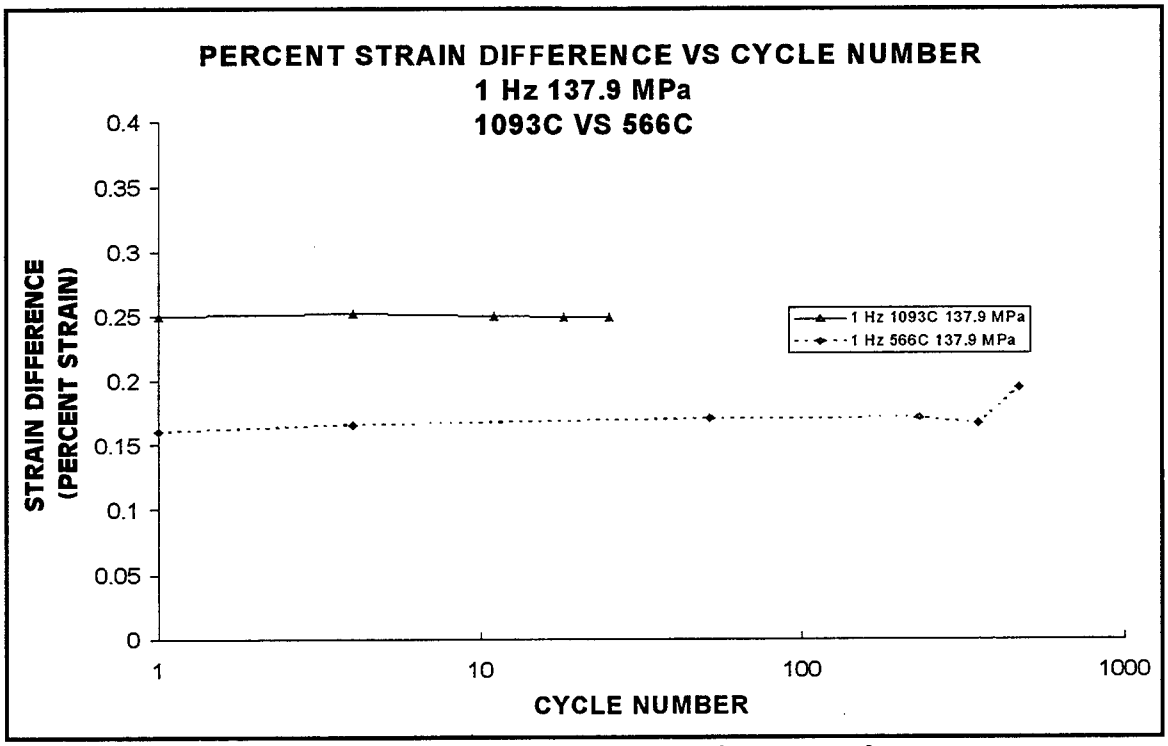

Figure 60. Strain Difference 1 Hz 137.9 MPa 566 °C vs 1093 °C

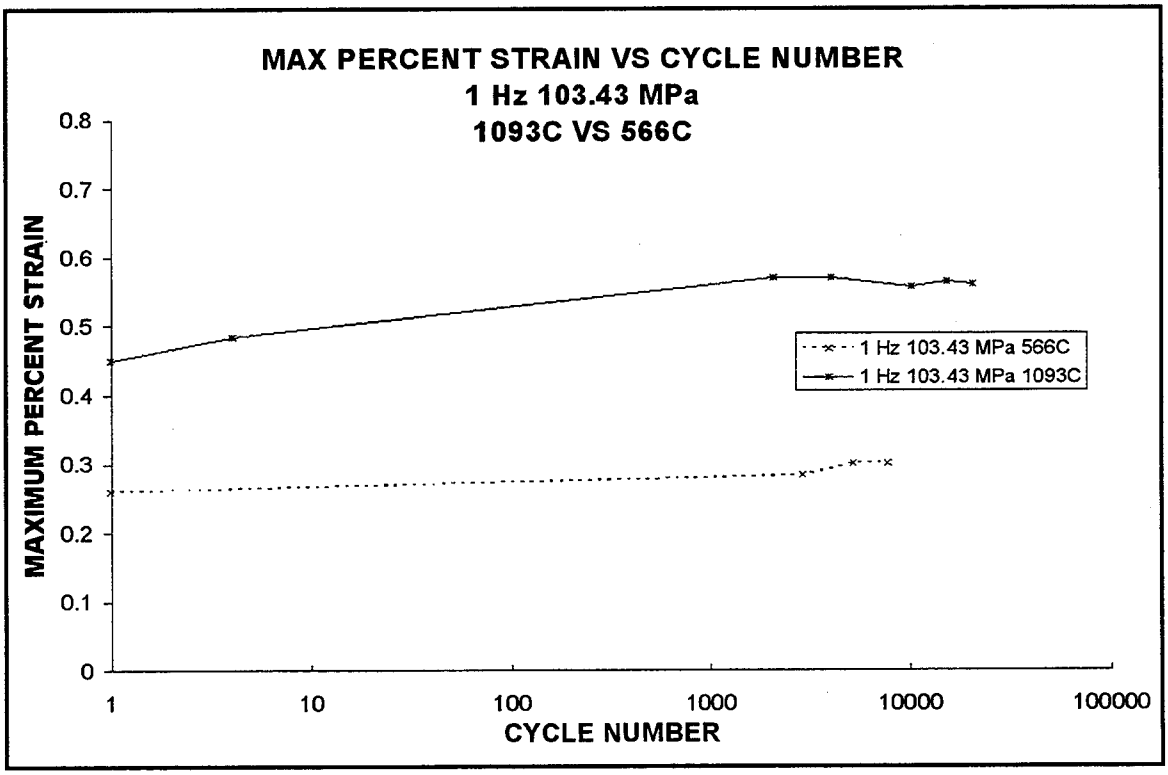

Figure 61. Maximum Strain 1 Hz 103.43 MPa 566 °C vs 1093 °C

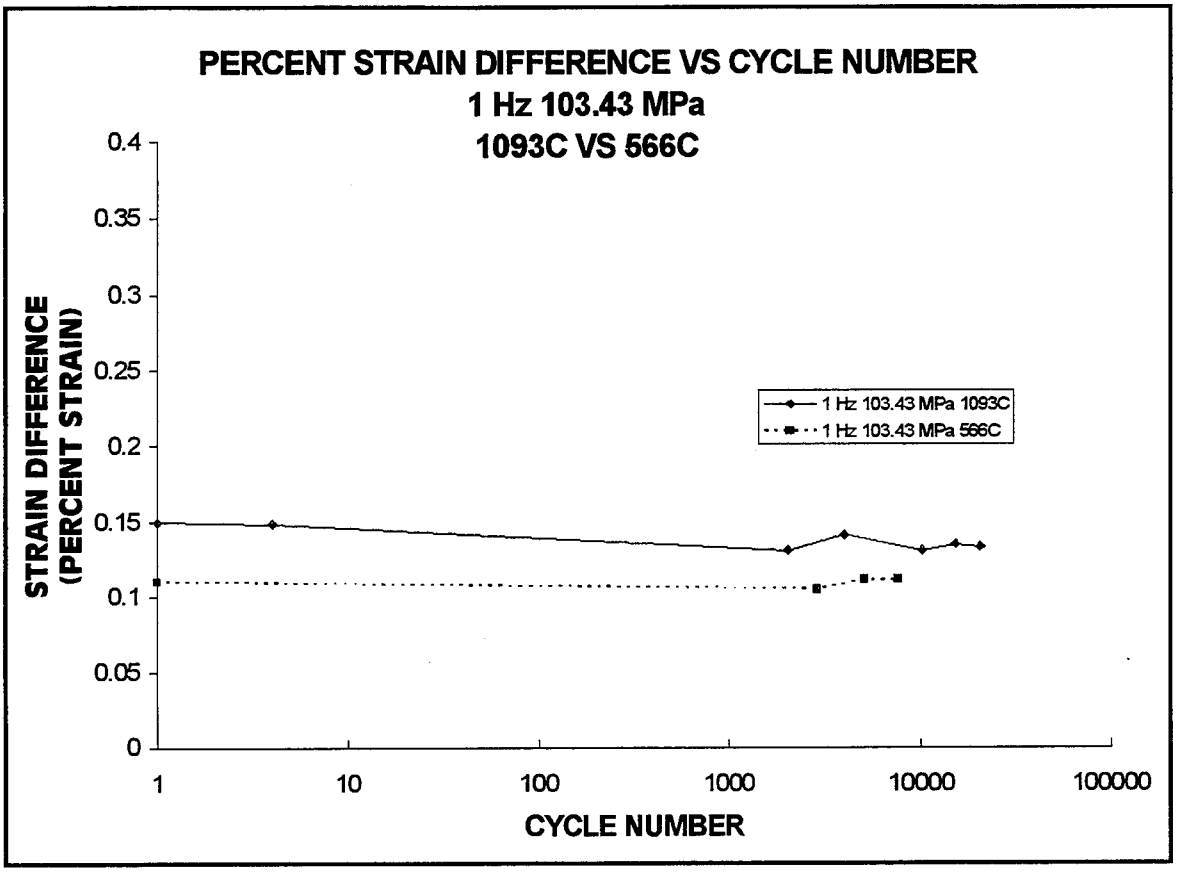

Figure 62. Strain Difference 1 Hz 103.43 MPa 566 °C vs 1093 °C

In summary, analysis of the strain data shows that the material experiences the phenomenon of creep deformation at both of the temperatures investigated in this study. This can be seen by examining the strain difference trends of all the tests. Both temperature and frequency have an effect on the amount of creep. There is more creep at the higher temperature, as can be seen in sections D.7., and there is more creep at the lower frequency, as can be seen in sections D.3. and D.6. In this context, creep is a time dependent damage mechanism induced by a combination of stress and environmental effect (temperature).

E. Hysteresis Loops

Another way to look at the same data is to look at the area inside the hysteresis loops of the stress strain data. This gives a measure of the energy per unit volume that the specimen is absorbing at each cycle. This energy was computed from the area inside the stress-strain hysteresis recorded during cycling.

E.1. Energy Loops 566°C. Figure 63 shows how the area inside the hysteresis loop varies as the specimens are cycled for the tests run at 566°C/1050°F and 10 Hz. This graph shows that the amount of energy absorbed by the material decreases from a maximum at the first cycle until about 10,000 cycles. At this point the amount of energy absorbed increases until the specimen eventually fails. The greater the stress applied to the specimen, the more energy per unit volume it is absorbing.

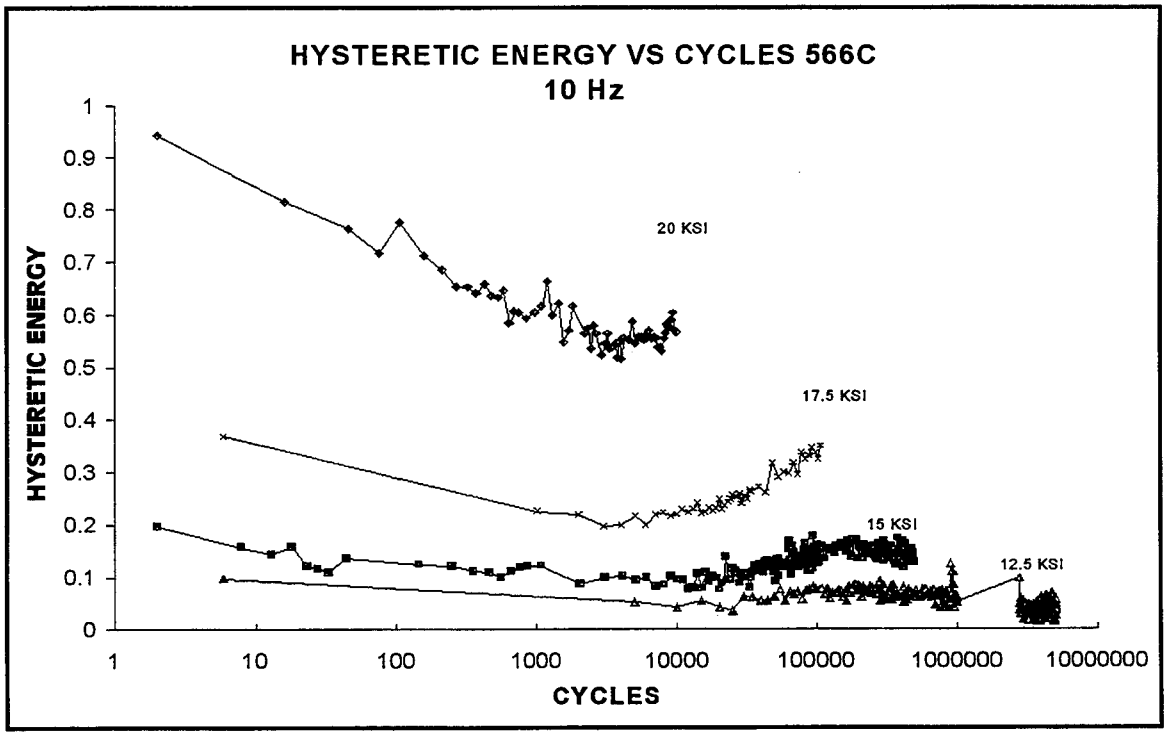

Figure 63. Hysteretic Energy 10 Hz 566°C

Figure 64 shows how the area inside the hysteresis loop varies as the specimens are cycled for the tests run at 566°C/1050°F and 1 Hz. This graph shows that the amount of energy absorbed by the material decreases from a maximum at the first cycle until about 1,000 cycles. At this point the amount of energy absorbed increases until the specimen eventually fails. This indicates that the point at which the specimen begins to absorb more energy and approach failure is a function of the amount of time the specimen has been cycled. This indicates that the frequency of the cyclic loading is not as big a factor as the length of exposure in determining the length of the test. This lends support to the results from the analysis of the fatigue life curves, which indicate that the fatigue life of this material is dependent on the temperature of the environment but not the frequency of the loading.

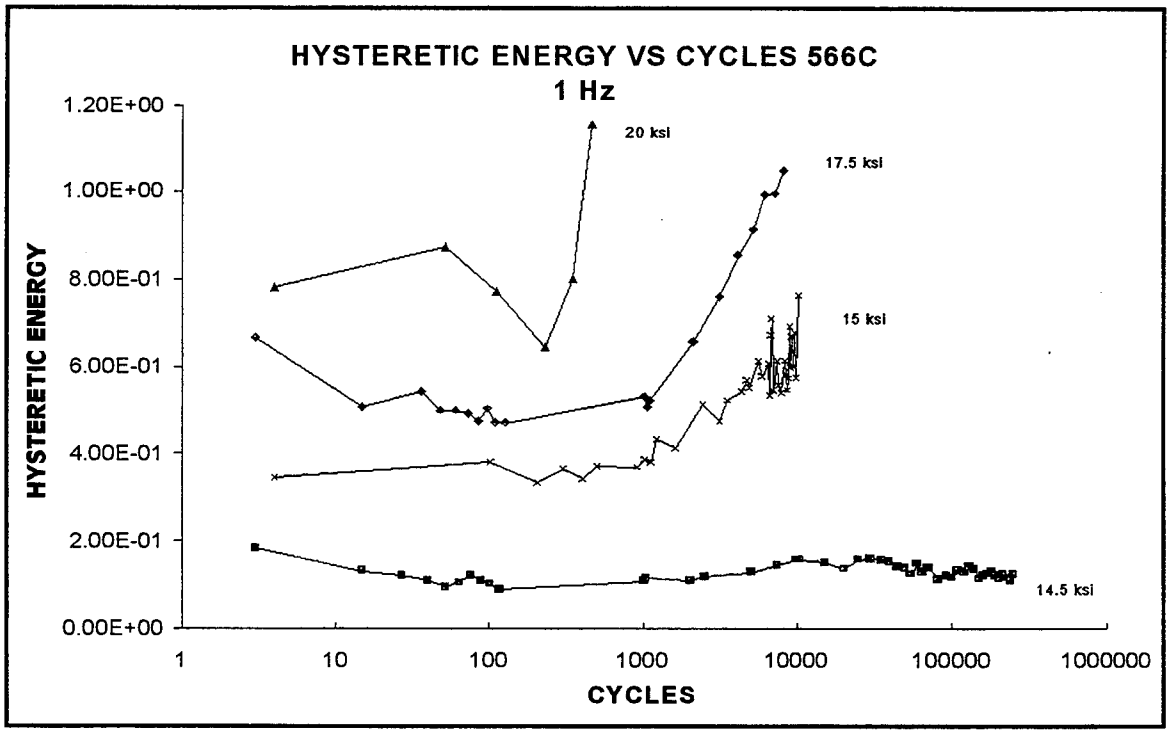

Figure 64. Hysteretic Energy 1 Hz 566°C

This point is illustrated in Figure 65, which compares the two tests run at 566°C/1050°F and a maximum stress of 120.66 MPa. The specimen that was run at 1 Hz absorbed more energy but the specimens both failed in the same amount of time and they both began to absorb more energy at the same time into the test. This point is again

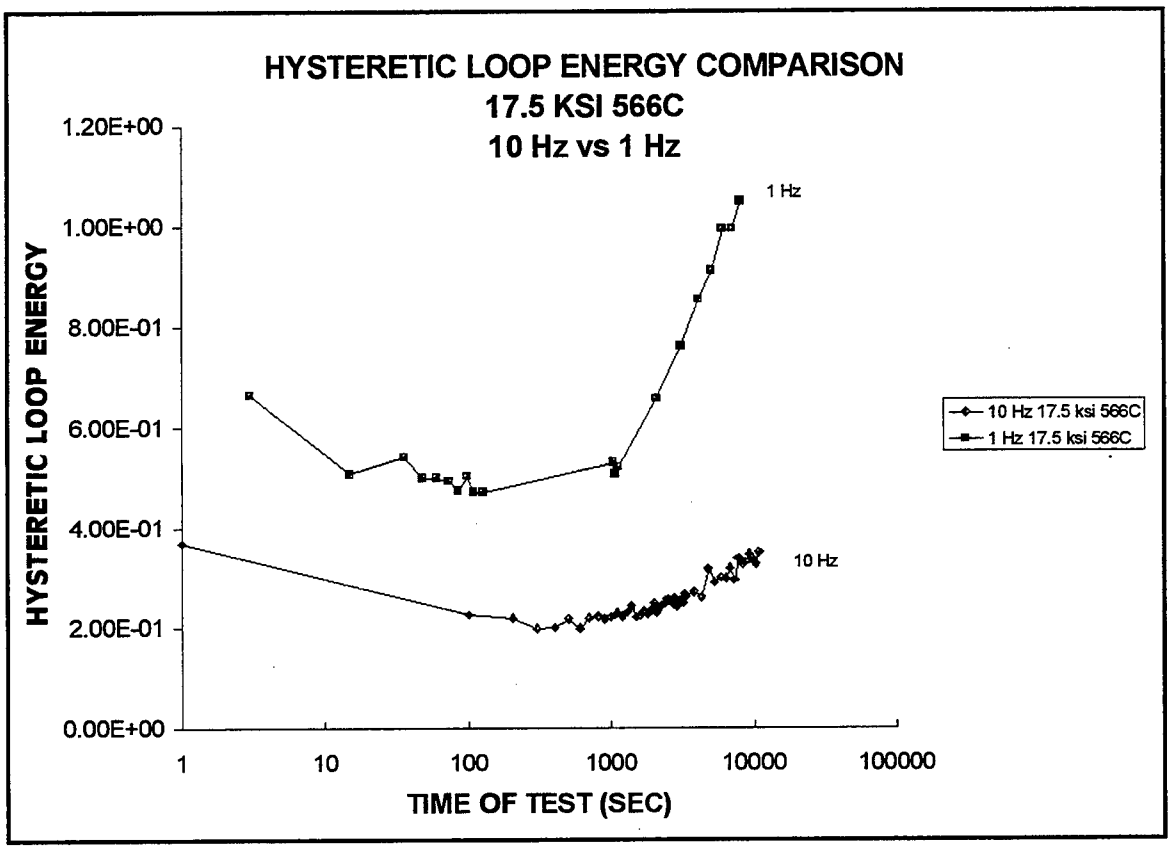

Figure 65. Hysteretic Energy 566°C 120.66 MPa 1 Hz vs 10 Hz

illustrated in Figure 66, which compares the two tests run at 566°C/1050°F and a maximum stress of 103.43 MPa. The similarity of the curves in these two charts support the idea that the fatigue behavior is the same for 1 Hz and 10 Hz.

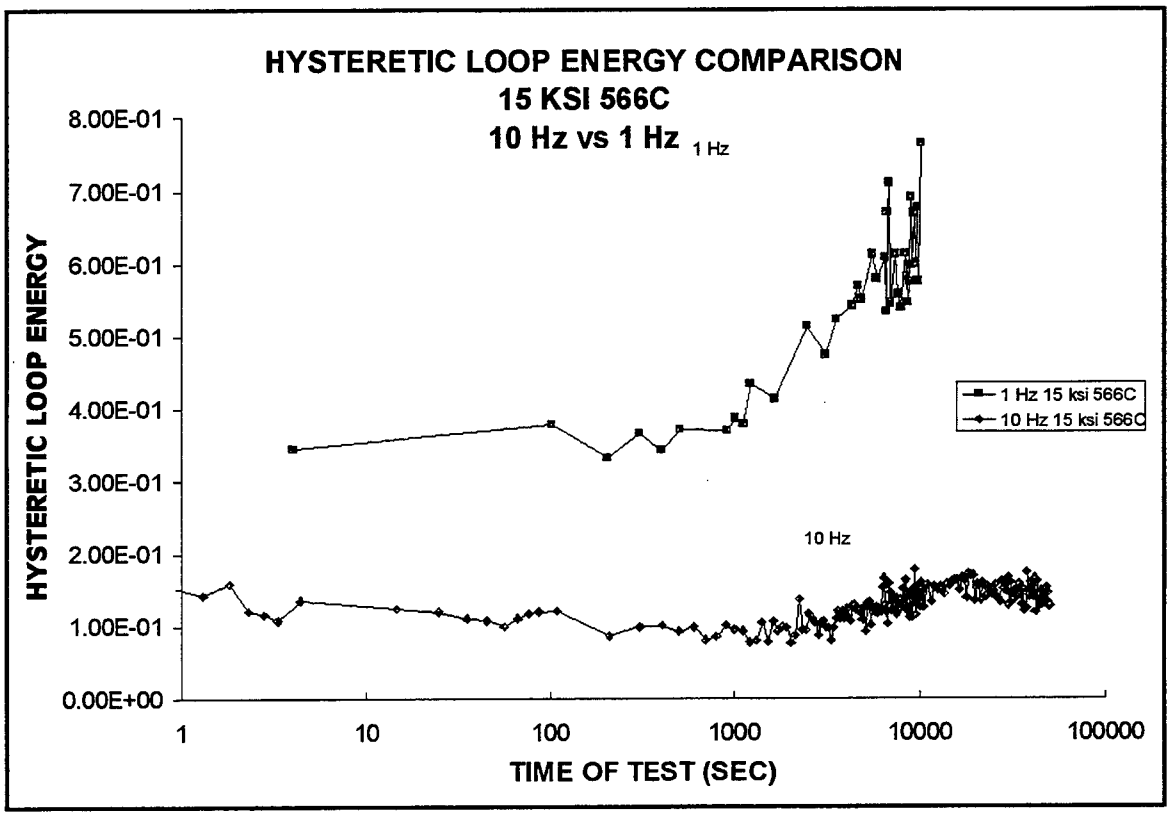

Figure 66. Hysteretic Energy 566°C 103.43 MPa 1 Hz vs 10 Hz

E.2. Energy Loops 1093°C. Figure 67 shows how the area inside the hysteresis loop varies as the specimens are cycled for the tests run at 1093°C/2000°F and 10 Hz. This graph shows that the amount of energy absorbed by the material decreases, from a maximum at the first cycle, until failure. The greater the stress applied to the specimen, the more energy per unit volume it is absorbing. This is the same pattern as was exhibited by the specimens that were tested at 566°C/1050°F and 10 Hz

Figure 68 shows how the area inside the hysteresis loop varies as the specimens are cycled for the tests conducted at 1093°C/2000°F and 1 Hz. This graph shows that the

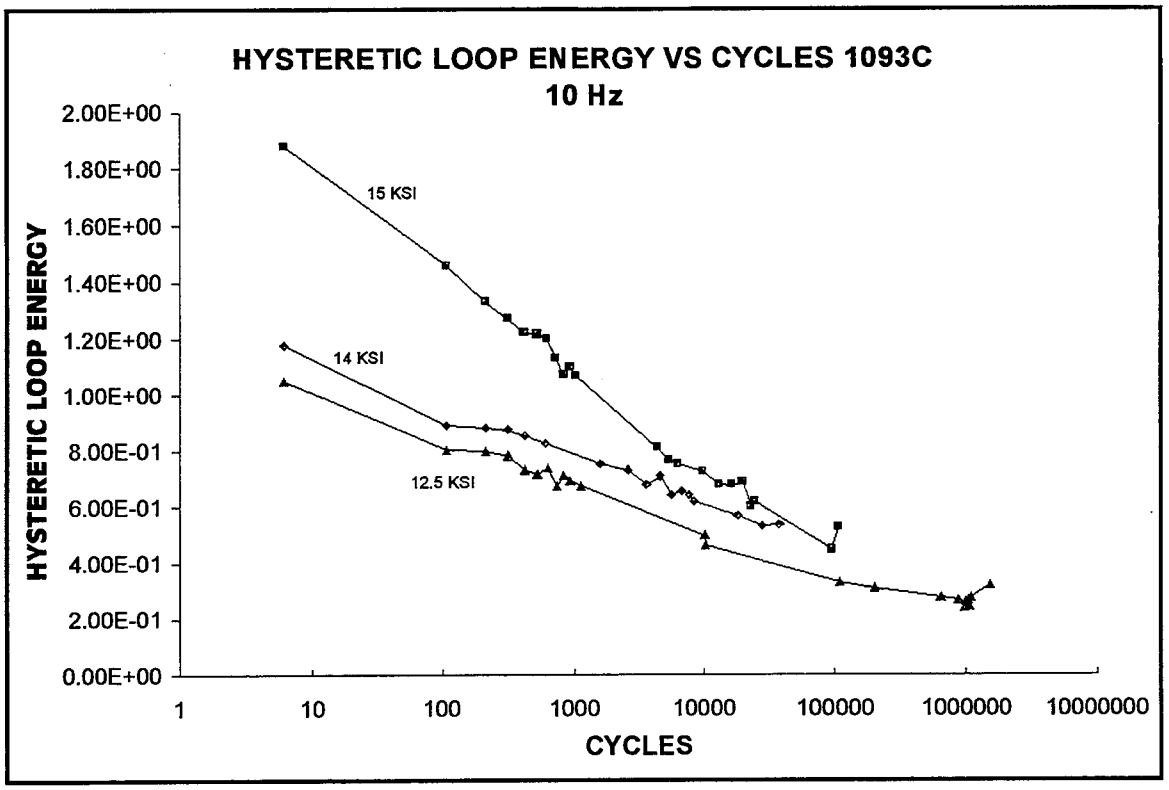

Figure 67. Hysteretic Energy 1093°C 10 Hz

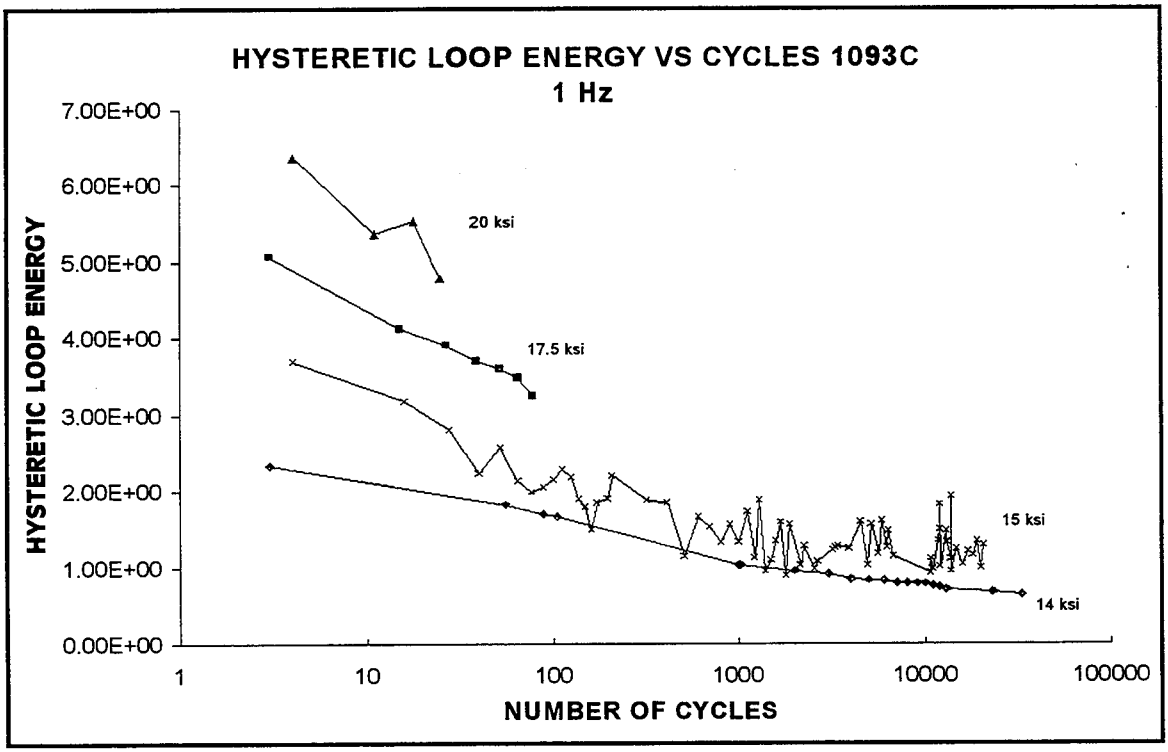

Figure 68. Hysteretic Energy 1093°C 1 Hz

amount of energy absorbed by the material decreases from a maximum at the first cycle until failure.

Figure 69 is a comparison of tests conducted at a temperature of 1093°C/2000°F with a maximum stress of 96.53 MPa. It indicates that at this temperature, for a given stress level, the material will degrade to a point where it is unable to absorb enough energy per cycle and will fail, regardless of the rate at which the load is applied. Figure 70 makes the same comparison for the 103.43 MPa stress level and leads to the same conclusion. This again indicates the similarity of the fatigue behavior at 1 Hz and 10 Hz.

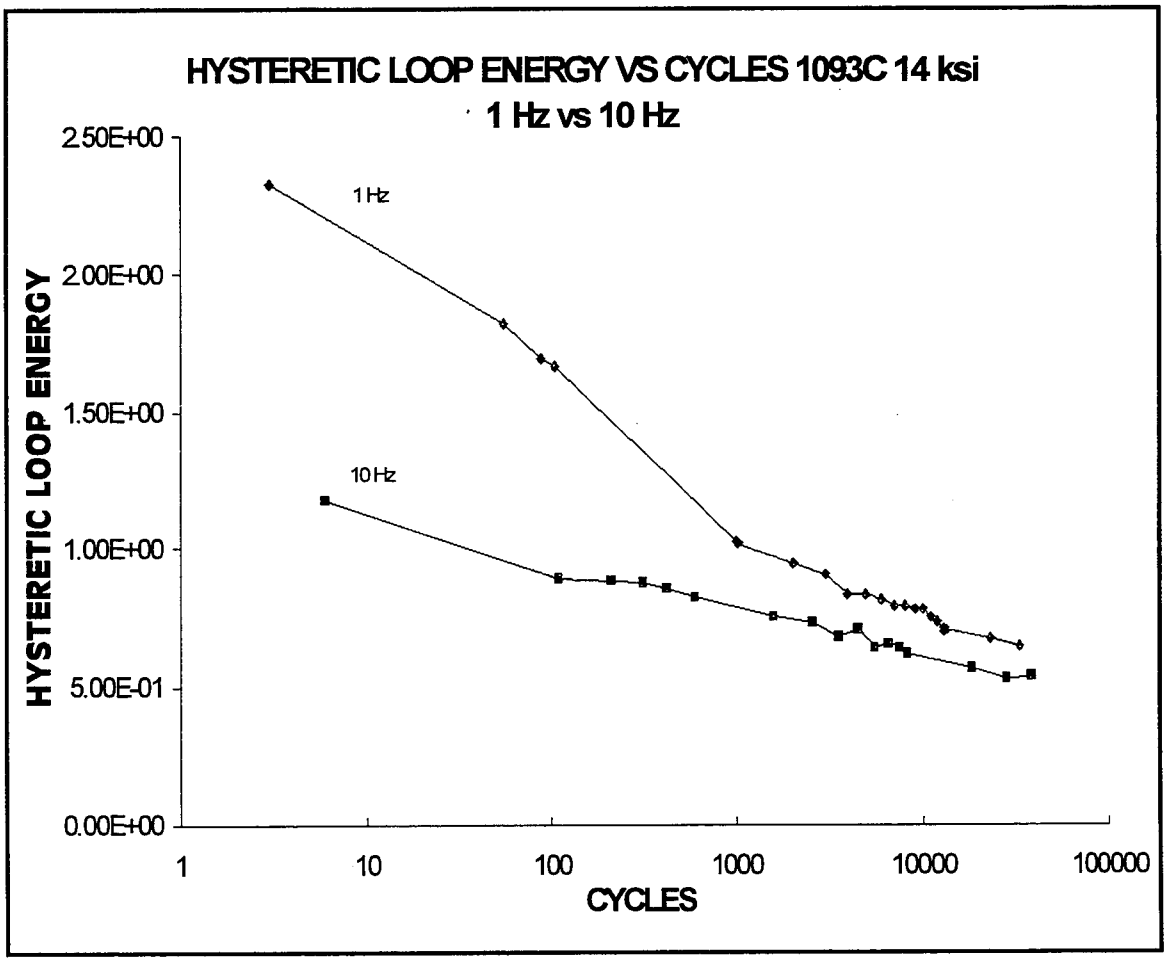

Figure 69. Hysteretic Energy 1093°C 96.53 MPa 1 Hz vs 10 Hz

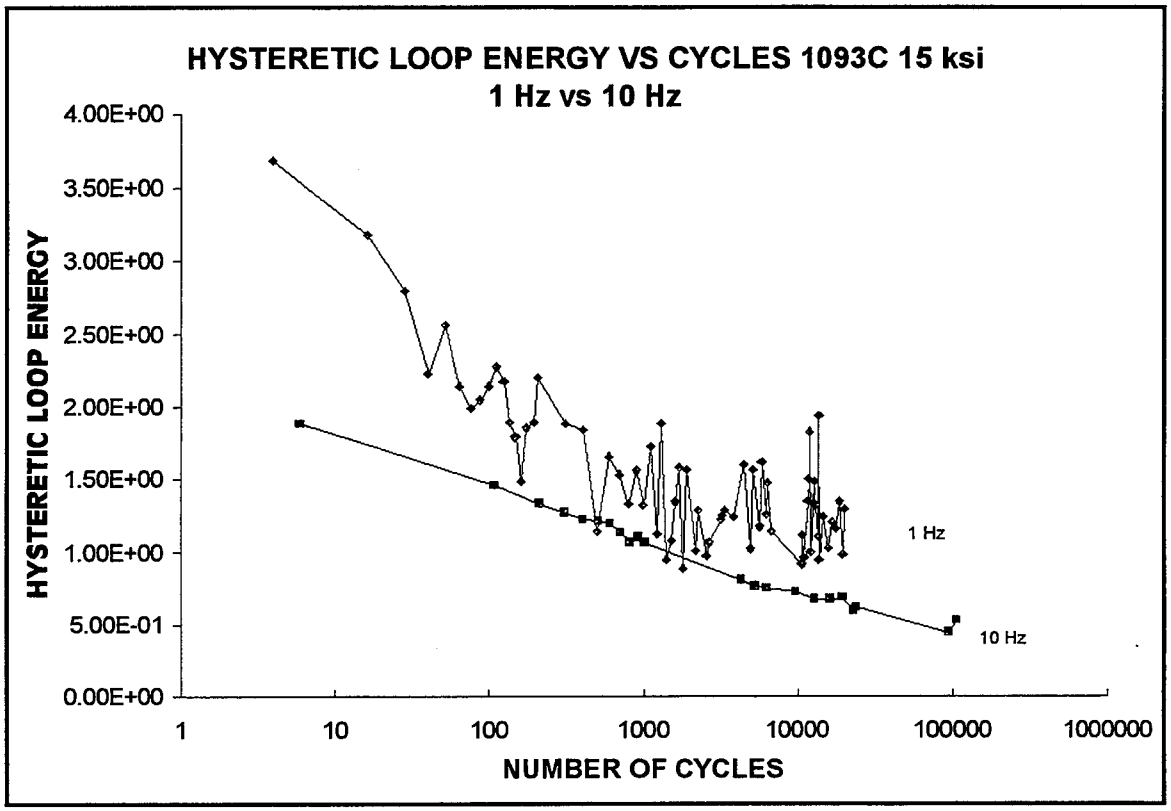

Figure 70. Hysteretic Energy 1093°C 103.43 MPa 1 Hz vs 10 Hz

F. Damage Mechanisms

Postmortem microscopic examination of the failed specimens showed that the primary failure mechanisms for this material under tension-tension fatigue loading were a combination of the development of matrix cracks in both the 0° and 90° plies and then coalescence of these cracks along fiber-matrix interfaces and an environmentally assisted crack growth due to the oxidation of the fiber matrix interface. This resulted in the transfer of load to the debonded fibers which eventually caused fracture due to tensile overload. This observation was consistent across both temperatures and both frequencies. There were two types of examinations performed. The first was the examination of the

polished edge of the specimens using optical microscopy and the second was the inspection of the fracture surface using a scanning electron microscope.

The term oxidation is used in two different contexts in the following discussion. There is an oxidation of the fiber-matrix interface which strengthens the bond between the fiber and matrix and causes a more brittle fracture. This type of oxidation is manifested in the form of a planar fracture surface with very little fiber pullout. The other type of oxidation referred to in this discussion is the progression of the effect of the environment along the debonded fiber-matrix interfaces. This form of oxidation is manifested in the form of a rough surface on the lengths of fibers that have pulled out.

F.1. Monotonic Tensile Tests. The first step towards the understanding of the damage mechanisms of the specimens tested under monotonic tension tests was to observe the fracture profiles of the failed specimens. Figure 71 shows the fracture profile of the specimen that was tested at 566°C. This specimen exhibits a very jagged and uneven profile which is indicative of a weak interfacial bond between the fibers and the matrix. This observation is similar to the fast fracture results obtained by Larsen [7] with this material and the profile is similar in appearance to that obtained by Agins [2] at 700°C with the SiC/CAS system. Figure 72 is a profile of the monotonic tensile specimen which was tested at a temperatures of 1093°C. This specimen exhibits a profile which is much more planar and exhibits a short amount of fiber pullout. The planar nature of the fracture surface of the fast fracture test specimen at high temperature is indicative of the strengthening of the fiber matrix interface by the process of oxidation. This oxidation strengthens the initially weak bond between the fiber and matrix and causes the specimen to have a fracture surface which is more brittle in nature. This is the same as the results

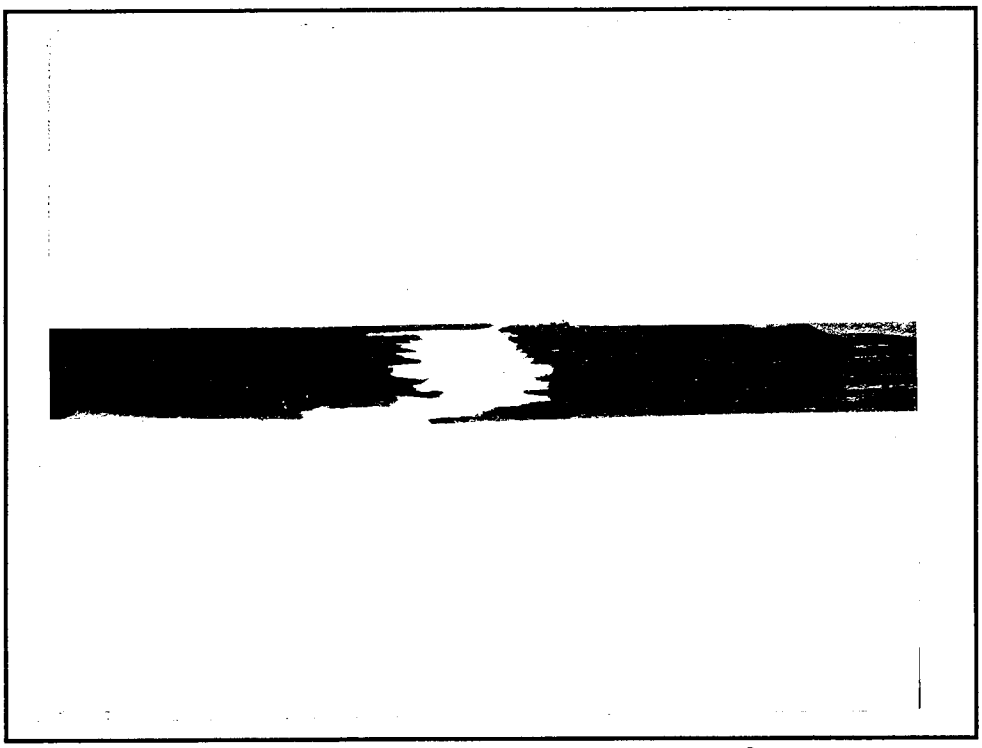

Figure 71. Fracture Profile, Monotonic Tensile, 566°C, 7X

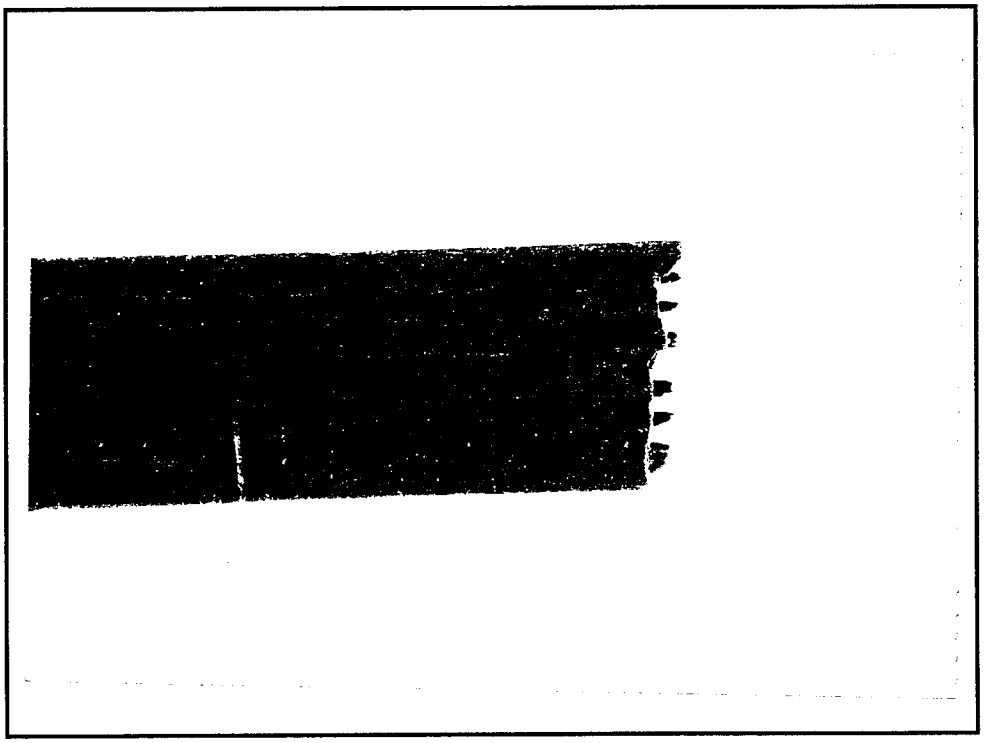

Figure 72. Fracture Profile, Monotonic Tensile, 1093°C, 10X

obtained by Larsen [7] and Grant [5] with this CMC system. Figure 73 is an oblique view of the fracture surface of the specimen tested at 1093°C and confirms that the oxidation progressed inward from the cut edges as evidenced by the flat planar fracture surface along the outer edge of the specimen.

Figure 74 is an oblique view of the fracture surface of the monotonic tensile specimen which was tested at 566°C. This photograph illustrates the rough, irregular, fibrous nature of the fracture surface which is indicative of a lot of matrix damage and minimal interface strengthening through the process of oxidation.

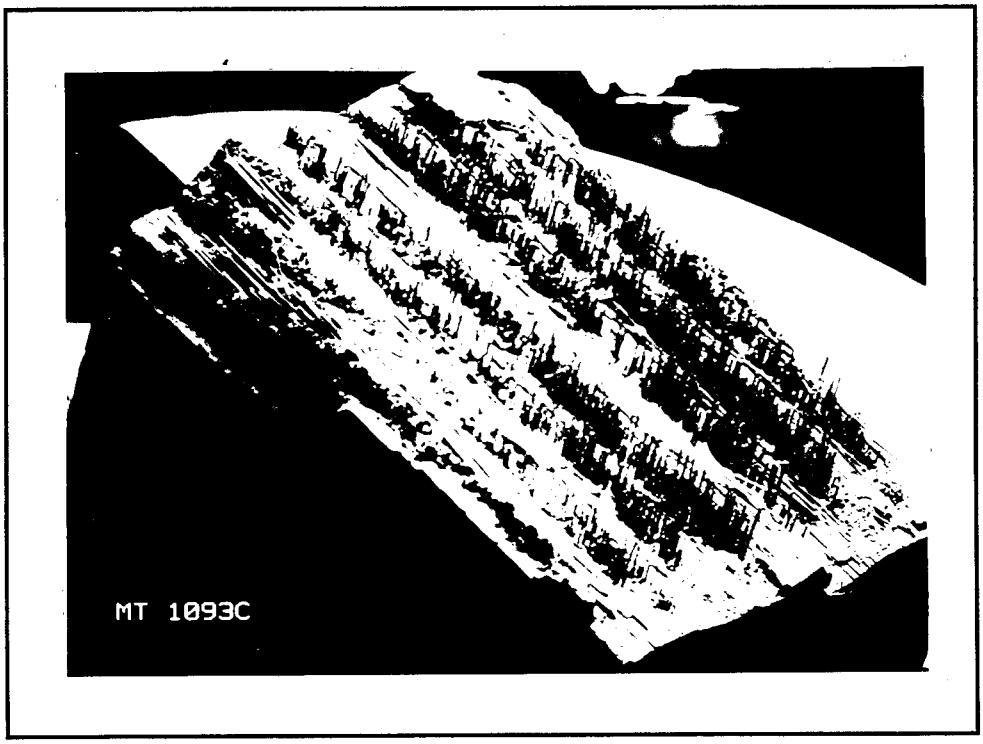

Figure 73. Fracture Surface, Monotonic Tensile, 1093 °C, 20.4X

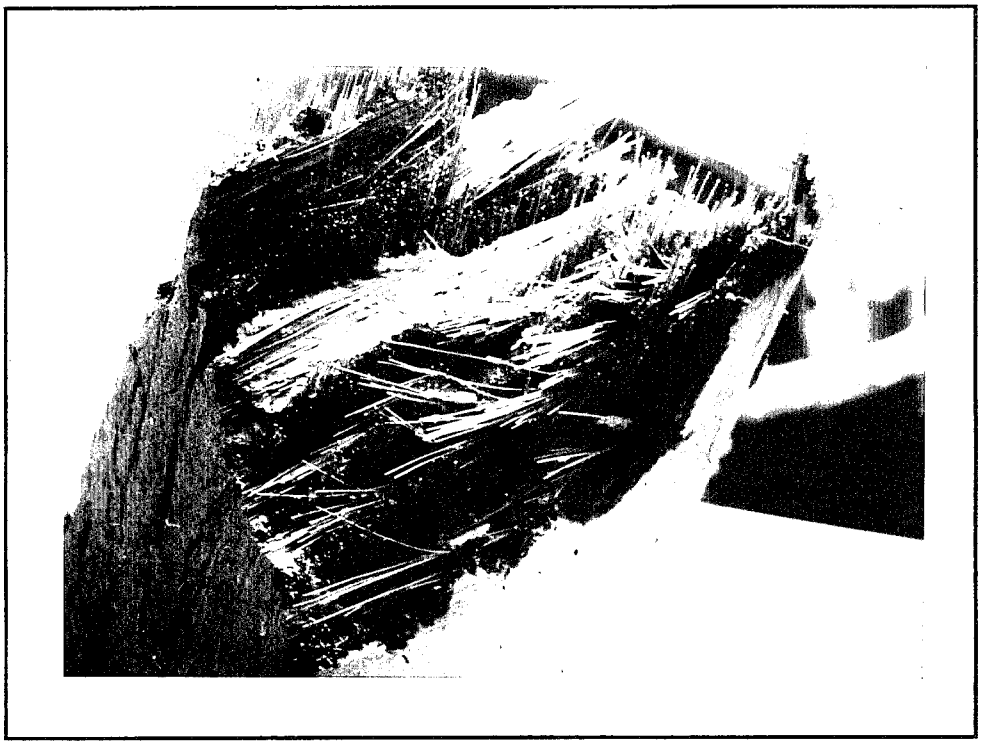

Figure 74. Fracture Surface, Monotonic Tensile, 566°C, 15.2X

F.2. Fracture Surface 10 Hz 566°C. The first step in the analysis of the fracture surfaces from this series of tests was the examination of the polished edges of the failed specimens using an optical microscope. This examination showed that there was some amount of matrix microcracking near the fracture surface. This matrix cracking is consistent with the behavior of ceramic matrix composites which will develop cracks in the 90° plies, transverse to the loading direction, when loaded beyond the proportional limit. Each of the tests performed in this study was conducted at a maximum stress level above the proportional limit. Transverse cracks were found in all specimens tested at a frequency of 10 Hz and a temperature of 566°C and typically extended across an entire

90° ply and in some cases extended through the fibers of a 0° ply. An example of a crack found in this series of tests can be seen in Figure 75.

Figure 75. Matrix Crack, 10 Hz, 566°C, 137.9 MPa, 100X

This figure is a photograph of the polished edge of the specimen tested at a maximum stress of 137.9 MPa. The presence of these cracks is consistent with the results from the analysis of the modulus degradation plots which showed that there was some amount of degradation of the modulus of elasticity in each of the specimens. The degradation of the modulus is usually associated with the development of cracks in the matrix.

An examination of the fracture profiles of the specimens in this series of tests showed them to be jagged and irregular. They were similar in appearance to the fracture profile of the monotonic tensile test at this temperature. Figure 76 is a representative

fracture profile of the specimens from this series. This figure is a photograph of the unpolished edge of the specimen tested at a maximum stress of 103.43 MPa.

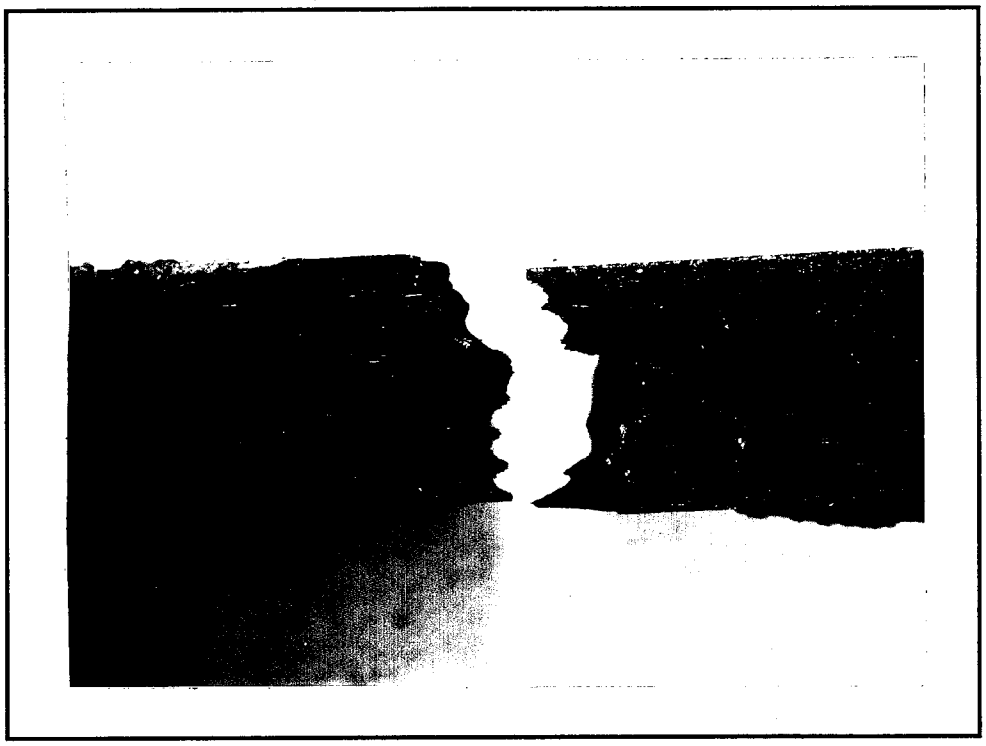

Figure 76. Fracture Profile, 10 Hz, 566°C, 103.43 MPa, 10X

Inspection of the fracture surfaces of the specimens from this series of tests, using scanning electron microscopy, revealed that all surfaces exhibited short fiber pullout over a portion of the surface of the fracture. This is the same observation as was made by Tuznik [12] with the SiC/CAS system. Figure 77 is an SEM microphotograph of the fracture surface of the specimen tested at a maximum stress of 137.9 MPa and it exhibits short fiber pullout over a portion of the fracture surface. This pullout can be attributed to the effect of the cyclic loading causing debonding of the fibers from the matrix along the

weak fiber-matrix interface. A similar effect was seen by Tuznik [12] with the SiC/CAS cross-ply system and Grant [5] with this SiC/MAS system.

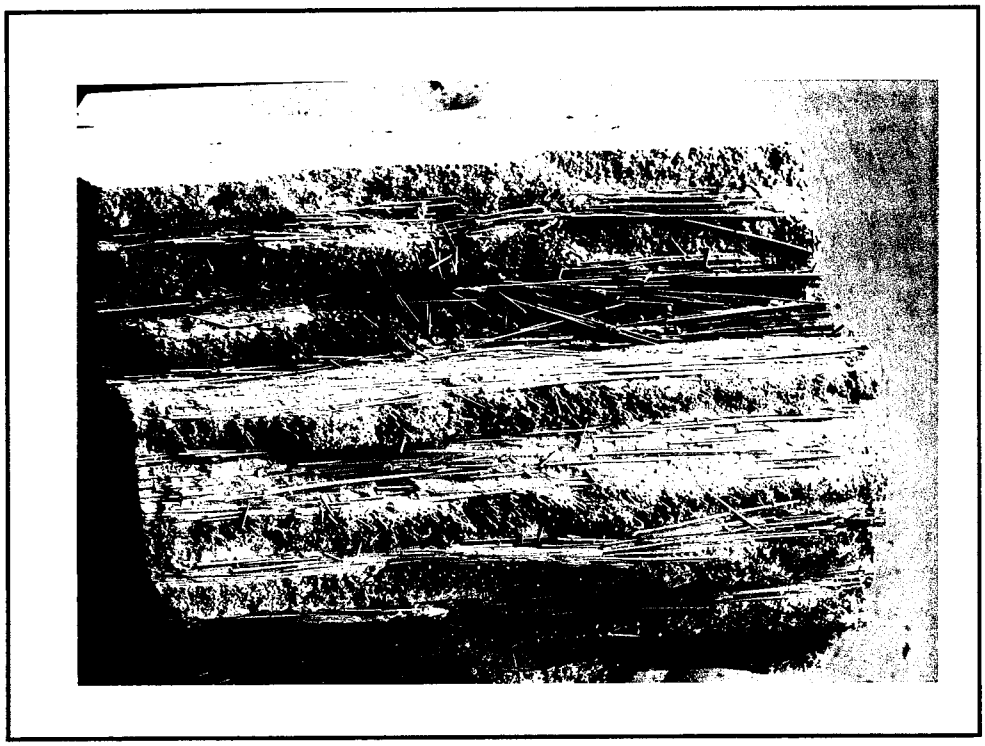

Figure 77. Fracture Surface, 10 Hz, 566°C, 137.9 MPa, 15.7X

Figure 78 is an SEM microphotograph of the fracture surface of the specimen tested at a maximum stress of 103.43 MPa. This specimen exhibits the same short fiber pullout as the specimen in Figure 77, but over a smaller area. The specimen depicted in Figure 77 was tested at a higher stress level and had a much shorter fatigue life. This observation indicates that the extent of the fiber-matrix interface oxidation and strengthening, leading to brittle fracture, is a function of the length of fatigue life for each specimen.

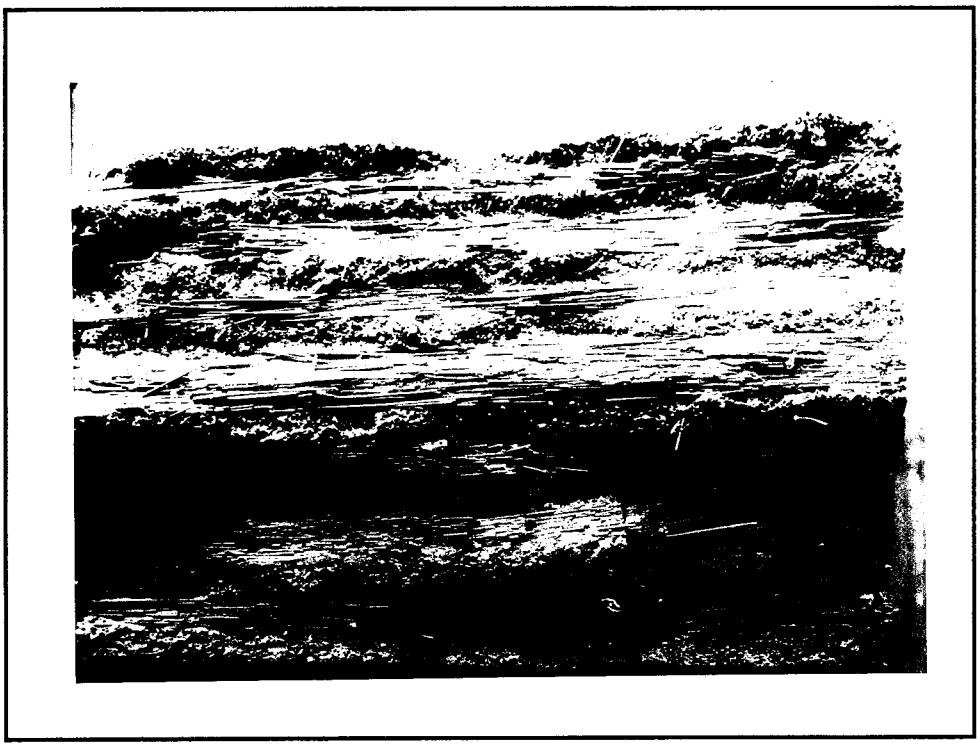

Figure 78. Fracture Surface, 10 Hz, 566°C, 103.43 MPa, 26.2X

The next step of the inspection of the fracture surface was to determine the condition of the surface of the fibers that had debonded and pulled out. Figure 79 is an SEM microphotograph of the surface of some of the fibers that had debonded during the 137.9 MPa (high stress) fatigue test at a frequency of 10 Hz and a temperature of 566 °C. These fibers are relatively clean and smooth and show little evidence of oxidation on the interface between the fiber and the matrix. Figure 80 is an SEM microphotograph of some of the fibers that had debonded during the 103.43 MPa (low stress) test at a frequency of 10 Hz and a temperature of 566 °C. These fibers show evidence of a lot of interfacial oxidation as would be expected for a test of long duration, even at the lower temperature. The oxidation, in this context, is an environmental effect of the air and the temperature

Figure 79. Fiber Surface, 10 Hz, 566°C, 137.9 MPa, 685X

Figure 80. Fiber Surface, 10 Hz, 566°C, 103.43 MPa, 470X

penetrating along the debonded interface, as opposed to the oxidation of the fiber matrix interface which causes a strengthening and embrittlement of the interface allowing for a planar crack growth. A comparison of Figures 79 and 80 shows that the longer times of the tests that result from the lower stress levels will allow more exposure to the atmosphere and more oxidative attack of the debonded fiber-matrix interface.

Figure 81 is an SEM microphotograph of a representative area of the fracture surface away from an area of fiber pullout. The fracture surface in this area is generally smooth and flat in appearance, indicating that the specimen failed due to an environmentally assisted crack growth, similar to that observed by Grant [5]. Figure 81 also illustrates the combination of mechanisms occurring in these tests. There is some

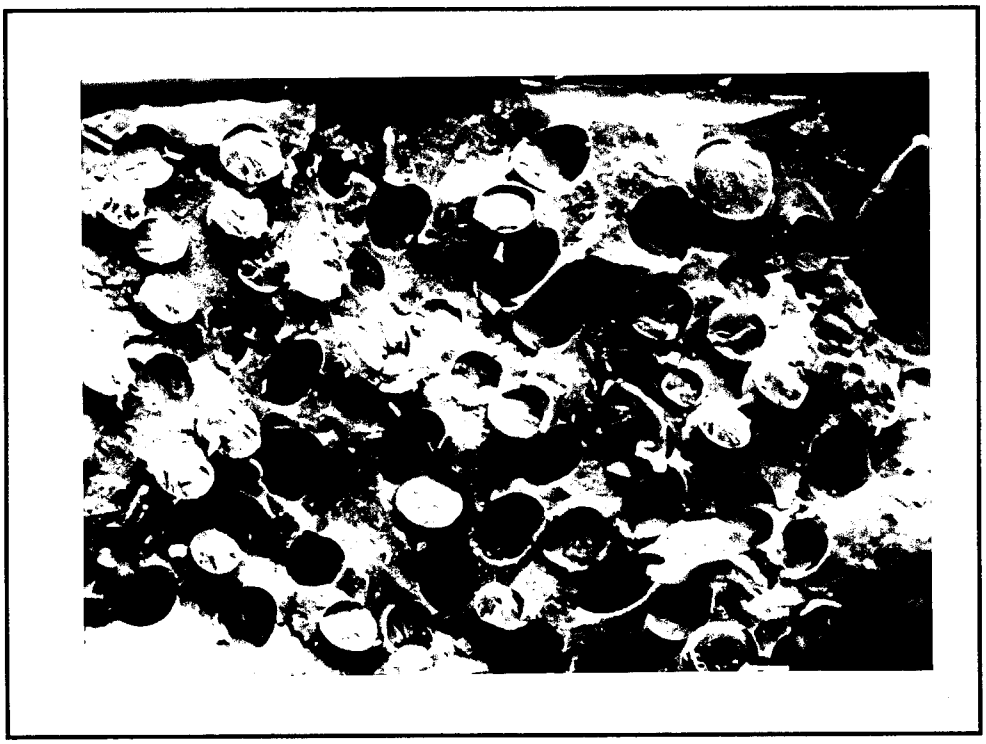

Figure 81. Fracture Surface, 10 Hz, 120.66 MPa, 566°C, 560X

evidence of debonding indicated by the few short lengths of fiber pullout on some of the fibers and there is also evidence of the environmentally assisted crack growth through the strengthened interfacial bonds, resulting in a flat planar surface.

F.3. Fracture Surface 1 Hz 566 °C. The first step in the analysis of the damage mechanisms of the specimens from series of tests was the examination of the polished edges of the failed specimens, using an optical microscope. This examination showed that there was some amount of matrix microcracking near the fracture surface, as was the case for the specimens tested at 10 Hz at this temperature. Transverse cracks were found in all the specimens tested at a frequency of 1 Hz and a temperature of 566°C and typically extended across an entire 90° ply and in some cases extended through the fibers of a 0°

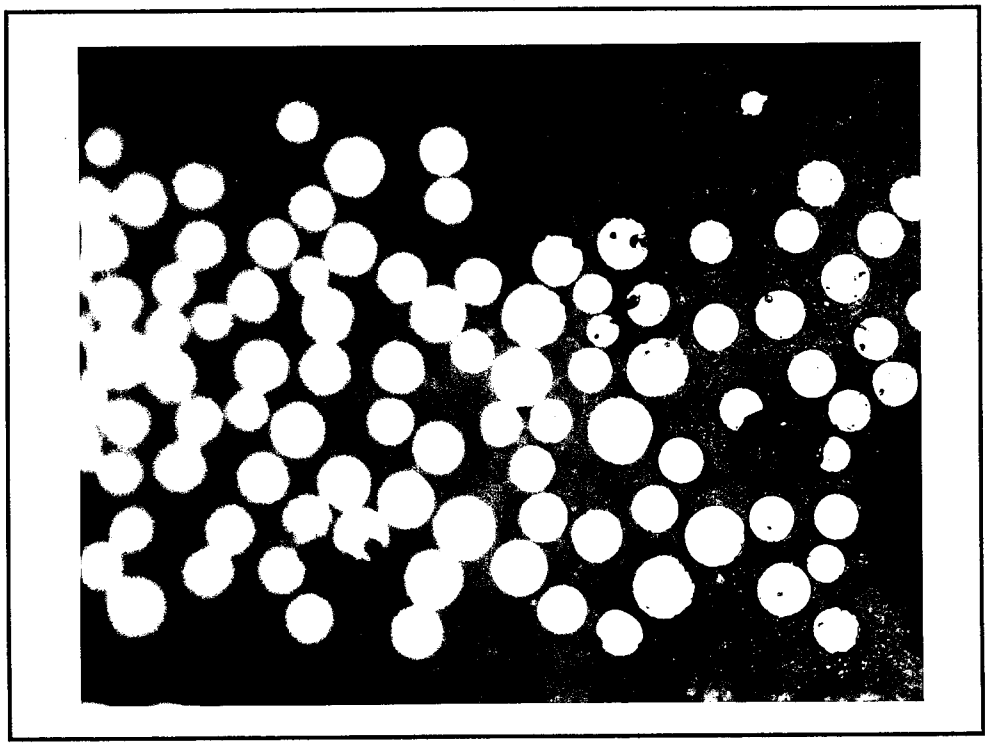

Figure 82. Matrix Crack, 1 Hz, 120.66 MPa, 566°C, 100X

ply. An example of a crack found in this series of tests can be seen in Figure 82. This figure is a photograph of the polished edge of the specimen tested at 120.66 MPa. The presence of these cracks is consistent with the results from the analysis of the modulus degradation plots for this series of tests, which showed that there was some amount of degradation of the modulus of elasticity in each of the specimens. The degradation of the modulus is usually associated with the development of matrix cracks.

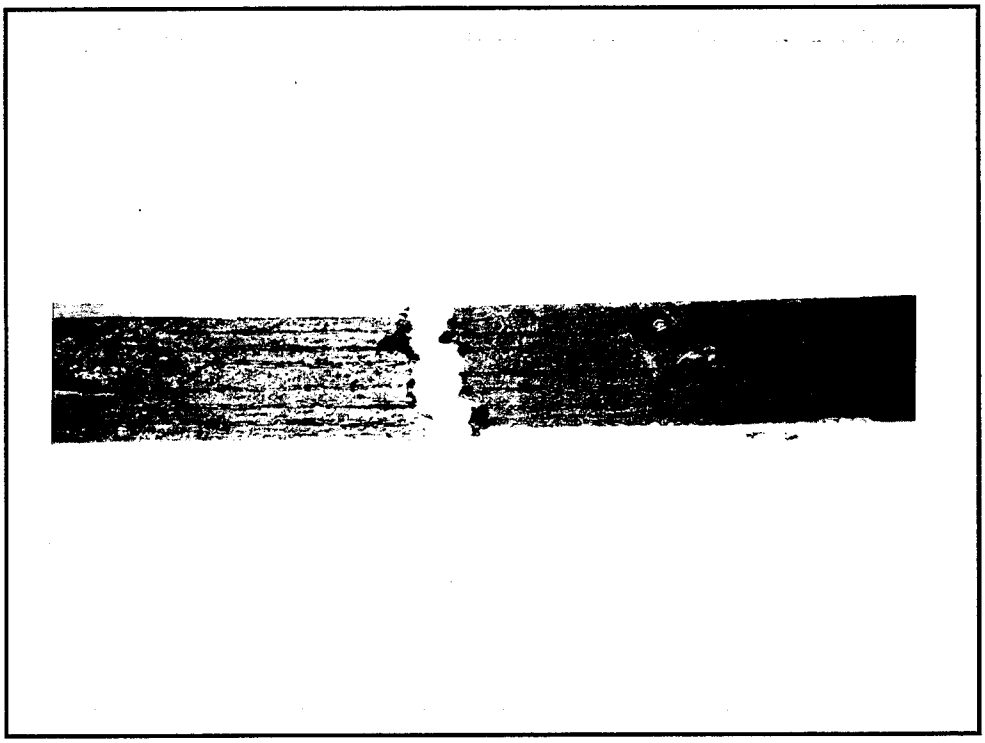

Figure 83. Fracture Profile, 1 Hz, 137.9 MPa, 566°C, 10X

An examination of the fracture profiles of the specimens from this series of tests showed them to be slightly jagged and irregular. They were slightly more planar in appearance than the fracture profiles of the monotonic tensile and 10 Hz fatigue tests at this temperature. Figure 83 is a representative fracture profile of the specimens from this

series of tests. This figure is a photograph of the unpolished edge of the specimen tested at a maximum stress of 137.9 MPa.

Inspection of the fracture surfaces of the specimens from this series of tests, using scanning electron microscopy, revealed that the surfaces all exhibited short fiber pullout over a portion of the fracture surface. This is the same observation as was made for the tests conducted at a frequency of 10 Hz at this temperature. Figure 84 is a an SEM microphotograph of the fracture surface of the specimen tested at 137.9 MPa (high stress) exhibiting short fiber pullout over a portion of the fracture surface. This fiber pullout can be attributed to the effect of the cyclic loading causing a debonding of the fibers from the matrix along the weak fiber-matrix interface.

Figure 84. Fracture Surface, 1 Hz, 566°C, 137.9 MPa, 20.8X

Figure 85 is an SEM microphotograph of the fracture surface of the specimen tested at 103.43 MPa (low stress) which exhibits a smaller area of fiber pullout than the specimen depicted in Figure 84. This is the same trend as was seen in the specimens tested at a frequency of 10 Hz at this temperature. The longer tests showed a smaller area of fiber pullout and a correspondingly larger area of planar, brittle fracture surface. The smaller area of pullout, and correspondingly larger area of planar fracture surface, again indicates that the progression of oxidation of the fiber matrix interface through the cross section of the specimen is a function of the length of time of the test. The longer test will allow the oxidation and strengthening of the fiber-matrix interface to progress over a larger area of the specimen cross section. This is the same effect as was seen in the tests by Grant [5] and Larsen [7].

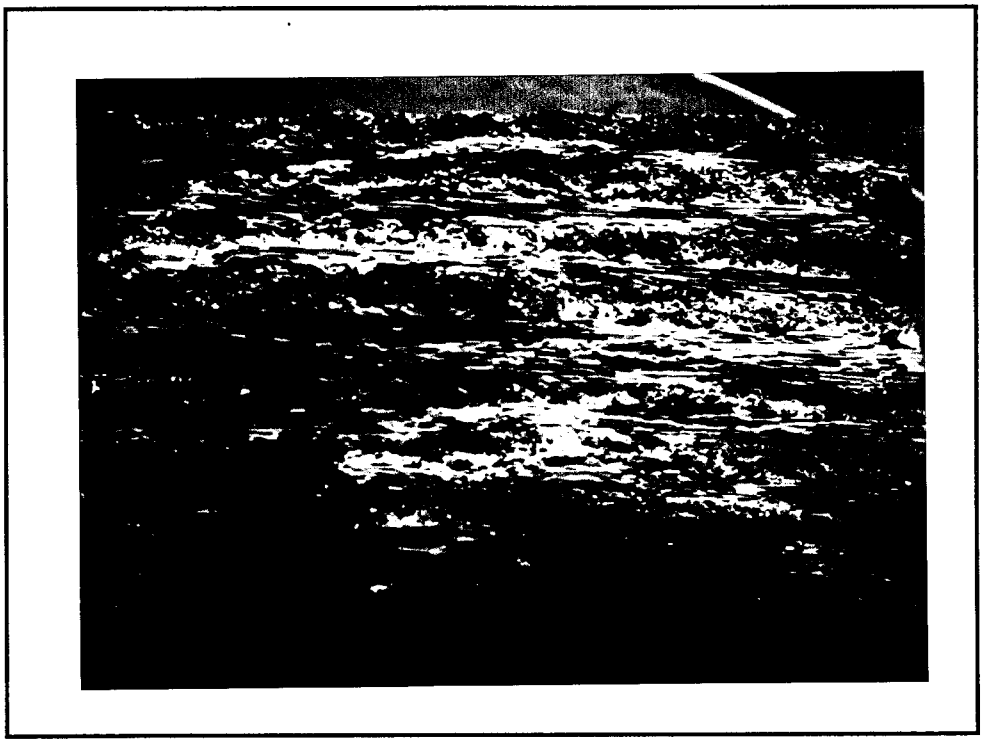

Figure 85. Fracture Surface, 1 Hz, 566°C, 103.43 MPa, 28.8X

The next step of the inspection of the fracture surface was to determine the condition of the surface of the fibers that debonded and pulled out. Figure 86 is an SEM microphotograph of the surface of some of the fibers that had debonded during the test conducted at 137.9 MPa (high stress) at a frequency of 1 Hz and a temperature of 566 °C. These fibers are relatively clean and smooth and show little evidence of damage due to the progression of oxidation along the debonded interface between the fiber and the matrix. Figure 87 is an SEM microphotograph of some of the fibers that had debonded during the test conducted at 120.66 MPa (low stress) at a frequency of 1 Hz and a temperature of 566 °C. These fibers show evidence of a greater degree of oxidation penetrating along the

Figure 86. Fiber Surface, 1 Hz, 566°C, 137.9 MPa, 685X

Figure 87. Fiber Surface, 1 Hz, 566°C, 120.66 MPa, 525X

debonded interface, as would be expected for a test of longer duration. A comparison of Figures 86 and 87 shows that the longer times of the tests that result from the lower stress levels will allow more exposure to the atmosphere and more penetration of the oxidative attack of the debonded fiber-matrix interface.

Figure 88 is an SEM microphotograph of a representative area of the fracture surface away from an area of fiber pullout in this series of tests. The fracture surface in this area is generally smooth and flat in appearance, indicating that the specimen failed due to an environmentally assisted crack growth, similar to that observed by Grant [5]. Figure 88 also illustrates the combination of mechanisms occurring in these tests. There is some evidence of debonding indicated by the few short lengths of fiber pullout and there is also

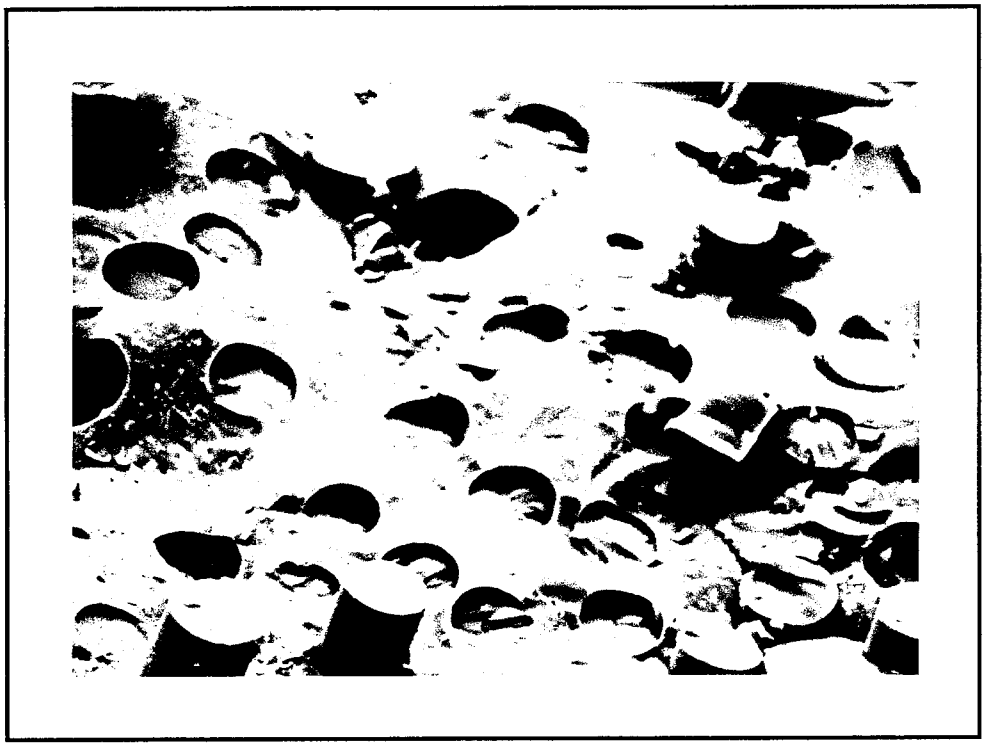

Figure 88. Fracture Surface, 1 Hz, 566°C, 660X

evidence of the environmentally assisted crack growth through the strengthened interfacial bonds resulting in a flat planar surface.

Examination of the fracture surfaces from both series of tests at this temperature has been shown that there is no difference between the damage mechanisms in the specimens tested at a frequency of 10 Hz and those tested at a frequency of 1Hz. This independence of frequency supports the results of the analysis of the fatigue-life curves which showed that the fatigue life of this material is independent of frequency of the loading at this temperature. The time dependence of the damage mechanisms is the same as was seen in the analysis of the fatigue-life curves, modulus degradation, strain progression, and hysteresis loop analysis.

F.4. Fracture Surface 10 Hz 1093 °C. The first step in the analysis of the fracture surfaces of the specimens from this series of tests was the examination of the polished edges of the failed specimens using an optical microscope. This examination showed that there was some amount of matrix microcracking near the fracture surface, as was the case for the specimens tested at 10 Hz at the lower temperature. Transverse cracks were found in all the specimens tested at a frequency of 10 Hz and a temperature of 1093°C and typically extended across an entire 90° ply and in some cases extended through the fibers of a 0° ply. An example of a crack found in this series of tests can be seen in Figure 89. This figure is a photograph of the polished edge of the specimen tested at a maximum stress of 96.53 MPa. The presence of these cracks is consistent with the results from the

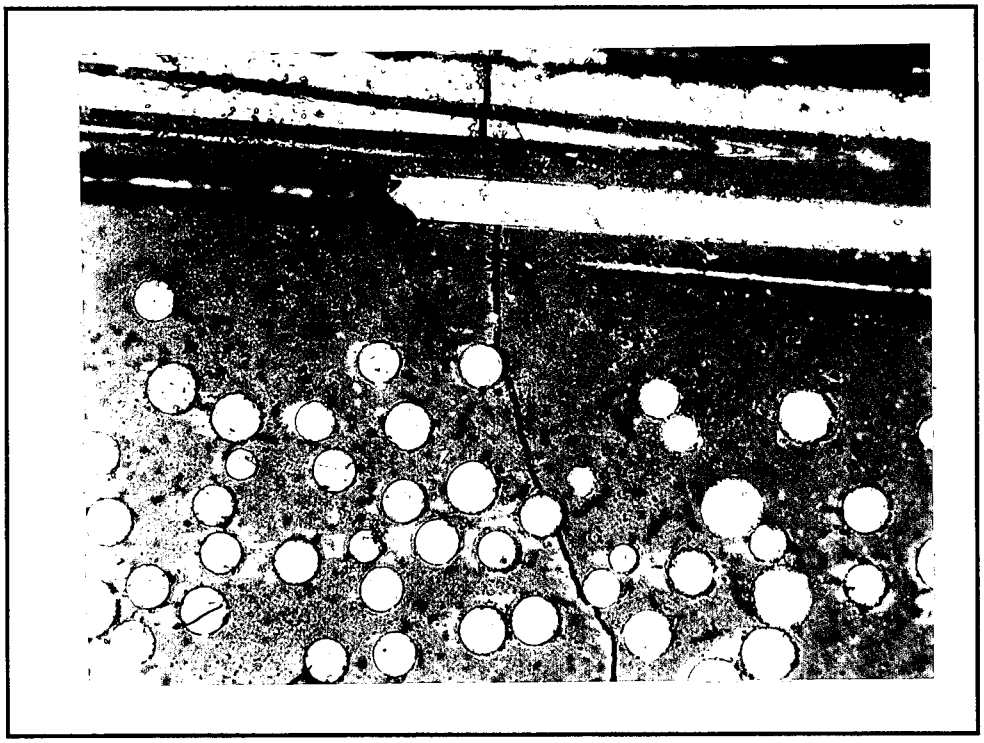

Figure 89. Matrix Crack, 10 Hz, 1093°C, 96.53 MPa, 100X

analysis of the modulus degradation plots for this series of tests which showed that there was some amount of degradation of the modulus of elasticity in each of the specimens. The degradation of the modulus is usually associated with the development of cracks in the matrix.

An examination of the fracture profiles of the specimens from this series of tests showed them to be fairly jagged and irregular, but more planar than the profiles of the tests that were conducted at 566°C. They were similar in appearance to the fracture profile of the monotonic tensile test at this temperature. Figure 90 is a representative fracture profile of the specimens from this series of tests. This figure is a photograph of the unpolished edge of the specimen tested at a maximum stress of 137.9 MPa.

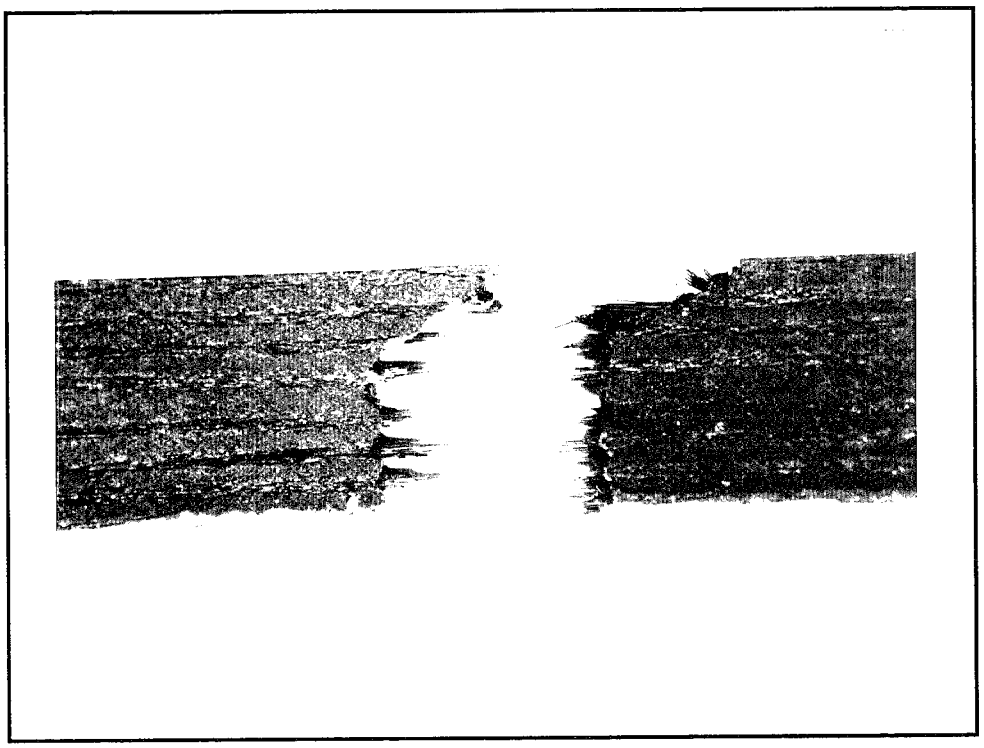

Figure 90. Fracture Profile, 10 Hz, 1093°C, 137.9 MPa, 10X

Inspection of the fracture surfaces of the specimens from this series of tests, using scanning electron microscopy, revealed that the surfaces of the specimens in this series of tests all exhibited fiber pullout over a portion of the surface of the fracture. Figure 91 is a an SEM microphotograph of the fracture surface of the specimen tested at 137.9 MPa (high stress) exhibiting fiber pullout over a portion of the fracture surface. This fiber pullout can be attributed to the effect of the cyclic loading causing a debonding of the fibers from the matrix along the weak fiber-matrix interface.

Figure 92 is an SEM microphotograph of the fracture surface of the specimen tested at 103.43 MPa (low stress) which exhibits a smaller area of fiber pullout than the specimen shown in Figure 91. The specimen in Figure 91 was tested at a higher stress

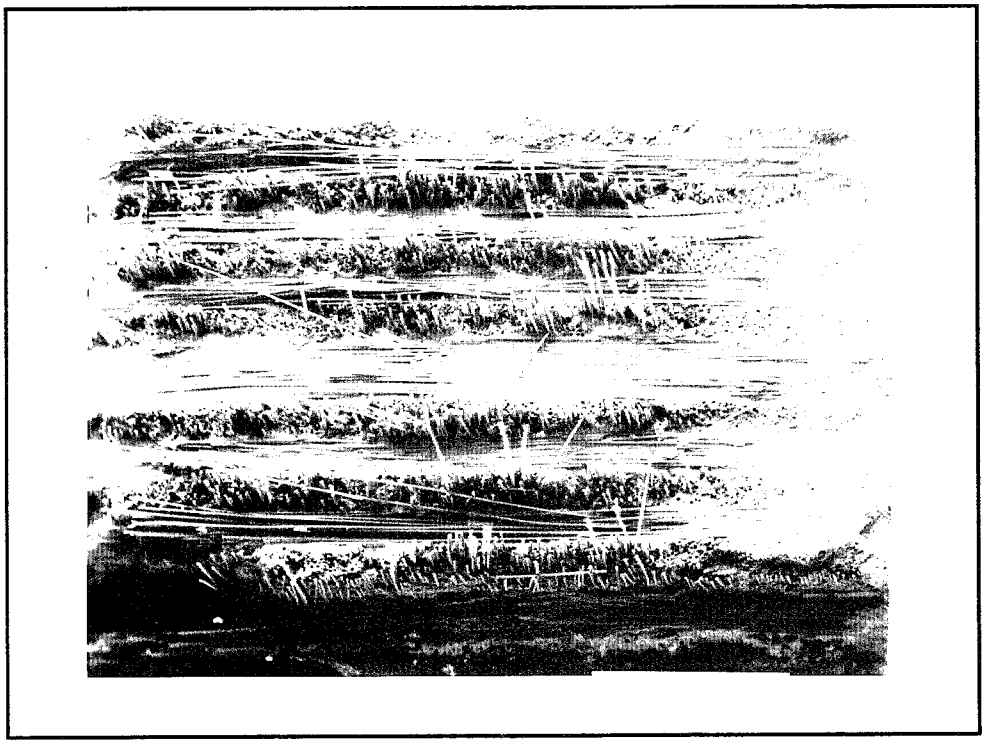

Figure 91. Fracture Surface, 10 Hz, 1093°C, 137.9 MPa, 18.4X

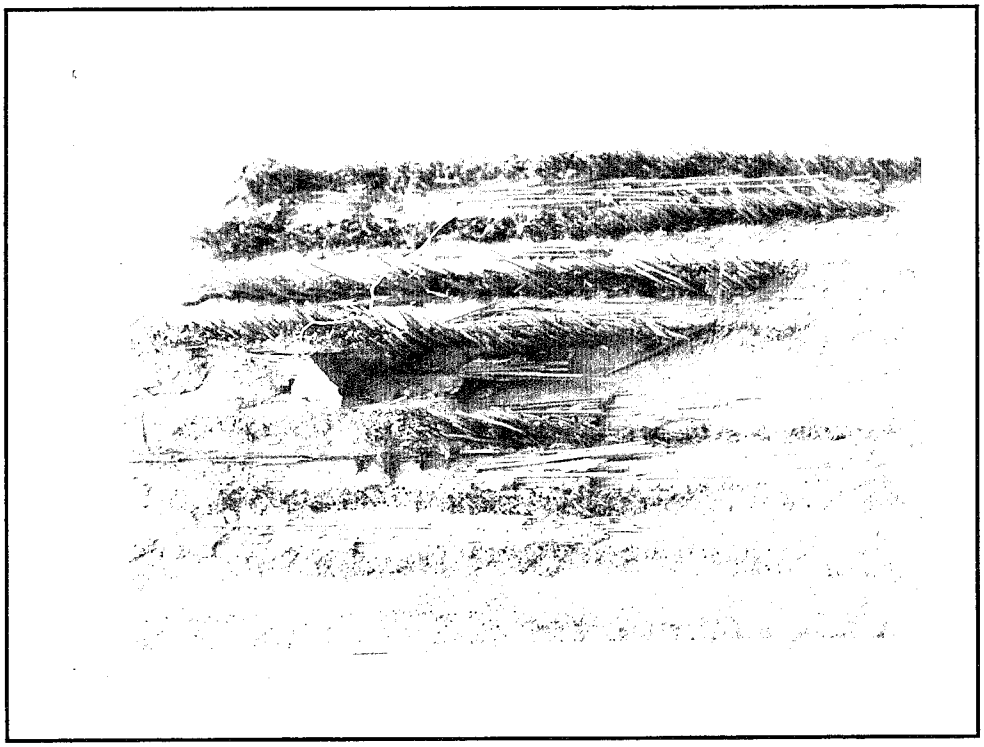

Figure 92. Fracture Surface, 10 Hz, 1093°C, 103.43 MPa, 18X

level and had a shorter fatigue life than the specimen shown in Figure 92. The difference in the amount of area of fiber pullout can again be attributed to the length of the tests. The increase in the planar area on the fracture surface of the specimen tested at the low stress level again indicates that the length of time of the test is the overriding factor in determining the extent of the oxidation and strengthening of the fiber-matrix interface through the specimen cross-section. This is consistent with observations made for both of the series of tests conducted at a temperature of 566°C.

The next step of the inspection of the fracture surface was to determine the condition of the debonded fiber surfaces from the specimens in this series of tests. Figure 93 is an SEM microphotograph of some of the fibers that had debonded during the test

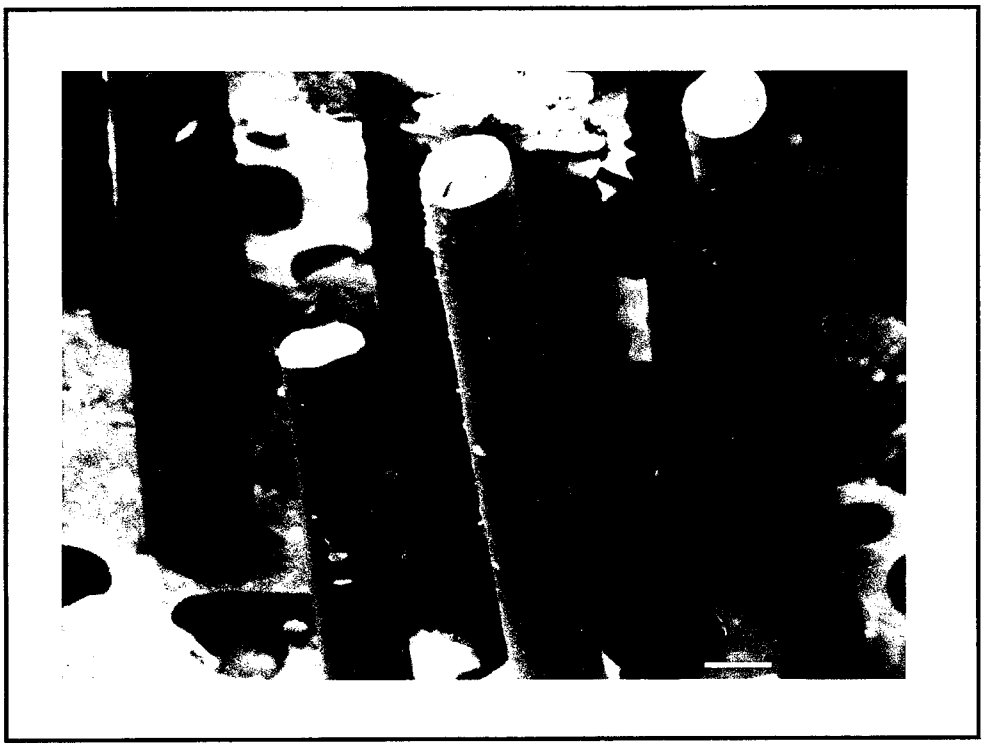

Figure 93. Fiber Surface, 10 Hz, 1093°C, 137.9 MPa, 815X

conducted at 137.9 MPa (high stress) at a frequency of 10 Hz and a temperature of 1093 °C. These fibers show a good deal of evidence of damage due to penetration of oxidation along the debonded interface between the fiber and the matrix, despite the short duration of the test.

Figure 94 is an SEM microphotograph of some of the fibers that had debonded during the test conducted at 96.53 MPa (low stress) at a frequency of 10 Hz and a temperature of 1093 °C. These fibers show evidence of a lot of fiber damage along the debonded interface due to oxidation, as would be expected for a test of long duration and high temperature. A comparison of Figures 93 and 94 shows that the longer times of the tests that result from the lower stress levels will allow more exposure to the atmosphere

and more oxidative attack of the debonded fiber-matrix interface. This is consistent with the observations made for both the series of tests conducted at 566°C.

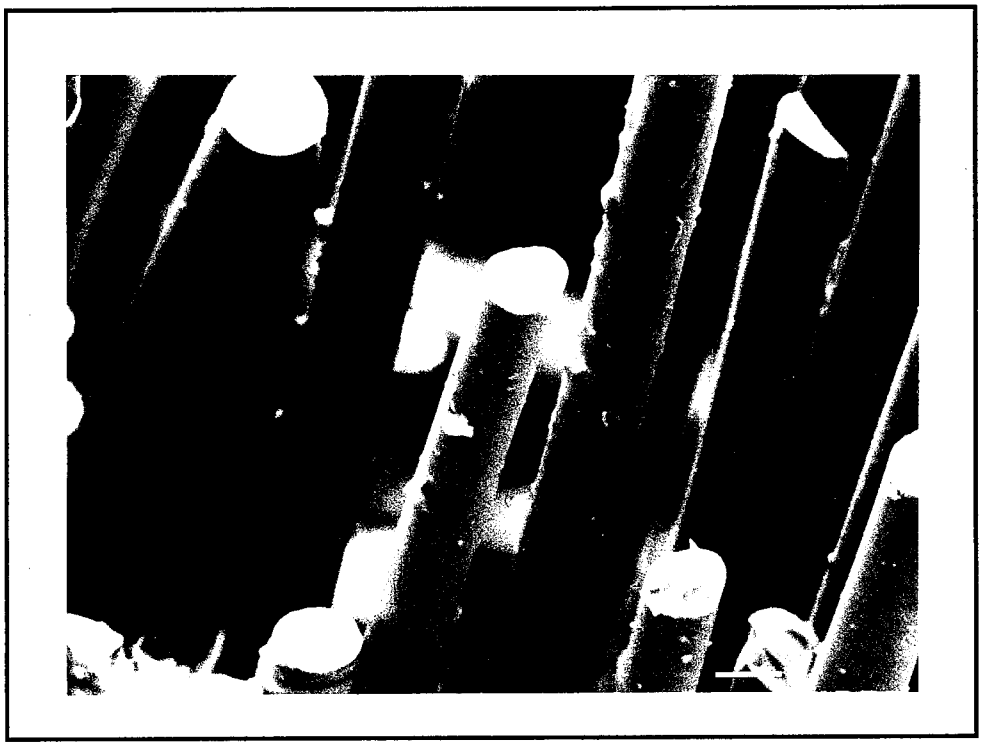

Figure 94. Fiber Surface, 10 Hz, 1093°C, 96.53 MPa, 855X

Figure 95 is an SEM microphotograph of a representative area of the fracture surface away from an area of fiber pullout. The fracture surface in this area is generally smooth and flat in appearance, indicating that the specimen failed due to an environmentally assisted crack growth, similar to that observed by Grant [5]. Figure 95 also illustrates the combination of mechanisms occurring in these tests. There is some evidence of debonding indicated by the few short lengths of fiber pullout and there is also evidence of the environmentally assisted crack growth through the strengthened interfacial bonds, resulting in a flat planar surface.

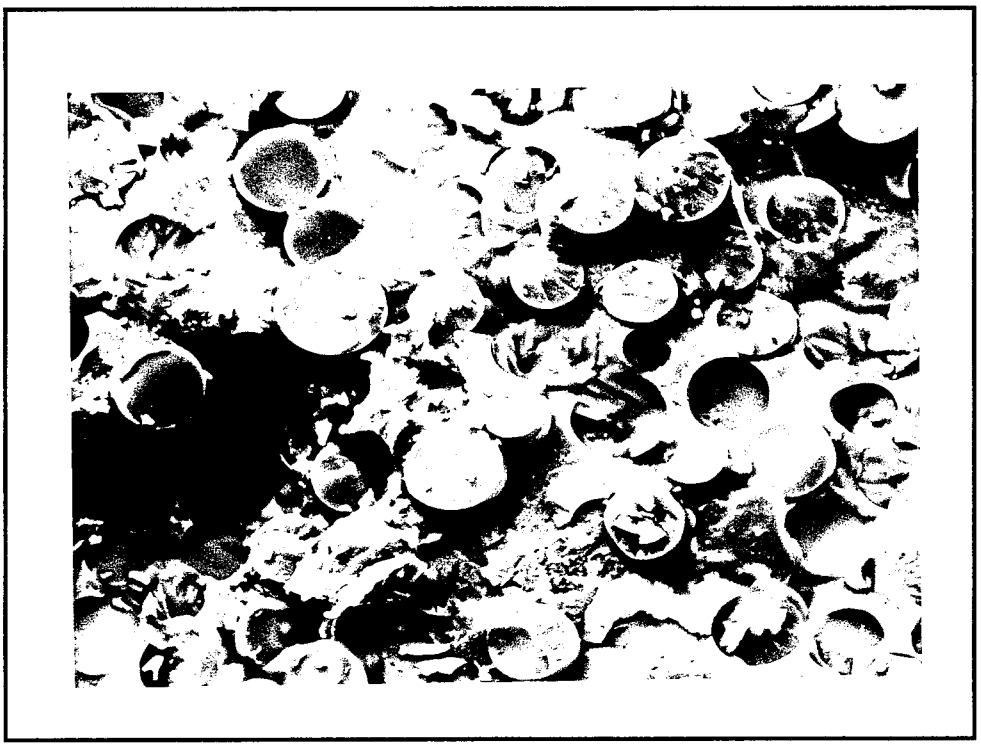

Figure 95. Fracture Surface, 10 Hz, 1093°C, 720X

F.5. Fracture Surface 1 Hz 1093 °C. The first step in the analysis of the fracture surfaces of the specimens from this series of tests was the examination of the polished edges of the failed specimens, using an optical microscope. This examination showed that there was some amount of matrix microcracking near the fracture surface, as was the case for the specimens tested at 10 Hz at this temperature and at 1 Hz for the lower temperature. Transverse cracks were found in all the specimens tested at a frequency of 1 Hz and a temperature of 1093°C. An example of a crack found in this series of tests can be seen in Figure 96. This figure is a photograph of the polished edge of the specimen tested at a maximum stress of 96.53 MPa. The presence of these cracks is consistent with the results from the analysis of the modulus degradation plots for this series of tests which showed that there was some amount of degradation of the modulus of elasticity in each of these specimens.

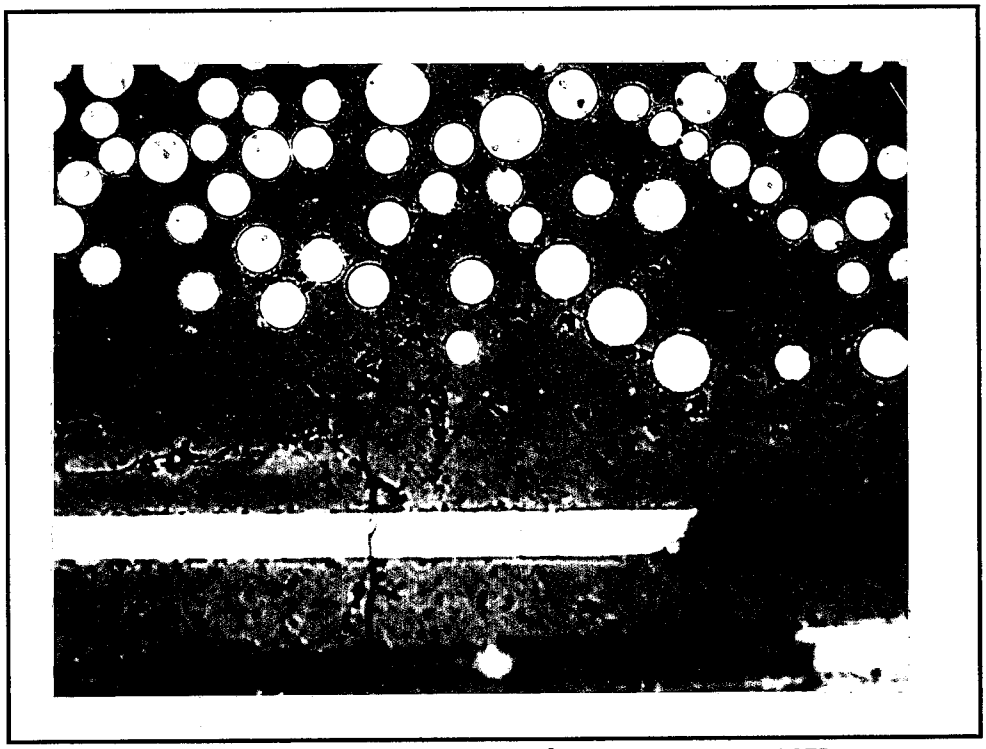

Figure 96. Matrix Crack, 1 Hz, 1093°C, 96.53 MPa, 100X

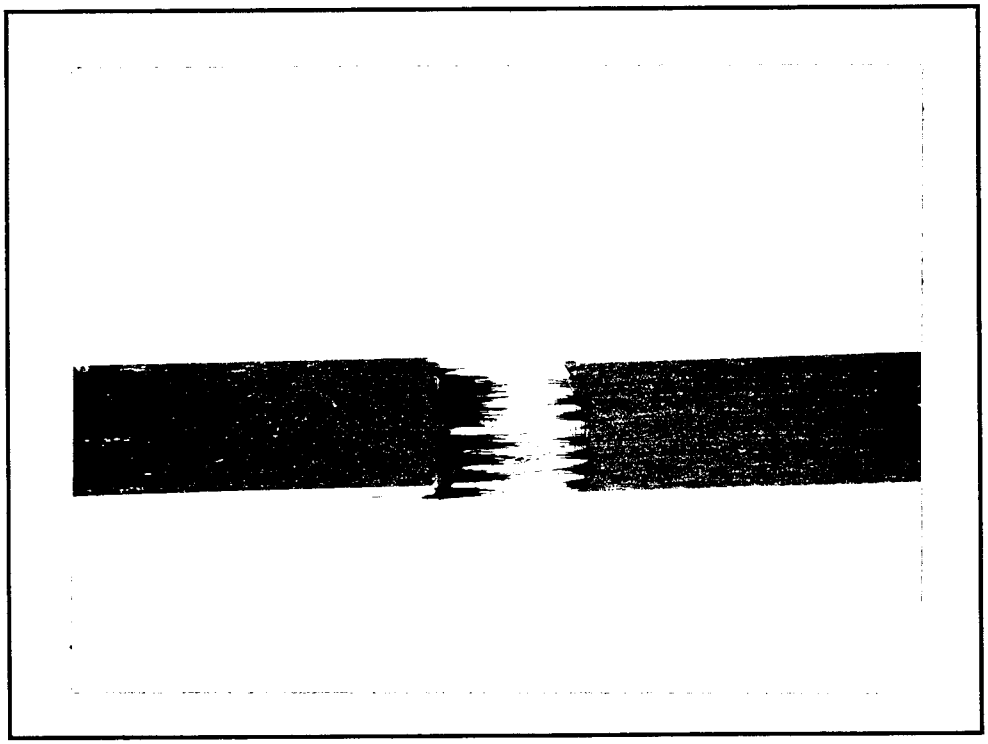

Figure 97. Fracture Profile, 1 Hz, 1093°C, 137.9 MPa, 10X

Figure 97 is a representative fracture profile of the specimens from this series of tests. This figure is a photograph of the unpolished edge of the specimen tested at a maximum stress of 137.9 MPa. Figure 97 can be compared to Figure 90 to show that the fracture profiles of the tests conducted at 1 Hz and 10 Hz are similar in appearance at this temperature.

Inspection of the fracture surfaces of the specimens from this series of tests, using scanning electron microscopy, revealed that the surfaces of all the specimens from this series of tests exhibited fiber pullout over a portion of the fracture surface and a flat planar region over the rest of the surface. This is the same observation as was made for the tests conducted at a frequency of 10 Hz at this temperature. Figure 98 is a an SEM

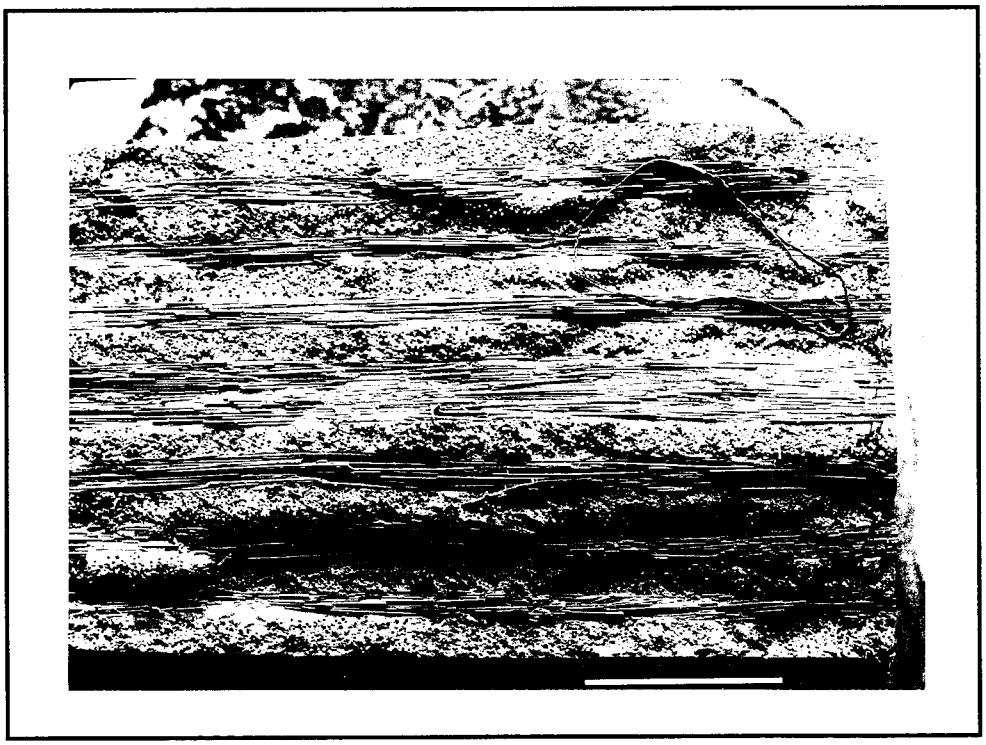

Figure 98. Fracture Surface, 1 Hz, 1093°C, 137.9 MPa, 11.4X

microphotograph of the fracture surface of the specimen tested at 137.9 MPa (high stress) exhibiting fiber pullout. This fiber pullout can be attributed to the effect of the cyclic loading causing a debonding of the fibers from the matrix along the weak fiber-matrix interface.

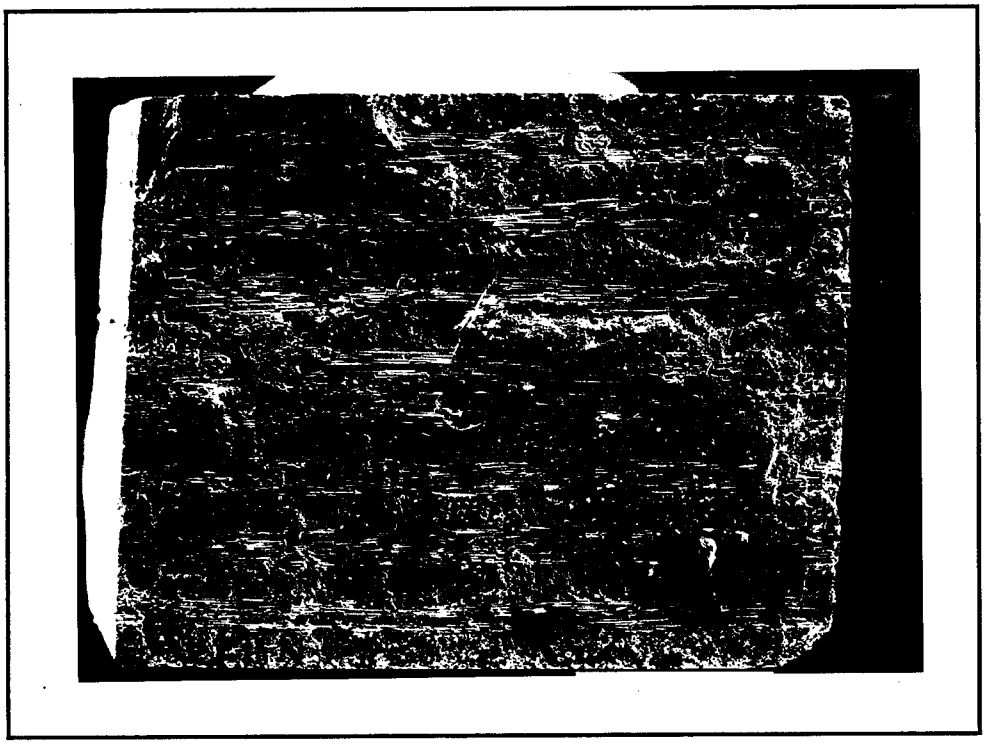

Figure 99. Fracture Surface, 1 Hz, 1093°C, 103.43 MPa, 25X

Figure 99 is an SEM microphotograph of the fracture surface of the specimen tested at 103.43 MPa (low stress) which exhibits a smaller area of fiber pullout than the specimen which was tested at 137.9 MPa (high stress). This difference in the area of fiber pullout between the two tests can again be attributed the difference in the length of the tests. The specimen shown in Figure 98 was tested at a higher stress level and had a shorter fatigue life than the specimen shown in Figure 99. This increased length of time

corresponds to a greater amount of time for the oxidation of the fiber-matrix interfaces to progress through the cross section of the specimen and is evidenced by the larger areas of planar, brittle fracture surface. This was seen by both Larsen [7] and Grant [5].

The next step of the inspection of the fracture surface was to determine the condition of the surface of the debonded fibers that had pulled out. Figure 100 is an SEM microphotograph of some of the fibers that had debonded during the test conducted at 137.9 MPa (high stress) at a frequency of 1 Hz and a temperature of 1093 °C. These fibers show a lot of evidence of damage due to oxidation of the debonded interface between the fiber and the matrix. Figure 101 is an SEM microphotograph of some of the fibers that had debonded during the test conducted at 96.53 MPa (low stress) at a

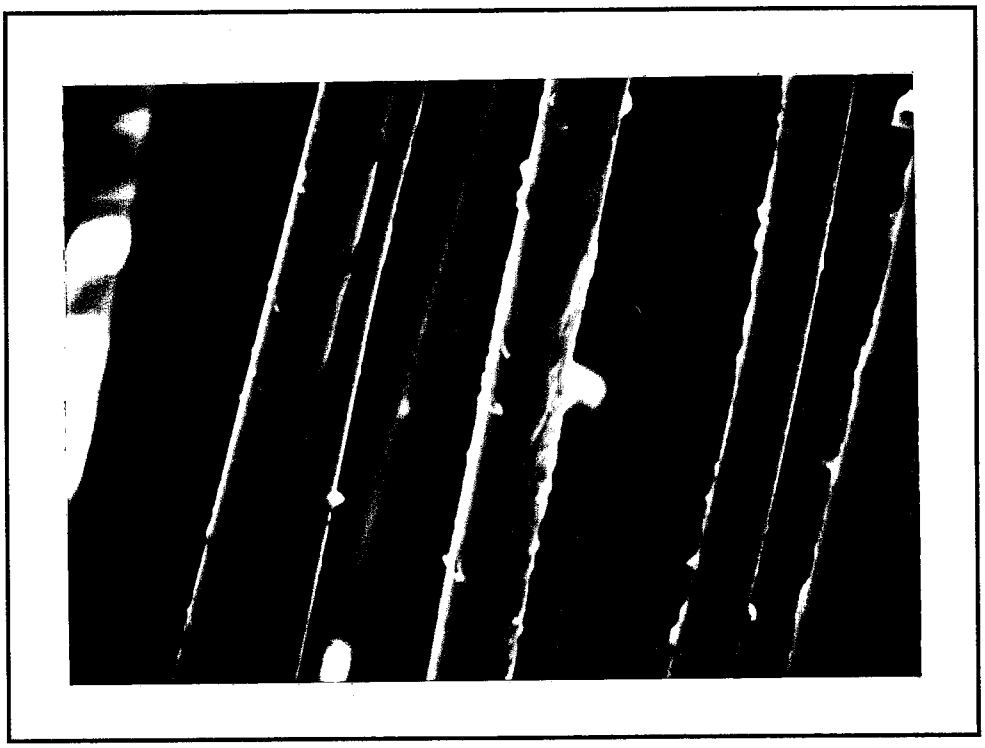

Figure 100. Fiber Surface, 1 Hz, 1093°C, 137.9 MPa, 625X

Figure 101. Fiber Surface, 1 Hz, 1093°C, 96.53 MPa, 575X

frequency of 1 Hz and a temperature of 1093 °C. These fibers show evidence of a lot of interfacial oxidation as would be expected for a test of long duration at a high temperature. A comparison of Figures 100 and 101 shows that the longer times of the tests that result from the lower stress levels will allow more exposure to the atmosphere and more oxidative attack of the debonded fiber-matrix interface. This is consistent with the observations from the series of tests conducted at 10 Hz at this temperature.

Figure 102 is an SEM microphotograph of a representative area of the fracture surface away from an area of pullout. The fracture surface in this area is generally smooth and flat in appearance, indicating that the specimen failed due to an environmentally assisted crack growth, similar to that observed by Grant [5]. Figure 102 also illustrates

the combination of damage mechanisms occurring in these tests. There is some evidence of debonding indicated by the few short lengths of fiber pullout and there is also evidence of the environmentally assisted crack growth through the strengthened interfacial bonds resulting in a flat planar surface.

Figure 102. Fracture Surface, 1 Hz, 137.9 MPa, 1093°C, 655X

The results of this section, along with the previous section (F.4), show a similar combination of damage mechanisms between the specimens tested at 1 Hz and 10 Hz at a temperature of 1093°C. Examination of the fracture surfaces from both series of tests at this temperature have shown that there is no difference between the damage mechanisms in the specimens tested at a frequency of 10 Hz and those tested at a frequency of 1Hz. This independence of frequency supports the results of the analysis of the fatigue-life

curves which showed that the fatigue life of this material is independent of frequency of the loading at this temperature. The time dependence of the damage mechanisms is the same as was seen in the analysis of the fatigue-life curves, modulus degradation, strain progression, and hysteresis loop analysis.

F.6 Over-all Comparison. In summary, examination of the fracture surfaces of all the failed specimens showed that there was a combination of fiber-matrix debonding and environmentally assisted crack growth caused by the oxidation and strengthening of the fiber-matrix interface. It can also be seen that the amount of environmentally assisted crack growth and oxidation penetrating along the debonded fiber-matrix interface is dependent on the length of the test. This was seen for both of the frequencies at both of the temperatures.

The tests which were conducted at the lower stress levels exhibited more oxidation along the debonded fiber-matrix interface and smaller areas of debonded, pulled out fibers than the tests conducted at the higher stress levels. The increased amount of oxidation along the debonded fiber-matrix interface can be attributed to more exposure to the air due to the increased length of the test. The smaller areas of fiber pullout in the specimens tested at a low stress can be attributed to more exposure to the air due to the increased length of the test. This increased exposure allowed the oxidation and strengthening of the fiber-matrix interface to progress further through the specimen cross-section and was evidenced by the larger brittle fracture surface.

The difference in the amount of oxidation penetrating along the fiber-matrix interface can be seen by comparing Figure 79, the fiber surface of a test conducted 10 Hz and 566 °C, to Figure 80, the fiber surface of a test conducted at 10 Hz and 566°C. The longer test showed more oxidation of the debonded interface than the shorter test.

The time dependence of the difference in the area of fiber pullout can also be seen by comparing Figure 103, the fracture surface of the specimen tested at 1 Hz and 1093°C at a stress level of 120.66 MPa with a fatigue life of 88 seconds, to Figure 104, the fracture surface of the specimen tested at 10 Hz and 1093°C at a stress level of 96.53 MPa with a fatigue life of 5.4 hours. Figure 104 can, in turn, be compared to Figure 105, which is the fracture surface of the specimen tested at 1 Hz and 566°C at a stress level of 103.43

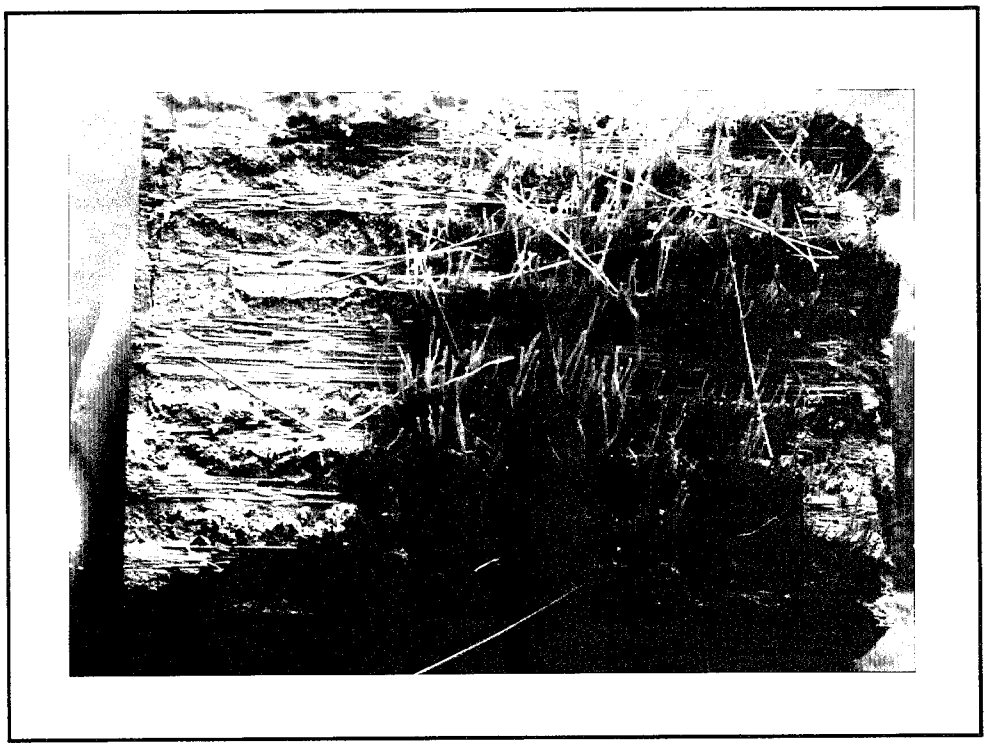

Figure 103. Fracture Surface, 1 Hz, 120.66 MPa, 1093°C, 17.6X

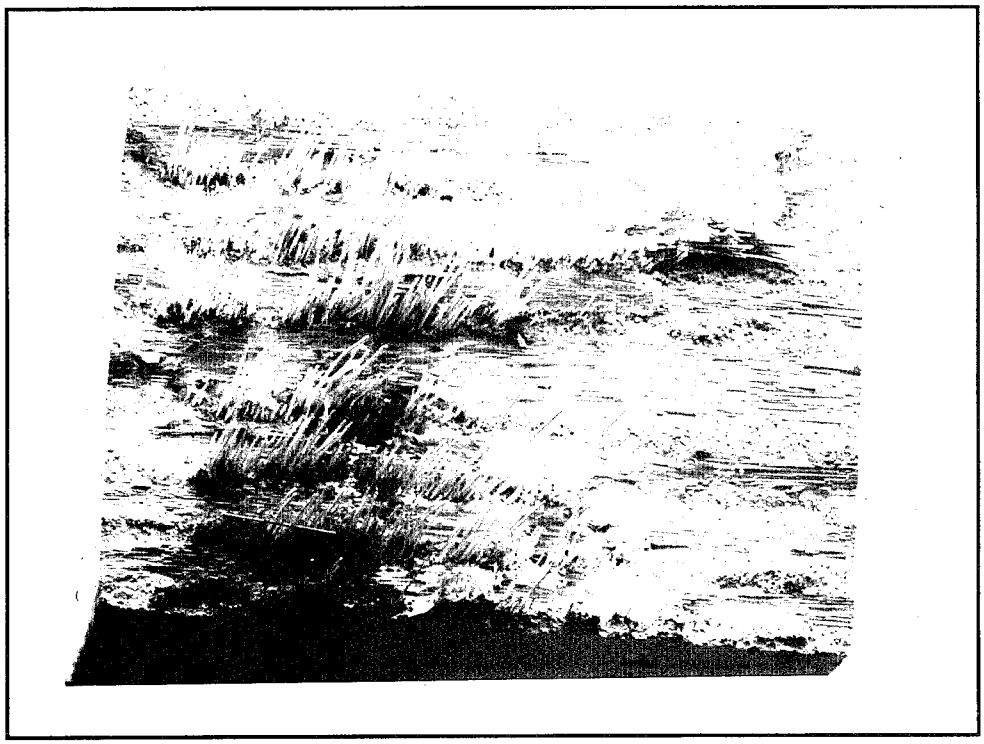

Figure 104. Fracture Surface, 10 Hz, 96.53 MPa, 1093°C, 19.9X

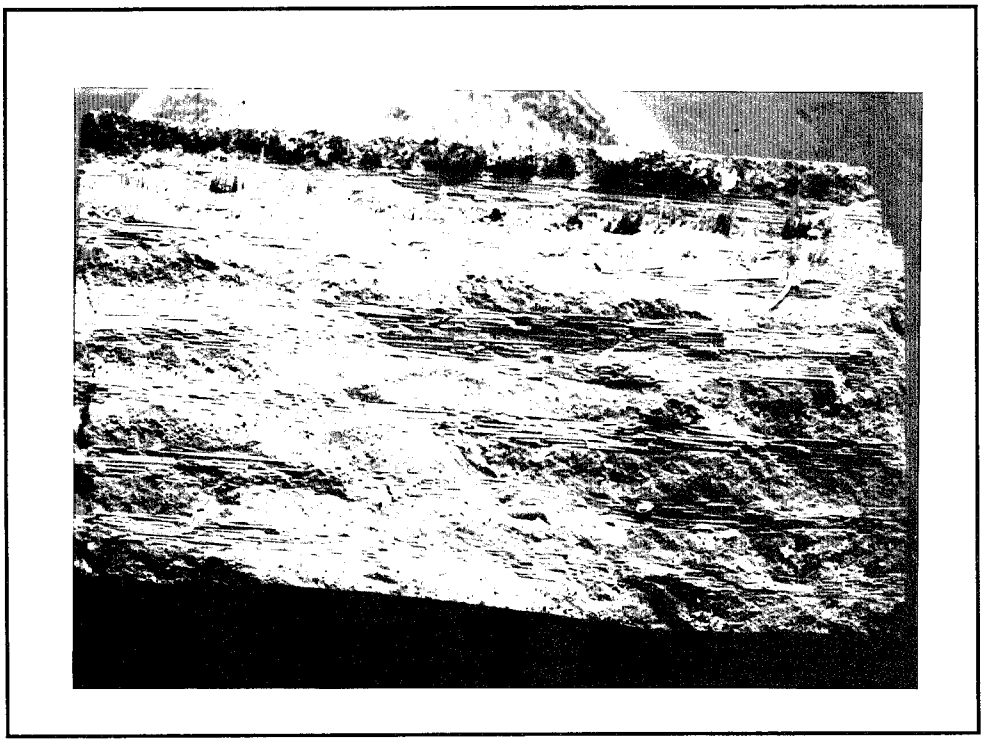

Figure 105. Fracture Surface, 1 Hz, 96.53 MPa, 1093°C, 20X

MPa with a fatigue life of 118 hours.

This time dependence of the damage mechanisms is consistent with the results of the analysis of the fatigue life curves which indicated that the fatigue life of this material is independent of the frequency of the loading, but dependent on the exposure time.

V. Conclusions

The purpose of this study was to investigate the effect of loading rate and elevated temperature on the fatigue behavior and damage mechanisms of a model ceramic matrix composite with a cross-ply lay-up. The material used in this study was a potassium borosillicate glass (BSG) doped (5%) magnesium aluminosilicate (MAS) cordierite matrix reinforced with Nicalon (silicon carbide, SiC) fibers in a $[0/90]_{4s}$ lay-up. The composite was forty percent fiber by volume. The BSG dopant in the MAS matrix serves as a source of boron which diffuses into the interface between the fiber and the matrix during hot consolidation. The boron serves to keep the interface thin and more oxidatively stable than a purely carbon interface, which is present in the earlier version of this ceramic composite, SiC/CAS. Monotonic tensile tests and tension-tension fatigue tests were conducted at two frequencies of 1 Hz and 10 Hz and two temperatures of 566°C and 1093°C. The test results showed that the damage mechanisms and fatigue life were independent of the frequency of the cyclic loading. The fatigue life was dependent on the temperature of the environment and the damage mechanisms were independent of the temperature of the environment.

The fatigue life curves, when plotted against time, showed that the fatigue life of this SiC/MAS system is independent of the frequency of the loading at both temperatures. The fatigue life curves also showed that the fatigue life of the material was shorter at the higher temperature for both of the frequencies investigated. The normalized fatigue life curves for both of the frequencies showed that the material performed slightly better at the

higher temperature on the basis of a percentage of the ultimate strength at that temperature. A comparison of the normalized fatigue life curves of the SiC/MAS system with the SiC/CAS system at the higher temperature showed the SiC/MAS system has achieved a slightly improved fatigue response at elevated temperature.

The examination of the fracture surfaces showed that there was a combination of two separate damage mechanisms occurring. There was a debonding of the fibers from the matrix due to the effects of the fatigue loading, allowing a coalescence of matrix cracks along the debonded interface, and an oxidation of the fiber-matrix interface, allowing an environmentally assisted crack growth. These two mechanisms were evidenced by areas of fiber pullout and areas of flat, smooth, planar fracture surface respectively. There was evidence of more oxidation and strengthening of the fiber-matrix interface as the tests became longer, indicated by a more planar fracture surface, but it was not possible to determine which mechanism was primarily responsible for the final fracture.

The modulus degradation, strain data, hysteretic energy, and fracture surfaces showed that the progression of the damage mechanisms was independent of the temperature and the frequency, but the rate and amount of the damage was dependent on temperature and, to some small degree, frequency. All the tests showed a modulus degradation through the first ten cycles and then a creep like mechanism which was a time dependent, environmentally assisted crack growth caused by a combination of the stress and the environment. The amount of modulus degradation was a function of the

temperature, frequency, and stress level. The lower frequency tests showed a slightly greater decrease in modulus as did the higher temperature tests.

VI. Recommendations

The tension-tension fatigue behavior of the Nicalon/MAS cross-ply ceramic matrix composite is well characterized at elevated temperature. It is clear that the main damage mechanisms under fatigue loading at elevated temperature are fiber debonding due to fatigue loading and environmentally assisted crack growth due to oxidation and strengthening of the fiber matrix interface. Further investigation of the effect of frequency of loading, in the form of lower and higher frequency tests, ought to be performed to further characterize the effect of frequency on fatigue behavior. Further testing ought to be performed with wider specimens, up to 0.5 inches, in an attempt to isolate the dominant damage mechanism in these fatigue tests.

Bibliography

1. Agarwal, B. D., and Broutman, L.J., Analysis and Performance of Fiber Composites, 2nd Ed., John Wiley and Sons, New York, 1990

2. Agins, D., Static Fracture Behavior of a Ceramic Matrix Composite at Elevated Temperatures, MS Thesis, AFIT/GAE/ENY/93D-1, School of Engineering, Air Force Institute of Technology (AU), Wright Patterson AFB, Ohio, December 1993

3. Allen, R.F., Beevers C.J., and Bowen P. "Fracture and Fatigue of a Nicalon/CAS Continuous Fiber Reinforced Glass-Ceramic Matrix Composite". Composites, Volume 24, Number 2: 150-156 (1993).

4. Headinger M.H. Dupont Lanxide Composites Inc., Newark Delaware. Fax of test data. May 1994.

5. Grant, S., Fatigue Behavior of a Cross-Ply Ceramic Matrix Composite Subjected to Tension-Tension Cycling with Hold Time, MS Thesis, AFIT/GAE/ENY/94D-1, Graduate School of Engineering, Air Force Institute of Technology (AETC), Wright Patterson AFB, Ohio, December 1994.

6. Holmes, J.W. "Fatigue of Fiber Reinforced Ceramics". The University of Michigan, Ann Arbor, MI, 48109-2125, 10 June 1991.

7. Larsen D.C., Godard, H.T., Stewart, R.L., Chyung, K., Linsey, G.D., and Murphy, D.S., "BSG Doped CMC's for Thermal Durability". Proceedings of the 17th Annual Conference on Composites, Materials, and Structures. New York: Corning Inc., January 1993.

8. Lee, S. S. Damage Analysis and Mechanical Response of As-Received and Heat-Treated Nicalon/CAS-II Glass-Ceramic Matrix Composites. PhD dissertation. Virginia Polytechnic Institute and State University, Blacksburg, VA, 1992.

9. Opalski, F. A., Fatigue Behavior of a Cross-Ply Ceramic Matrix Composite Under Tension-Tension and Tension Compression Loading, MS Thesis, AFIT/GAE/ENY/92D-02, Graduate School of Engineering, Air Force Institute of Technology (AETC), Wright Patterson AFB, Ohio, December 1992.

10. Rousseau, C.Q. Monotonic and Cyclic Behavior of a Silicon Carbide/Calcium-Aluminosilicate Ceramic Composite, Thermal and Mechanical Behavior of Metal Matrix and Ceramic Matrix Composites, ASTM SPT 1080.

11. Sanders Brian P. Characterization of Fatigue Damage in a Metal Matrix Composite (SCS-6/Ti-15-3) at Elevated Teperature. PhD Dissertation, AFIT/DS/AA/93-4. Graduate School of Engineering, Air Force Institute of Technology, Wright-Patterson Air Force Base, Ohio, Dec 1993.

12. Sorensen, B.F., Talreja, R., and Sorensen, O.T., "Damage Development in a Ceramic Matrix Composite under Mechanical Loading," Proceedings of the 5th European Conference on Composite Materials, Bordeaux, France, April 1992.

13. Tuznik, R. J., Fatigue Behavior of a Cross-Ply Ceramic Matrix Composite at Elevated Temperatures Under Tension-Tension Loading, MS Thesis, AFIT/GAE/ENY/93D-28, Graduate School of Engineering, Air Force Institute of Technology (AETC), Wright Patterson AFB, Ohio, December 1993.

14. Worthem D.W. Thermomechanical Fatigue Behavior of Three Ceramic Matrix Composites. Contract NAS3-25266. Brook Park, Ohio: Sverdup Technology, Inc., 1993.

15. Zawada, L.P., Butkus, L.M. and Hartman, G.A., "Tensile and Fatigue Behavior of Silicon Carbide Fiber-Reinforced Aluminosilicate Glass," Journal of the American Ceramic Society, Vol 144, No 2, August 1993, pp 30-35.

APPENDIX A

This Appendix contains a figure pertaining to the over all dimensions and appearance of the specimens that have been prepared for testing.

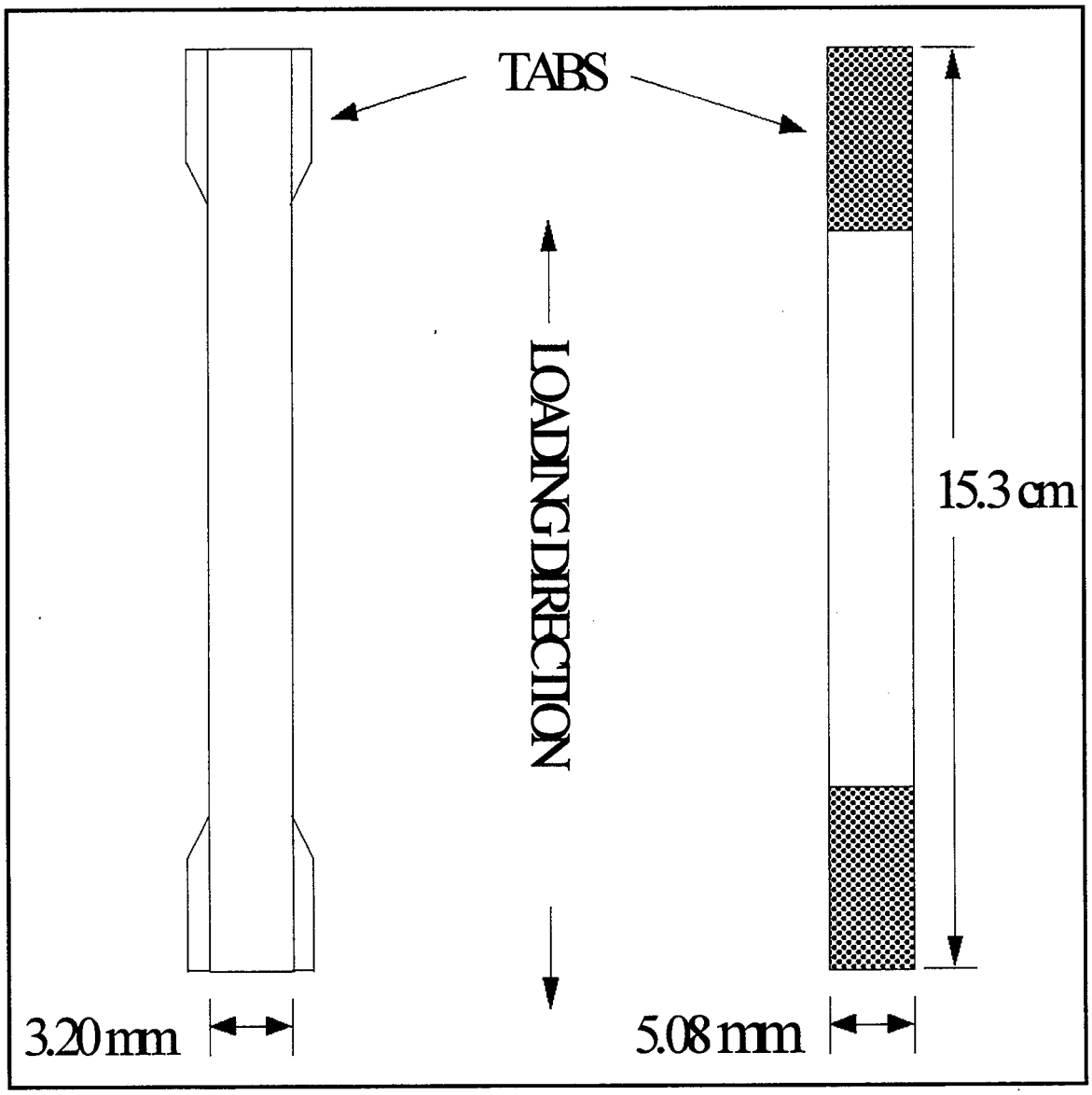

APPENDIX B

This Appendix contains figures pertaining to the monotonic stress-strain relationships of the SiC/MAS material at 566oC and 1093oC. The figures in this appendix compare those curves obtained in this study to those reported by Larsen [7].

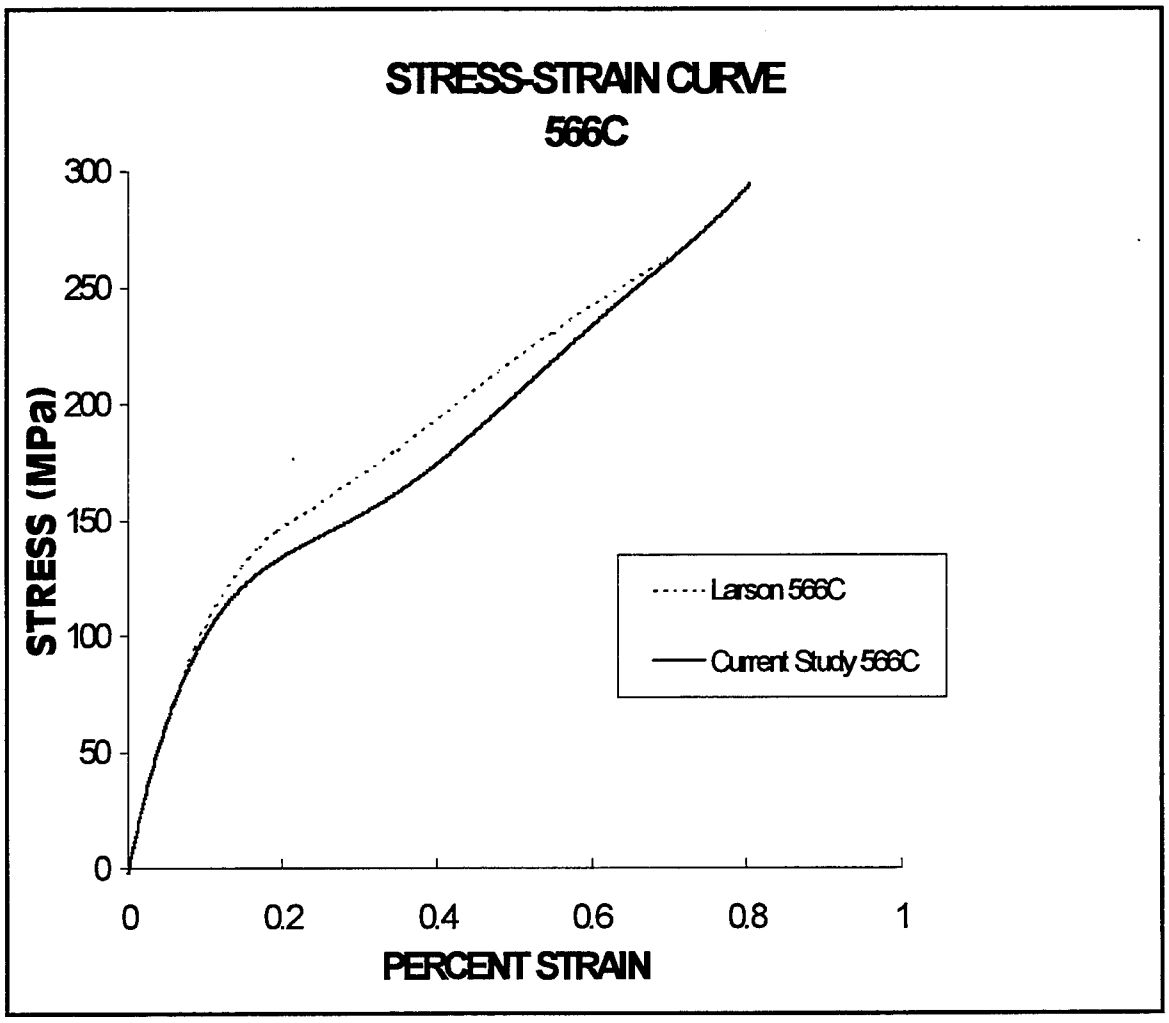

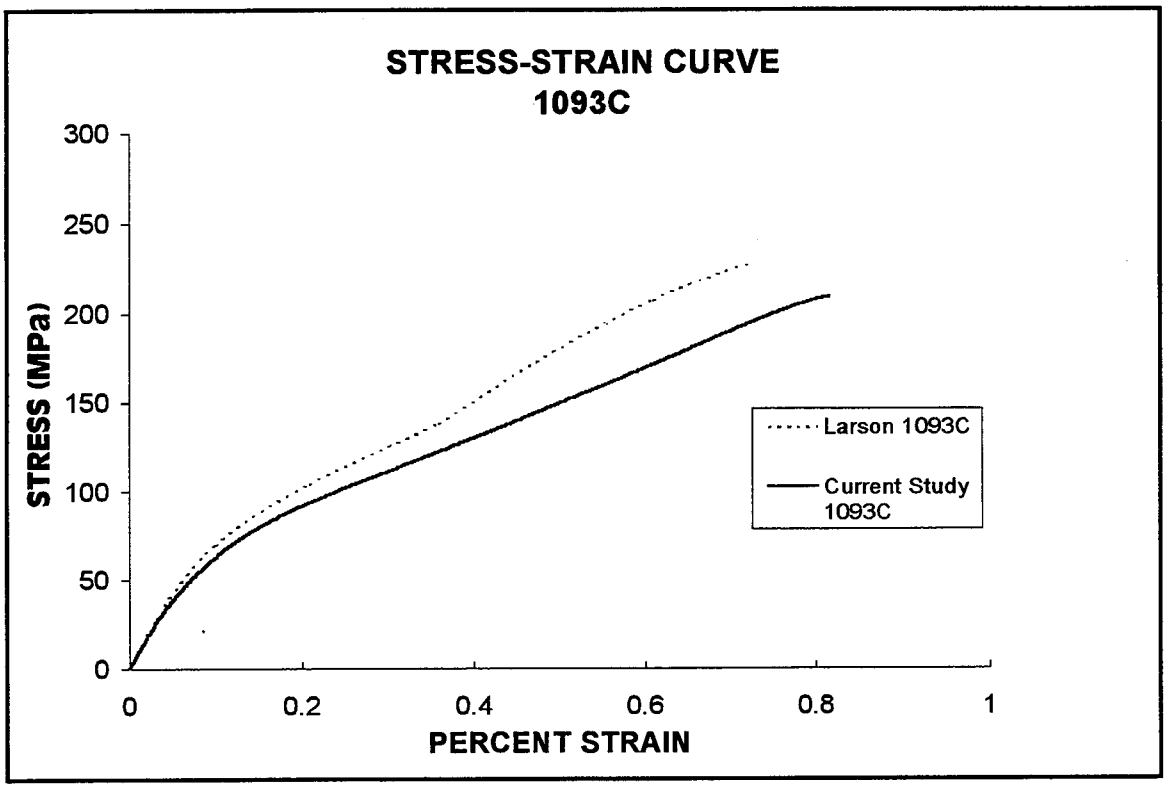
STRESS-STRAIN CURVE
1093C
300
250
200
150
100
50
0
STRESS (MPa)
0
0.2
0.4
0.6
0.8
1
PERCENT STRAIN
Larson 1093C
Current Study 1093C

APPENDIX C

The figures in this Appendix contain the stress-strain hysteresis loops for selected tests. These loops represent trend lines drawn through the raw data obtained in the tests for selected cycles. The loops have been shifted in most cases for clarity. Additional loops for tests not shown can be found in the work done by Grant [5].

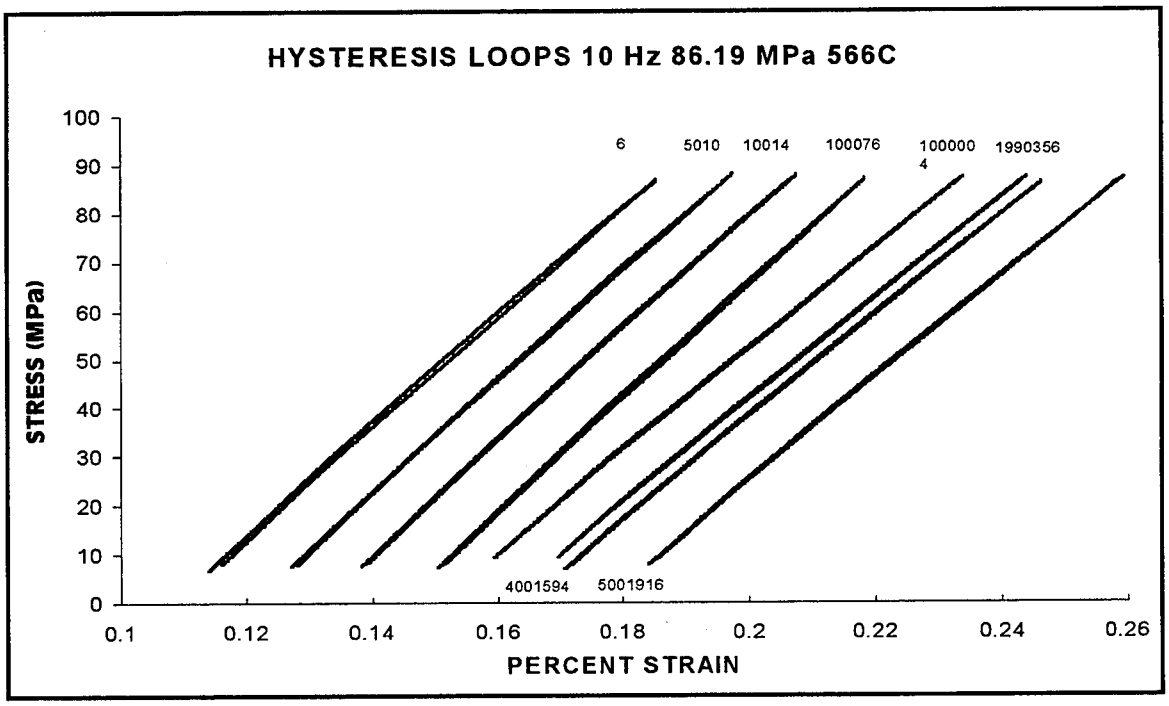

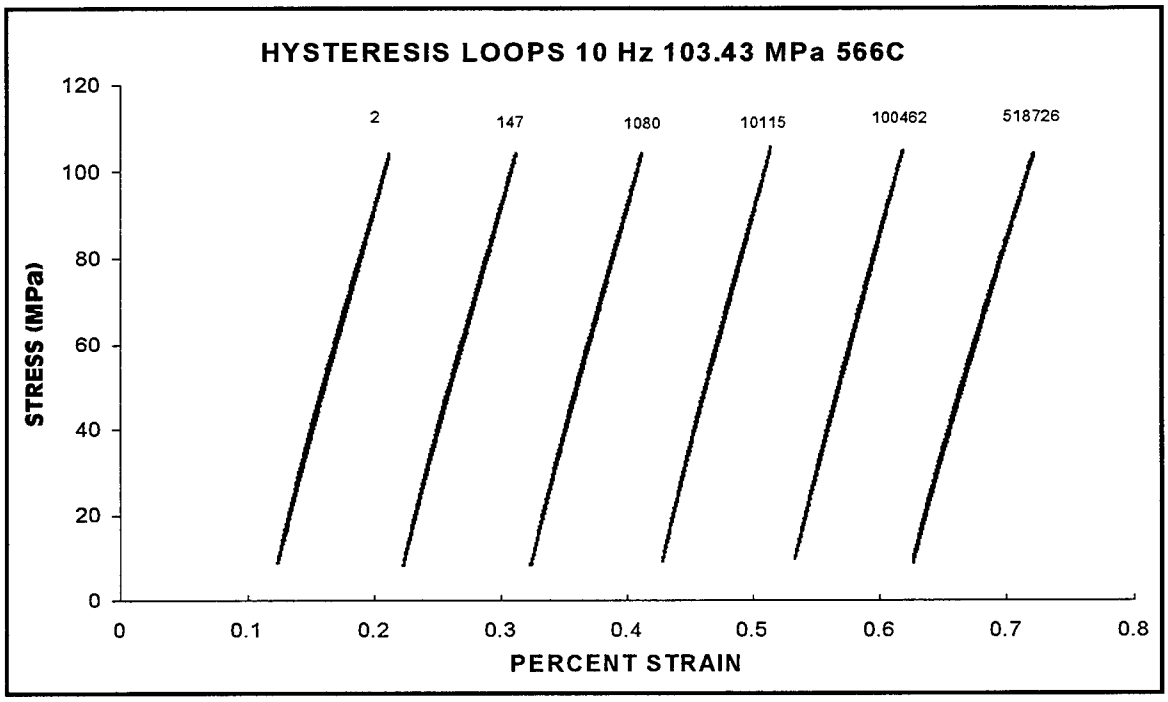
HYSTERESIS LOOPS 10 Hz 103.43 MPa 566C
STRESS (MPa)
PERCENT STRAIN
2
147
1080
10115
100462
518726
0
20
40
60
80
100
120
0
0.1
0.2
0.3
0.4
0.5
0.6
0.7
0.8

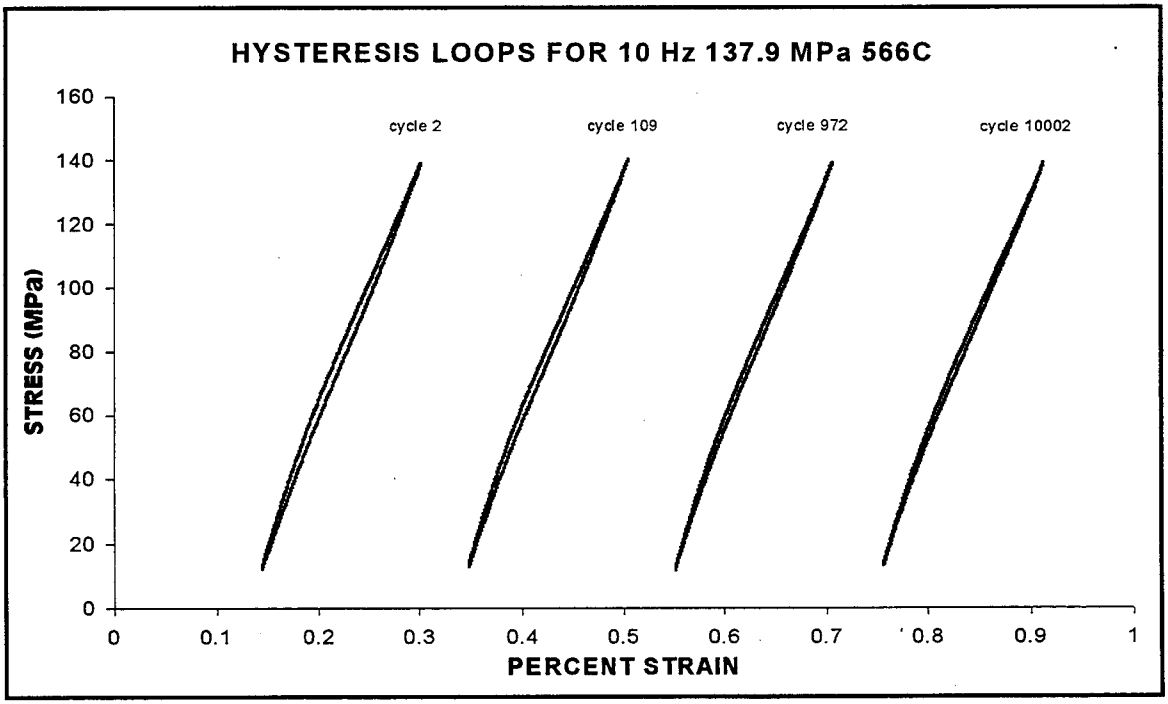
HYSTERESIS LOOPS FOR 10 Hz 137.9 MPa 566C
STRESS (MPa)
PERCENT STRAIN
cycle 2
cycle 109
cycle 972
cycle 10002
0
20
40
60
80
100
120
140
160
0
0.1
0.2
0.3
0.4
0.5
0.6
0.7
0.8
0.9
1

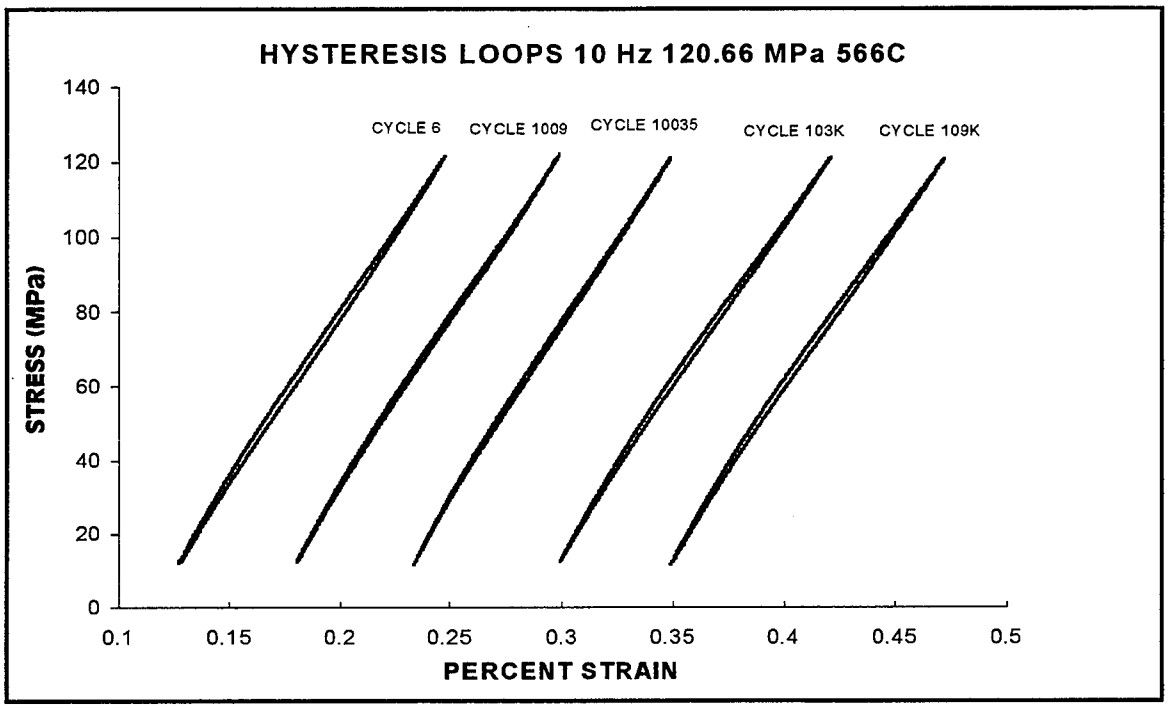
HYSTERESIS LOOPS 10 Hz 120.66 MPa 566C
CYCLE 6
CYCLE 1009
CYCLE 10035
CYCLE 103K
CYCLE 109K
STRESS (MPa)
140
120
100
80
60
40
20
0
0.1
0.15
0.2
0.25
0.3
0.35
0.4
0.45
0.5
PERCENT STRAIN

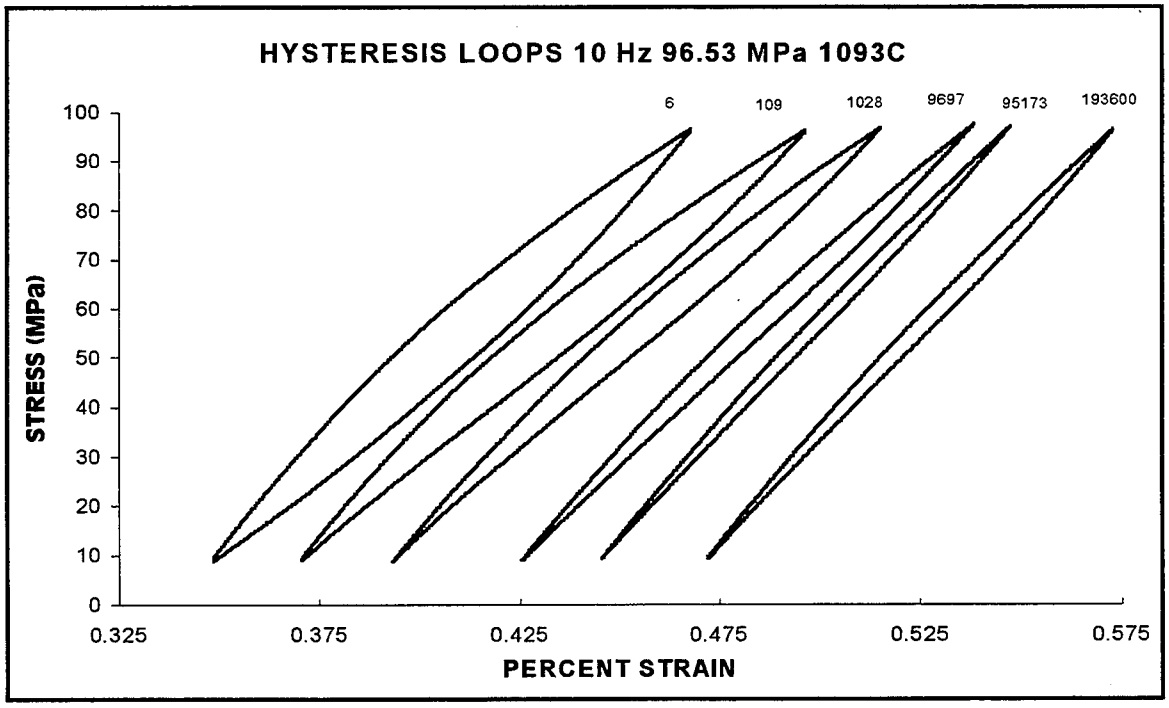
HYSTERESIS LOOPS 10 Hz 96.53 MPa 1093C
6
109
1028
9697
95173
193600
STRESS (MPa)
100
90
80
70
60
50
40
30
20
10
0
0.325
0.375
0.425
0.475
0.525
0.575
PERCENT STRAIN

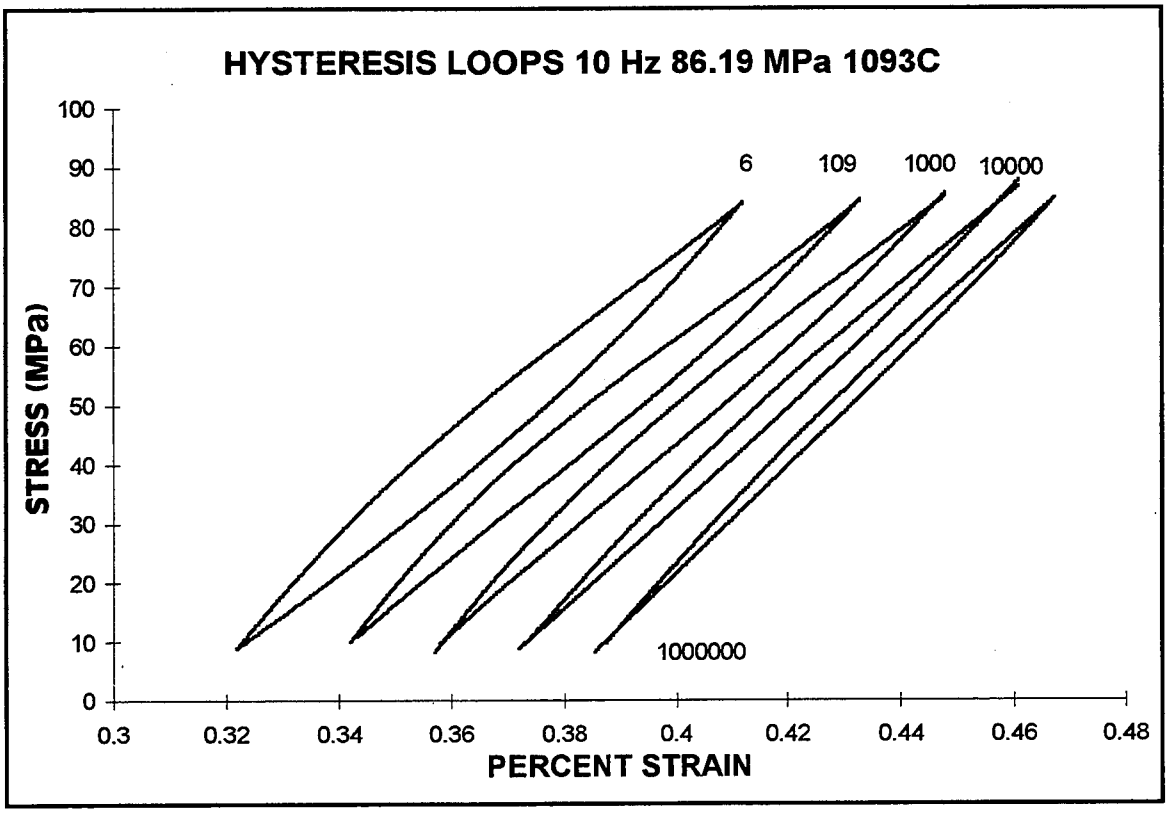
HYSTERESIS LOOPS 10 Hz 86.19 MPa 1093C
STRESS (MPa)
PERCENT STRAIN
6
109
1000
10000
1000000
100
90
80
70
60
50
40
30
20
10
0
0.3
0.32
0.34
0.36
0.38
0.4
0.42
0.44
0.46
0.48

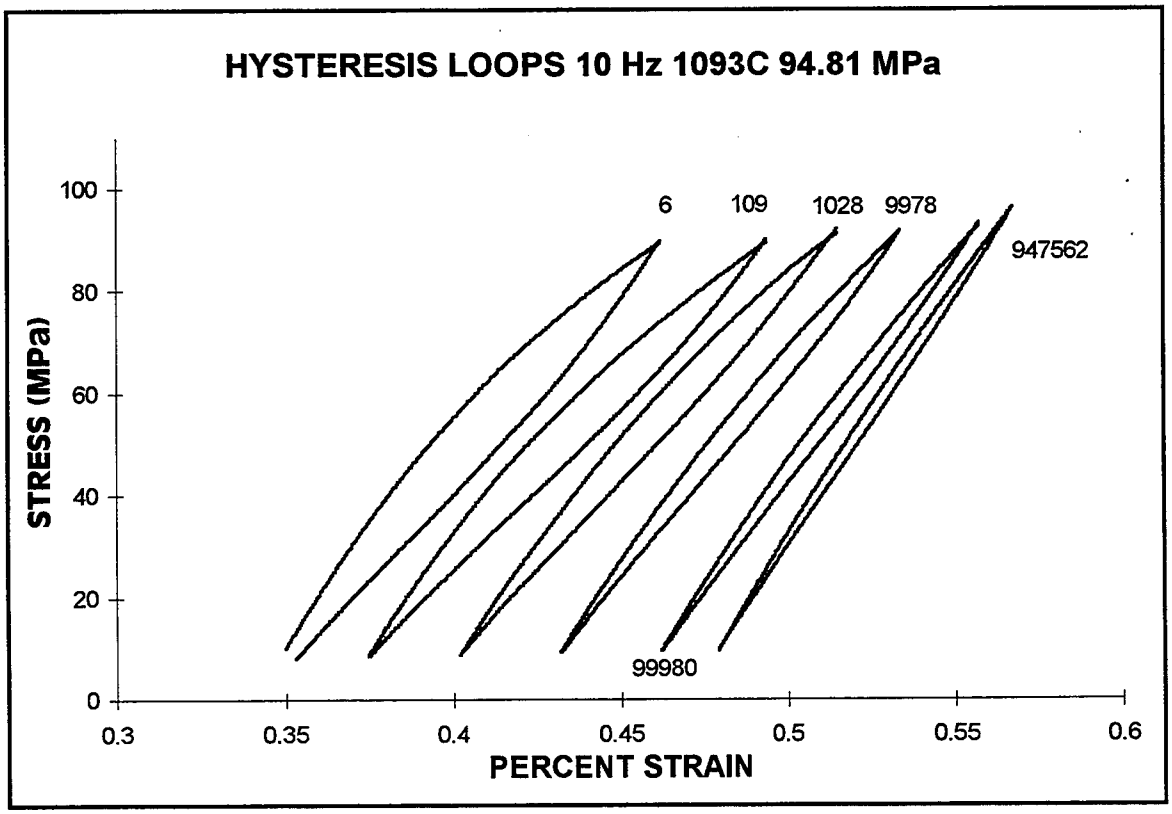
HYSTERESIS LOOPS 10 Hz 1093C 94.81 MPa
STRESS (MPa)
PERCENT STRAIN
6
109
1028
9978
947562
99980
100
80
60
40
20
0
0.3
0.35
0.4
0.45
0.5
0.55
0.6

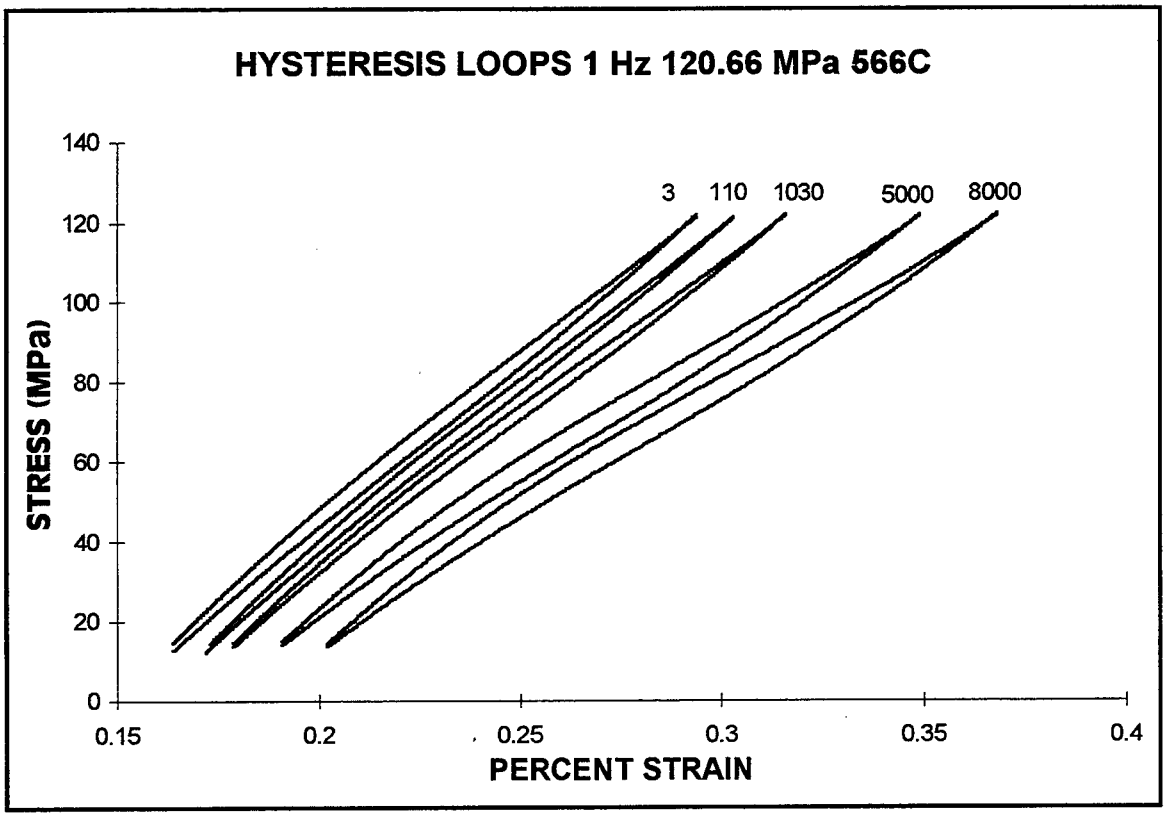
HYSTERESIS LOOPS 1 Hz 120.66 MPa 566C
STRESS (MPa)
PERCENT STRAIN
140
120
100
80
60
40
20
0
0.15
0.2
0.25
0.3
0.35
0.4
3
110
1030
5000
8000

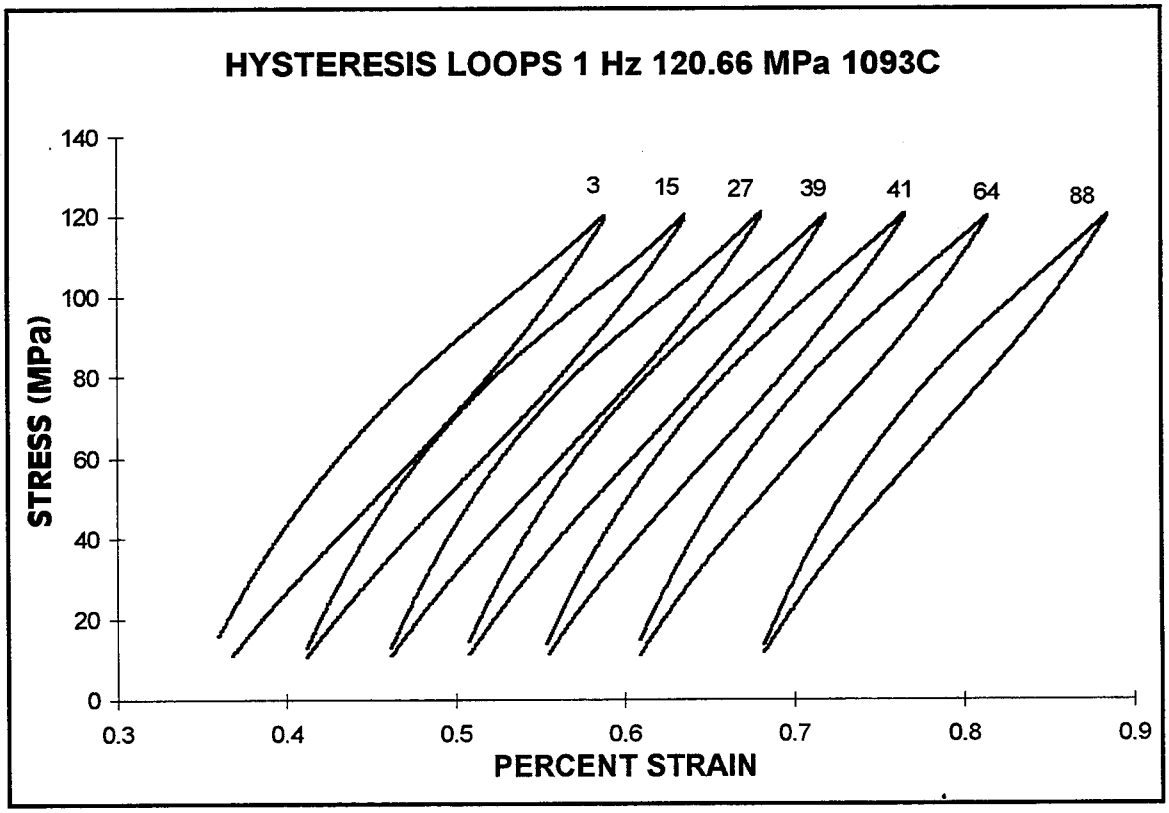
HYSTERESIS LOOPS 1 Hz 120.66 MPa 1093C
STRESS (MPa)
PERCENT STRAIN
140
120
100
80
60
40
20
0
0.3
0.4
0.5
0.6
0.7
0.8
0.9
3
15
27
39
41
64
88

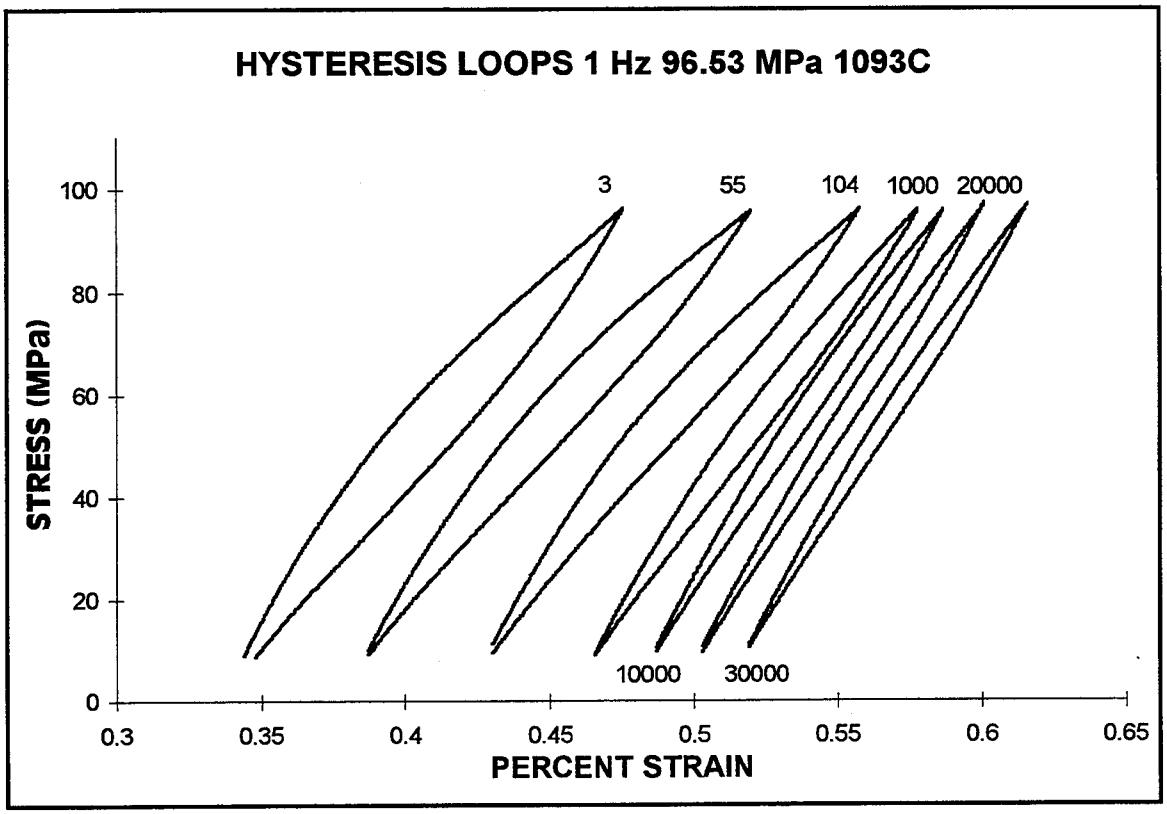
HYSTERESIS LOOPS 1 Hz 96.53 MPa 1093C
STRESS (MPa)
100
80
60
40
20
0
0.3
0.35
0.4
0.45
0.5
0.55
0.6
0.65
PERCENT STRAIN
3
55
104
1000
20000
10000
30000

Vita

Captain Craig D. Steiner was born in Annapolis, Maryland. He graduated from Portsmouth High School, Portsmouth, Rhode Island in 1986. He then attended the United States Air Force Academy in Colorado Springs, Colorado, from 1986 until 1990 and graduated with a Bachelor of Science Degree in Engineering Mechanics.

Captain Steiner's military assignment includes engineering project officer in the SATCOM System Program Office (SPO) at Los Angeles Air Force Base, California.

Captain Steiner entered the School of Engineering, Air Force Institute of Technology, in June 1994.

REPORT DOCUMENTATION PAGE

Form Approved
OMB No. 0704-0188

1. AGENCY USE ONLY (Leave blank)	2. REPORT DATE	3. REPORT TYPE AND DATES COVERED
	December 1994	Master's Thesis

4. TITLE AND SUBTITLE
FATIGUE BEHAVIOR OF A CROSS-PLY CERAMIC MATRIX COMPOSITE AT ELEVATED TEMPERATURE UNDER TENSION-TENSION LOADING

5. FUNDING NUMBERS

6. AUTHOR(S)

Craig D. Steiner, Captain, USAF

7. PERFORMING ORGANIZATION NAME(S) AND ADDRESS(ES)

Air Force Institute of Technology
2750 P Street
WPAFB OH 45433-6583

8. PERFORMING ORGANIZATION REPORT NUMBER

AFIT/GAE/ENY/94D-9

9. SPONSORING / MONITORING AGENCY NAME(S) AND ADDRESS(ES)

Mr. Ted Fecke
WL/POTC
WPAFB, OH, 45433-6583

10. SPONSORING / MONITORING AGENCY REPORT NUMBER

11. SUPPLEMENTARY NOTES

12a. DISTRIBUTION / AVAILABILITY STATEMENT

Approved for public release; distribution unlimited

12b. DISTRIBUTION CODE

13. ABSTRACT (Maximum 200 words)

This study investigated the fatigue behavior and damage mechanisms of a $[0/90]_{4s}$ SiC/MAS ceramic matrix composite under tension-tension loading at two elevated temperatures and two frequencies. Stress and strain hystereses, maximum and minimum strain, and modulus of elasticity were evaluated to characterize the material behavior. Microscopy and fractography were used to evaluate damage progression and mechanisms. Fatigue life was independent of frequency at both temperatures.

14. SUBJECT TERMS
Ceramic matrix composites, Elevated temperature, Fatigue testing, Silicon carbide fibers, Glass Ceramics

15. NUMBER OF PAGES
147

16. PRICE CODE

17. SECURITY CLASSIFICATION OF REPORT	18. SECURITY CLASSIFICATION OF THIS PAGE	19. SECURITY CLASSIFICATION OF ABSTRACT	20. LIMITATION OF ABSTRACT
Unclassified	Unclassified	Unclassified	UL